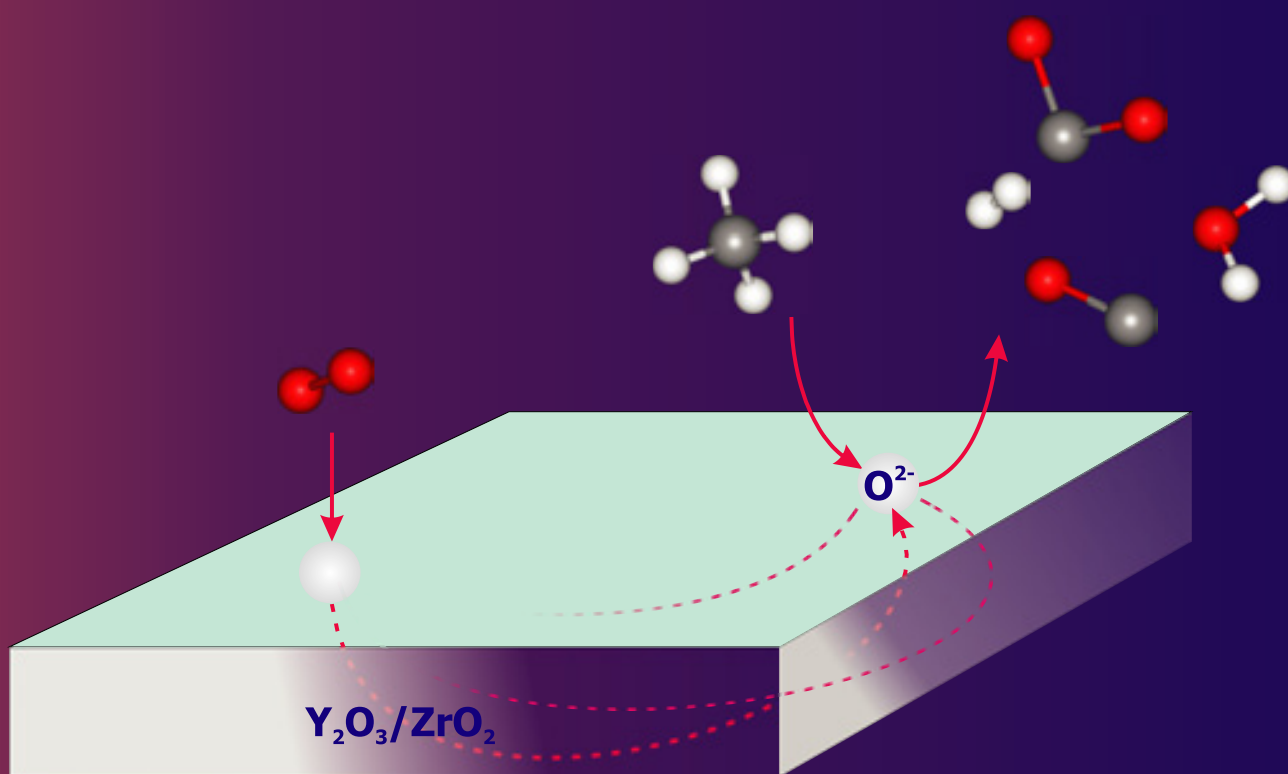


Catalytic Partial Oxidation of Methane to Synthesis Gas over ZrO_2 -based Defective Oxides



Jianjun Zhu

**Catalytic Partial Oxidation of Methane to Synthesis Gas
over ZrO₂-based Defective Oxides**

Jianjun Zhu

Dissertation committee

Prof. dr. U. Karst, chairman	University of Twente
Prof. dr. ir. L. Lefferts, promotor	University of Twente
Dr. J.G. van Ommen, assistant promotor	University of Twente
Prof. dr. A.O.I. Krause	Helsinki University of Technology, Finland
Prof. dr. ir. G.J. Kramer	Eindhoven University of Technology
Prof. dr. ir. W.P.M. van Swaaij	University of Twente
Prof. dr. ir. J.A.M. Kuipers	University of Twente
Prof. dr. ir. T.H. van der Meer	University of Twente
Dr. H.J.M. Bouwmeester	University of Twente
Dr. E.R. Stobbe	Energy research Centre of the Netherlands

The research described in this thesis was performed under the auspices of NIOK, the Netherlands Institute of Catalysis Research, and financially supported by Stichting technische wetenschappen (STW, the Dutch technology foundation) under project number UPC-5037.

Publisher:

Printpartners Ipskamp B.V., P.O. Box 333, 7500 AH Enschede, The Netherlands.

Cover designer: Ing. Bert Geerdink

Copyright © 2005 by Jianjun Zhu, Enschede, The Netherlands.

No part of this book may be reproduced in any form of print, photo print, microfilm or any other means without written permission from the author / publisher.

ISBN 90-365-2142-4

**CATALYTIC PARTIAL OXIDATION OF METHANE
TO SYNTHESIS GAS OVER ZRO₂-BASED
DEFECTIVE OXIDES**

DISSERTATION

to obtain
the doctor's degree at the University of Twente,
on the authority of the rector magnificus,
prof. dr. W.H.M. Zijm,
on account of the decision of the graduation committee,
to be publicly defended
on Thursday, March 24th, 2005 at 16.45

by

Jianjun Zhu

born on April 8th, 1966
in Jiangsu, P.R. China

This dissertation has been approved by the promotor

Prof. dr. ir. L. Lefferts

and the assistant promotor

Dr. J.G. van Ommen

To my family

Table of Contents

Summary	1
Summary in Dutch	5
Summary in Chinese	9
Chapter 1 General Introduction	13
1.1. Introduction.....	14
1.2. Methane conversion technologies	14
1.2.1. Direct utilization of methane	14
(1) Oxidative coupling of methane C ₂ hydrocarbons (OCM)	15
(2) Selective oxidation of methane into formaldehyde and methanol (SOM).....	16
1.2.2. Indirect utilization of methane	16
(1) Methanol synthesis.....	16
(2) Fischer-Tropsch process	17
1.3. Synthesis gas production	18
(1) Steam reforming	18
(2) CO ₂ reforming	19
(3) Partial oxidation	20
1.4. Catalytic partial oxidation of methane to synthesis	21
1.4.1. Thermodynamic analysis of methane partial oxidation	21
1.4.2. CPOM over metallic catalysts	22
1.4.2.1. Metallic catalysts	22
(1) Supported Ni, Co or Fe catalysts	22
(2) Supported noble metal catalysts	23
1.4.2.2. Reaction mechanisms for CPOM over metal catalysts	24
(1) Two-step reaction mechanism	24
(2) Direct partial oxidation mechanism	24
1.4.2.3. Problems with metal catalysts	25
1.4.3. Oxide catalysts	27
1.4.3.1. CPOM over oxides	27
1.4.3.2. Yttrium-stabilized zirconia (YSZ)	27
1.5. Scope of this thesis	30
References	31
Chapter 2 Dual Catalyst Bed Concept for Catalytic Partial Oxidation of Methane to Synthesis Gas	33

Abstract	33
2.1. Introduction	34
2.2. Experimental	35
2.2.1. Catalyst preparation	35
2.2.2. Catalytic reaction	35
2.3. Results and Discussion	35
2.3.1. CPOM in a single catalyst bed	35
2.3.2. CPOM in the dual catalyst bed system	37
2.3.3. Adiabatic temperature changes	38
2.3.4. Productivity and reactor concepts	39
2.4. Conclusion	40
Acknowledgements	40
References	40

Chapter 3 Effect of Surface Composition of Yttrium-Stabilized Zirconia on Partial Oxidation of Methane to Synthesis Gas43

Abstract	43
3.1. Introduction	44
3.2. Experimental	45
3.2.1. Catalysts	45
3.2.2. Catalyst characterization	45
3.2.3. Catalytic measurement	46
3.3. Results	46
3.3.1. Surface composition	46
3.3.2. CPOM over YSZ	49
3.3.2.1. ZrO ₂ and YSZ	49
3.3.2.2. Influence of surface area.....	50
3.3.2.3. Methane conversion rate	51
3.3.3. CPOM over YSZ at temperatures above 900°C	51
3.3.4. Coupling CPOM with steam or CO ₂ reforming of CH ₄	52
3.3.5. Steam reforming of methane	52
3.3.6. CO ₂ reforming of methane	53
3.4. Discussion	53
3.4.1. Active surface of YSZ	53
3.4.2. Effects of contamination	54
3.4.3. Effects of calcination temperature	55
3.4.4. CPOM at high temperatures	55
3.5. Conclusions	56

Acknowledgements	57
References	57

Chapter 4 Reaction Scheme of Partial Oxidation of Methane to Synthesis Gas over Yttrium-stabilized Zirconia61

Abstract	61
4.1. Introduction	62
4.2. Experimental	63
4.2.1. Catalysts	63
4.2.2. Catalytic measurements	63
4.2.3. <i>In-situ</i> Infrared spectroscopy	64
4.2.4. Temperature-programmed desorption/decomposition (TPD/TPDE)	65
4.2.4.1. TPD/TPDE in the IR cell	65
4.2.4.2. TPD/TPDE in TPD setup	65
4.3. Results	65
4.3.1. Partial oxidation of methane over YSZ	65
4.3.2. <i>In-situ</i> IR study	66
4.3.3. TPD/TPDE of the formate on YSZ surface	67
4.3.4. Oxidative conversion of CH ₂ O	67
4.3.4.1. YSZ12A	67
4.3.4.2. Empty reactor	68
4.3.4.3. Co-feeding CH ₂ O with CH ₄ and O ₂	68
4.4. Discussion	70
4.4.1. Activation of methane	70
4.4.2. Reaction intermediates	71
4.4.3. Reaction scheme	72
4.4.4. Relative reaction rates	73
4.5. Conclusions	75
Acknowledgements	75
References	75

Chapter 5 Activation of O₂ and CH₄ on Yttrium-stabilized Zirconia for the Partial Oxidation of Methane to Synthesis Gas77

Abstract	77
5.1. Introduction	78
5.2. Experimental	79
5.2.1. Catalysts	79

5.2.2. Transient experiments	79
5.2.3. Isotopic $^{18}\text{O}_2$ exchange	80
5.3. Results	80
5.3.1. Isotopic oxygen exchange	80
5.3.1.1. $^{18}\text{O}_2$ exchange in the absence of methane	80
5.3.1.2. $^{18}\text{O}_2$ exchange in the presence of methane	81
5.3.2 Methane activation	82
5.3.2.1. CH_4 -pulse experiments	82
5.3.2.2. O_2 -pulse experiments	83
5.4. Discussion	84
5.4.1. Oxygen activation	84
5.4.2. Methane activation	85
5.4.3. Reaction model	87
5.5. Conclusions	88
Acknowledgements	89
References	89

Chapter 6 The Role of Defect Structure in Activation of N_2O and O_2 on ZrO_2 and Yttrium-stabilized ZrO_291

Abstract	91
6.1. Introduction	92
6.2. Experimental	93
6.2.1. Catalysts	93
6.2.2. Catalytic measurements	93
6.2.3. TPD of adsorbed oxygen species	93
6.2.4. SEM and XRD	94
6.3. Results	94
6.3.1. CPOM	94
6.3.2. Decomposition of N_2O	95
6.3.3. TPD of adsorbed oxygen species	95
6.3.4. Characterization	97
6.3.4.1. SEM	97
6.3.4.2. XRD	97
6.4. Discussion	98
6.4.1. Surface oxygen species	98
6.4.2. Activations of N_2O and O_2	99
6.4.3. Effect of calcination temperature	100
6.5. Conclusions	101

Acknowledgements	102
References	102
Chapter 7 Concluding Remarks and Recommendations: A Promising Concept for Catalytic Partial oxidation of Hydrocarbons to Synthesis Gas.....	105
7.1. CPOM over ZrO₂ and YSZ	106
7.1.1. Catalytic chemistry	106
1) Reaction scheme	106
2) Active sites	107
3) C-H bond activation	108
7.1.2. Technical concept for synthesis gas production	109
7.1.3. Challenges in the application	110
7.2. Catalytic partial oxidation of liquid hydrocarbons	111
References	113
List of Publications	115
Acknowledgements.....	117
Curriculum Vita	119

Summary

The impending decline in fossil-oil resources, and contemporarily, the large amounts of natural gas found worldwide have stimulated intensive research in utilizations of methane, the main component of natural gas. The direct conversion of natural gas to olefins via oxidative coupling, or to oxygenates, e.g. methanol and formaldehyde, via selective oxidation is not attractive due to the low yields obtained (either low conversion or poor selectivity). So far, most of the applications of natural gas still proceed via the indirect route, in which natural gas has to be converted to synthesis gas first. It has been estimated that in most of the indirect processes such as methanol synthesis, Fischer-Tropsch (F-T) synthesis and ammonia synthesis, over 60% of the cost of the overall process is associated with synthesis gas generation. Therefore, considerable academic and industrial research has been focused on production of synthesis gas. Steam reforming of methane is the conventional process for synthesis gas production. Compared with steam reforming, direct partial oxidation of methane to synthesis gas (POM) is attractive because of its mild exothermic heat of reaction and the suitable H_2/CO ratio for downstream processes, such as methanol and F-T syntheses. Especially, it becomes much more attractive when using a catalyst, which significantly reduces the reaction temperature required for POM. About 10-15% reduction in the energy requirement and 25-30% lower capital investment are expected for catalytic partial oxidation (CPOM) as compared to the steam reforming process. In last two decades, considerable amount of work has been done for CPOM, including fundamental studies on catalysis and technological investigations in reactor engineering. Almost all research in CPOM is based on metallic catalysts. However, in addition to difficulty in controlling the reaction temperature due to the highly exothermic reaction heat of the total oxidation ($\Delta H_{298}^{\circ} = -802 \text{ kJ/mol}$), metal catalysts, e.g. Rh, Pt, Ni, are suffering from deactivation via evaporation in the form of volatile metal oxides at high temperatures, especially in the presence of oxygen. Poor stability of the metal catalysts handicaps commercialization of CPOM on an industrial scale. As compared with metal catalysts, hardly reducible oxides are much more stable, although they are less active and selective. Therefore, the work presented in this thesis provides both fundamental scientific knowledge as well as a new technical dual-bed concept for synthesis gas production via catalytic partial oxidation of methane over defective ZrO_2 -based oxides.

The dual bed concept is demonstrated for synthesis gas production in Chapter 2. The direct partial oxidation of methane is found to proceed over yttrium-stabilized zirconia (YSZ). However, in addition to CO and H_2 , CO_2 and H_2O are also primary products. For a stoichiometric feedstock ($CH_4/O_2=2:1$), methane conversion is always less than 50% due to the unavoidable H_2O formation which consumes half of the oxygen added. To completely convert methane to synthesis gas, a dual catalyst bed concept is required. In the first reactor, a stoichiometric mixture of methane and oxygen is converted to a mixture of CO, H_2 , H_2O , CO_2 and unconverted CH_4 over an irreducible stable oxide, such as YSZ. The second catalyst bed

Summary

with a conventional reforming catalyst (e.g. supported Co), subsequently converts CO_2 and H_2O with the remaining CH_4 to CO and H_2 . Finally, synthesis gas with an equilibrium composition (almost 100% CO and H_2 yields) is produced at high GHSV. Compared with initial deep oxidation on metal catalysts, the partial-selective oxidation over oxide catalyst in the first bed significantly decreases the amount of heat generated. This results in milder temperature profiles in the reactor. Most importantly, all oxygen is completely consumed in the oxide catalyst bed. Exposure of metal catalyst in the second reactor to oxygen at high temperatures is prevented. Therefore, deactivation of metal catalyst via evaporation of volatile metal oxides is circumvented. As discussed in Chapter 7 a temperature of 650°C in the first reactor is high enough for complete consumption of oxygen, although 1000°C was used in this chapter. If this startup temperature can be further lowered, the concept of this dual catalyst bed system may be a very promising candidate for application in synthesis gas production.

ZrO_2 -based oxides are promising catalysts for CPOM. Therefore, it is worth further studying CPOM over ZrO_2 -based oxides. The effects of surface area, reaction temperature, and especially surface composition of YSZ on CPOM have been studied in Chapter 3. Much attention has been paid to the influence of surface contaminations, such as CaO, TiO_2 , and HfO_2 on catalytic performance. The catalysts are characterized by X-ray fluorescence (XRF), X-ray Photoelectron Spectroscopy (XPS) and low-energy ion scattering (LEIS). Compared with ZrO_2 , YSZ is much more active and selective. This improved catalytic performance is attributed to the creation of active sites by doping ZrO_2 with Y_2O_3 , although the role of oxygen vacancies generated is not completely clear yet in this chapter. CPOM is studied for YSZ catalysts with different Y_2O_3 contents. It is observed that the surface composition rather than the bulk composition determines the catalytic performance. Interestingly, as long as YSZ is not contaminated, the composition of the outermost surface of calcined YSZ is independent of both the concentration of Y_2O_3 in the bulk and calcination temperature above 900°C ; the surface always contains 12 ± 2 mol% Y_2O_3 due to segregation of Y_2O_3 . Calcination of uncontaminated YSZ at higher temperatures creates more active sites per m^2 , while the catalyst loses surface area via sintering. However, much lower activity is observed for YSZ containing traces of (earth) alkali oxides (contaminations). Two major impurities, TiO_2 and HfO_2 , detected in the bulk, have not been detected on the surface by LEIS. In contrast, CaO is detected on the surface but not in the bulk. Moreover, calcination at higher temperature results in higher surface coverage of the impurities (mainly CaO), thus lowering the catalytic activity. The impurities segregated to the surface either block active surface of YSZ catalyst or form new phases with different catalytic properties.

The roles of consecutive steam- and CO_2 - reforming reactions have been also investigated in this chapter. Heterogeneous reactions occur concurrently with homogeneous gas phase reactions at temperatures above 950°C during CPOM over YSZ catalysts. At such high temperatures, CPOM, steam- and CO_2 reforming, as well as reverse water-gas shift, occur in

competition during CPOM. These reforming reactions of methane result in a significant increase of synthesis gas selectivity, although the catalyst activity is still too low to reach thermodynamic equilibrium.

The work described in Chapter 4 allows the formulation of a reaction scheme for CPOM over YSZ catalyst, based on the results of *in-situ* FTIR and both steady state- and transient-experiments. Yields of CO, H₂, CO₂ and H₂O linearly depend on methane conversion, indicating all of them are primary products of CPOM. Traces of formaldehyde and formic acid are detected in the effluent from the reactor during steady state experiments. Formation of formate species is observed on the surface of YSZ at temperatures between 400 and 475°C in *in-situ* IR experiments. Rapid conversion of formaldehyde to formate on YSZ, even at room temperature, explains that adsorbed formaldehyde is never observed. Temperature-programmed decomposition of formate formed either by adsorption of formaldehyde at 50°C or by activation of methane at 400°C results in an essentially identical mixture of CO, CO₂, H₂ and H₂O as observed for normal CPOM. Moreover, addition of formaldehyde to the feed of CPOM does not influence selectivities to CO, CO₂ and H₂. These results indicate that formate and formaldehyde are two reaction intermediates for CPOM over YSZ. CO and H₂ are produced mainly via decomposition of formaldehyde. Surface formate formed by further oxidation of formaldehyde decomposes either to CO and H₂O via dehydration, or to CO₂ and H₂ via dehydrogenation. Finally, a complete reaction scheme is proposed, which contains exclusively reaction pathways that contribute significantly to the products. The ratios between the competing pathways are strongly influenced by temperature.

Formaldehyde added to the reaction feed competes for oxygen with methane. At temperatures above 600°C, methane conversion decreases with increasing amount of formaldehyde, indicating that oxidation of methane to formaldehyde is a rate-determining step.

To get much more insight of the reaction mechanism, the sites responsible for activation of both oxygen and methane on ZrO₂ and YSZ have been investigated, which are described in Chapter 5. Especially, the role of oxygen vacancies, which are generated by doping ZrO₂ with Y₂O₃, has been clarified by isotopic oxygen exchange with ZrO₂ or YSZ and transient pulse experiments. The results reveal that CPOM over both ZrO₂ and YSZ oxides proceeds via a Mars-van Krevelen mechanism. Exclusive ¹⁶O-containing oxidation products are detected during ¹⁸O₂-CH₄ pulses over YSZ. This indicates that methane is selectively oxidized by lattice oxygen ions on the surfaces of YSZ and ZrO₂, despite the presence of adsorbed oxygen species under reaction conditions. It is estimated that about 8% and 14% of lattice oxygen in the outermost surface layer of ZrO₂ and YSZ, respectively, can be extracted by methane at 900°C. Extraction of lattice oxygen results in the formation of surface oxygen vacancies. However, the routes to replenish the consumed lattice oxygen are different for ZrO₂ and YSZ. For ZrO₂, the extracted lattice oxygen ions are replenished by direct activation of molecular oxygen at the site of the surface vacancies that are formed by extraction of lattice oxygen. As compared with ZrO₂, YSZ has oxygen vacancies with a significantly higher concentration

Summary

both on the surface and in the bulk of YSZ, which are generated by doping ZrO_2 with Y_2O_3 . This feature enables fast activation of oxygen molecules at oxygen vacancies in the surface as well as fast lattice diffusion of oxygen ions in the bulk. Therefore, the surface lattice oxygen extracted by methane can be rapidly replenished, which results in a higher concentration of surface lattice oxygen during steady-state CPOM. This explains why YSZ is much more active in CPOM than ZrO_2 .

In Chapter 6 the relationship between the structure of both YSZ and ZrO_2 catalysts and their abilities to activate N_2O and O_2 is studied by catalytic testing and characterization with TPD, SEM and XRD. N_2O can be activated at both structural defects (e.g. Zr cations located at corners) and intrinsic oxygen vacancies ($\text{Zr}'_{\text{Zr}}-\text{V}_\text{O}^{\bullet\bullet}-\text{Zr}'_{\text{Zr}}$) and forms two types of oxygen species ($\alpha\text{-O}$ and $\beta\text{-O}$) on the surface, respectively. In contrast, only $\beta\text{-O}$ is formed when the catalysts are treated with molecular oxygen, which is active oxygen for methane activation during CPOM. This indicates that the structural defects are not active for oxygen activation during CPOM. Doping ZrO_2 with Y_2O_3 significantly decreases the number of the structural defects via replacement of Zr^{4+} cations by Y^{3+} cations, located at corners, steps, kinks and edges of the crystallites. Calcination at higher temperatures results in less structural defects due to both increasing crystallite size as well as transformation to more regular shaped crystallites. High temperature calcination also accelerates surface reconstruction to form low index surface planes, minimizing the surface energy. The reducibility of the surface is probably enhanced due to the resulting increase in the average coordination number of Zr in the exposed surface. This explains the increase in activity (per m^2) of CPOM over YSZ with calcination temperature.

Finally, in Chapter 7, the main results of this thesis are evaluated. Based on the knowledge obtained in this thesis, additional research is proposed in catalytic partial oxidation of liquid hydrocarbons to synthesis gas.

Samenvatting

De dreigende afname van fossiele olie voorraden en de grote hoeveelheden aardgas, die wereldwijd worden gevonden, hebben een intensief onderzoek naar het gebruik van methaan, de hoofdcomponent van aardgas, gestimuleerd. De directe omzetting van aardgas naar olefinen, via oxidatieve koppeling, of naar zuurstofhoudende verbindingen zoals methanol en formaldehyde, via selectieve oxidatie, zijn niet aantrekkelijk, als gevolg van de verkregen lage opbrengsten (of lage conversie of lage selectiviteit). Tot nu toe verlopen de meeste omzettingen van aardgas via de indirecte route, waarbij aardgas eerst moet worden omgezet in synthese gas. Er is geschat dat in de meeste indirecte processen, zoals methanol synthese, Fischer-Tropsch (F-T) synthese en ammoniak synthese, meer dan 60% van de kosten van het gehele proces een gevolg zijn van de synthese gas productie. Daarom is veel academische en industriële research gericht op de productie van synthese gas. Steam-reforming van methaan is het conventionele proces voor de synthese gas productie. Vergeleken met steamreforming is de directe partiele oxidatie van methaan (POM) naar synthese gas aantrekkelijk, vanwege zijn milde exotherme reactiewarmte en de geschikte H_2/CO verhouding voor volggprocessen, zoals methanol synthese en F-T synthese. Het wordt extra aantrekkelijk als we een katalysator gebruiken die de benodigde reactie temperatuur voor POM aanzienlijk verlaagt. Vergeleken met steamreforming levert katalytische partiele oxidatie (CPOM) een verlaging van de benodigde energie op van ongeveer 10-15% en een vermindering van de kapitaalinvestering van 25-30%. In de laatste twee decades is er een belangrijke hoeveelheid werk verricht aan CPOM, met name aan fundamenteel katalytisch en technologisch reactorkundig onderzoek. Bijna al het CPOM onderzoek is gericht op metallische katalysatoren. Deze metaal katalysatoren, zoals Rh, Pt en Ni, hebben naast de problemen met de moeilijke temperatuur controle, tengevolge van de grote exothermische reactiewarmte van de totale oxidatie ($\Delta H_{298}^\circ = -802 \text{ kJ/mol}$), ook nog problemen tengevolge van deactivering via het verdampen van vluchtige metaaloxides bij hoge temperaturen onder CPOM condities, speciaal in de aanwezigheid van zuurstof. De slechte stabiliteit van de metaal katalysatoren is een handicap voor de commercialisering van CPOM op een industriële schaal. Vergeleken met metaal katalysatoren zijn moeilijk reduceerbare oxiden veel stabiel, hoewel ze veel minder actief en selectief zijn. Het in dit proefschrift gepresenteerd werk geeft daarom, zowel fundamenteel wetenschappelijke kennis, als een nieuw technisch dual-bed concept voor de synthese gas productie via katalytische partiele oxidatie van methaan over defecte op ZrO_2 gebaseerde oxiden.

Het dual bed concept is gedemonstreerd voor synthese gas productie in Hoofdstuk 2. De directe partiele oxidatie van methaan vindt plaats over yttrium gestabiliseerd zirkoon oxide (YSZ). Naast CO en H_2 , worden CO_2 en H_2O gevonden als primaire producten. Dit betekent voor een stechiometrische voeding ($CH_4/O_2=2:1$), dat de methaan omzetting altijd minder is dan 50% tengevolge van de onvermijdelijke water vorming, die tenminste de helft van de

toevoegde O₂ consumeert. Om de methaan volledig naar synthese gas om te zetten is een dual bed nodig. In de eerste reactor wordt een stechiometrisch mengsel van methaan en zuurstof, over een niet reduceerbaar stabiel oxide als YSZ, omgezet naar een mengsel van CO, H₂, H₂O, CO₂ en onomgezet CH₄. Het tweede katalysator bed met een conventionele reformings katalysator (zoals b.v. gedragen Co), zet vervolgens de CO₂ en H₂O met de overblijvende CH₄ om naar CO en H₂. Tenslotte wordt bij een hoge GHSV synthese gas met de evenwichtssamenstelling (bijna 100% CO en H₂ opbrengst) geproduceerd. Vergeleken met initiele diepe oxidatie op een metaal katalysator reduceert de partiele oxidatie over een oxidische katalysator in het eerste bed de gegenereerde hoeveelheid warmte aanzienlijk. Dit resulteert in een milder temperatuur profiel in de reactor. Belangrijker is, dat alle zuurstof volledig wordt geconsumeerd in het oxidische katalysator bed. Zo wordt de blootstelling aan zuurstof van de metaal katalysator bij hoge temperaturen in de tweede reactor voorkomen. Daardoor wordt de deactivering van de metaal katalysator via het verdampen van vluchtige metaal oxiden vermeden. In hoofdstuk 7 wordt bediscussieerd, dat een temperatuur van 650°C in de eerste reactor hoog genoeg is voor volledige zuurstof consumptie, hoewel 1000°C gebruikt is in dit hoofdstuk. Indien deze start-op temperatuur verder verlaagd kan worden, kan het concept van deze dual bed katalysator een veel belovende kandidaat zijn voor de toepassing in de synthese gas productie door partiele oxidatie van methaan.

Op ZrO₂ gebaseerde oxiden zijn veelbelovende katalysatoren voor CPOM, vooral wanneer een metaal katalysator hun onvoldoende reformingscapaciteit compenseert in het dual bed katalysator systeem. Daarom is het aantrekkelijk CPOM over op ZrO₂ gebaseerde oxides verder te bestuderen. De invloed van oppervlaktgrootte, reactie temperatuur en vooral oppervlak samenstelling van YSZ, op CPOM zijn bestudeerd in hoofdstuk 3. Veel aandacht is gegeven aan de invloed van oppervlak verontreinigingen, zoals CaO, TiO₂ en HfO₂, op katalytische eigenschappen. De katalysatoren zijn gekarakteriseerd met X-ray fluorescence (XRF), X-ray Photoelectron Spectroscopy (XPS) and low-energy ion scattering (LEIS). Vergeleken met ZrO₂ is YSZ veel aktiever en selectiever. Deze toegenomen katalytische prestatie wordt toegeschreven aan het creëren van actieve plaatsen door het dopen van ZrO₂ met Y₂O₃, hoewel de rol van de gecreeerde zuurstof vacatures nog niet geheel duidelijk is in dit hoofdstuk.

CPOM wordt bestudeerd over YSZ met verschillende Y₂O₃ gehalten. Er wordt waargenomen dat de oppervlaksamenstelling meer dan de bulksamenstelling de katalytische eigenschappen bepaalt. Het interessante is, dat als YSZ niet verontreinigd is, de samenstelling van het buitenste oppervlak van gecalcineerd YSZ onafhankelijk is van zowel de bulk samenstelling als de calcinerings temperatuur (boven 900 °C), het oppervlak bevat altijd 12±2 mol% Y₂O₃ tengevolge van de uitscheiding van Y₂O₃. Het calcineren van niet verontreinigd YSZ bij hogere temperaturen, resulteert in meer actieve plaatsen per m², terwijl de katalysator oppervlak verliest via sintering. Echter voor YSZ, verontreinigd met sporen aardalkali oxiden, wordt in dit geval een erg lage activiteit per m² gevonden. Met LEIS worden de twee hoofd verontreinigingen TiO₂ en HfO₂, die in de bulk worden gevonden, niet gedetecteerd aan het

oppervlak. Daarentegen wordt calcium niet gevonden in de bulk maar wel aan het oppervlak. Daar komt nog bij, dat hogere calcinerings Temperaturen resulteren in een hogere bezetting van het oppervlak met de verontreinigingen voornamelijk CaO en zodoende de katalytische activiteit verlagen. De naar het oppervlak uitgescheiden verontreinigingen, blokkeren het actieve oppervlak van YSZ of vormen een nieuwe fase met andere katalytische eigenschappen. De rol van de volgreacties steam- en CO₂- reforming zijn ook onderzocht in dit hoofdstuk. Heterogene reacties concurreren met gasfase reacties bij temperaturen boven 950°C gedurende CPOM over YSZ katalysatoren. Bij deze hoge temperaturen zijn CPOM, stoom- en CO₂- reforming en ook de “reversed watergasshift” in competitie met elkaar gedurende CPOM. Deze reforming reacties van methaan resulteren in een belangrijke toename van de synthese gas selectiviteit, hoewel de activiteit van de katalysator nog steeds te laag is om thermodynamisch evenwicht te bereiken.

Het werk beschreven in Hoofdstuk 4 geeft de mogelijkheid tot het formuleren van een reactie schema gebaseerd op de resultaten van *in-situ* FTIR en zowel stationaire toestand als transiente experimenten. Opbrengsten van CO, H₂, CO₂ en H₂O hangen lineair af van de methaan conversie, hetgeen aangeeft dat allen primaire producten zijn van CPOM. Sporen formaldehyde en mierenzuur worden aan de uitgang van de reactor gedetecteerd, gedurende stationaire toestands experimenten. De vorming van een formiaat groep op het oppervlak van YSZ wordt waargenomen bij temperaturen tussen 400 and 475°C bij *in-situ* IR experimenten. Snelle omzetting van formaldehyde naar formiaat, zelfs bij kamertemperatuur, verklaart waarom geadsorbeerd formaldehyde nooit wordt waargenomen. Temperatuur-geprogrammeerde ontleding van formiaat gevormd door of adsorptie van formaldehyde of door activering van methaan bij 400°C resulteert in essentieel hetzelfde mengsel van CO, CO₂, H₂ en H₂O als wordt waargenomen bij normale CPOM. Bovendien beïnvloedt de toevoeging van formaldehyde aan de voeding van de CPOM niet de selectiviteiten naar CO, CO₂ en H₂. Deze resultaten geven aan dat formiaat en formaldehyde twee reactie intermediaren zijn voor CPOM over YSZ. CO and H₂ worden hoofdzakelijk geproduceerd via de ontleding van formaldehyde. Oppervlakte formiaat gevormd door verdere oxidatie van formaldehyde ontleedt of naar CO en H₂O *via* dehydratatie, of naar CO₂ and H₂ *via* dehydrogenering. Tenslotte wordt een compleet reactie schema voorgesteld, dat uitsluitend reactiepaden bevat, die een grote bijdrage leveren aan de product vorming. De verhoudingen tussen de concurrerende reactiepaden worden sterk beïnvloed door de temperatuur.

Formaldehyde toegevoegd aan de reactie voeding concurreert met methaan om de zuurstof. Bij temperaturen boven 600°C neemt de methaan conversie af met toenemende toegevoegde hoeveelheden formaldehyde, hetgeen aangeeft dat de oxidatie van methaan naar formaldehyde de snelheidsbepalende stap is.

Om meer inzicht te krijgen in het reactie mechanisme is het onderzoek van de plaatsen verantwoordelijk voor de activering van zowel zuurstof als methaan op ZrO₂ en YSZ beschreven in hoofdstuk 5. Speciaal de rol van de zuurstof vacatures gedurende CPOM over YSZ, welke zijn ontstaan door het dopen van ZrO₂ met Y₂O₃, is opgehelderd door zuurstof

isotoop uitwisseling op ZrO_2 of YSZ gedurende CPOM transiënte puls experimenten. De resultaten geven aan dat CPOM over zowel ZrO_2 als YSZ oxides verloopt via een Mars- van Krevelen mechanisme. Er worden uitsluitend ^{16}O -bevattende oxidatie producten gevormd gedurende $^{18}O_2$ - CH_4 pulsen over YSZ. Dit geeft aan dat methaan selectief wordt geoxideerd door rooster zuurstof ionen op het oppervlak van YSZ en ZrO_2 , ondanks de aanwezigheid van geadsorbeerde zuurstof deeltjes onder reactie condities. Er is geschat dat ongeveer 8% en 14% van de rooster zuurstof in de buitenste laag van respectievelijk ZrO_2 en YSZ kan worden geextraheerd door methaan bij $900^\circ C$. Extractie van rooster zuurstof resulteert in de vorming van oppervlak zuurstof vacatures. De routes voor de aanvulling van de gebruikte rooster zuurstof zijn echter verschillend voor ZrO_2 en YSZ. Bij ZrO_2 worden de geextraheerde zuurstof ionen aangevuld door directe activering van moleculaire zuurstof op de plaats van de oppervlakte zuurstof vacature, die gevormd zijn door de rooster zuurstof extractie. Vergeleken met ZrO_2 genereert Y_2O_3 gedoopt ZrO_2 zuurstof vacatures met een veel hogere concentratie zowel aan het oppervlak als in de bulk. Dit fenomeen maakt zowel een snelle activering van zuurstof molekulen aan de oppervlakte vacatures als een snelle rooster diffusie van zuurstof ionen in de bulk mogelijk. Hierdoor kan de oppervlakte rooster zuurstof geextraheerd door methaan snel worden aangevuld. Dit verklaart waarom YSZ veel aktiever is in CPOM dan ZrO_2 . In hoofdstuk 6 is de relatie bestudeerd tussen de structuur van zowel yttrium gestabiliseerd zirconia (YSZ) als ZrO_2 katalysatoren en hun geschiktheid om N_2O en O_2 te activeren. Deze relatie is bestudeerd met behulp van katalytisch testen en karakteriseren (TPD, SEM and XRD).

N_2O kan geactiveerd worden op zowel structurele defecten (bv Zr kationen op hoeken) als intrinsieke zuurstof vacatures ($Zr_{Zr}'-V_O^{**}-Zr_{Zr}'$) en vormt twee typen zuurstof deeltjes (α -O and β -O respectievelijk) op het oppervlak. In tegenstelling hiermee wordt er bijna alleen β -O gevormd als de katalysatoren zijn behandeld met moleculaire zuurstof, welke de actieve zuurstof is voor methaan activering tijdens CPOM. De structurele defecten (α -O) zijn dus niet aktief voor zuurstof activering gedurende CPOM. Als we ZrO_2 met Y_2O_3 dopen zal het aantal structurele defecten significant afnemen door de vervanging van Zr^{4+} kationen door Y^{3+} kationen op hoeken, stappen, kniken en randen van de kristallen. Calcineren bij hoge temperaturen resulteert in minder structurele defecten, hetgeen het gevolg is van zowel de toenemende kristal grootte, als de verandering in de richting van meer regelmatig gevormde kristallen. Hoge temperatuur calcineren versnelt ook de oppervlakte reconstructie in de richting van lage index kristalvlakken, om de oppervlakte energie te minimaliseren. De reduceerbaarheid van het oppervlak is waarschijnlijk versterkt tengevolge van de resulterende toename in het gemiddelde coordinatie getal van Zr in het blootgestelde oppervlak. Dit kan de toename van de activiteit per m^2 van CPOM over YSZ met de calcinerings temperatuur verklaren.

Tenslotte worden in hoofdstuk 7 de belangrijkste resultaten van dit proefschrift geëvalueerd. Er wordt voorgesteld op basis van de kennis in dit proefschrift, aanvullend onderzoek te doen naar de katalytische partiele oxidatie van vloeibare koolwaterstoffen naar synthese gas.

概 述

近年来，世界石油储量的急剧下降，与此同时大量的天然气被探明及开发。这大大地促进了在天然气利用方面的研究。天然气可以通过直接转化成其他化工原料而加以利用，如通过甲烷氧化耦合制备烯烃，选择性氧化制甲醇或甲醛等。然而，由于直接转化过程的单程转化率或选择性太低，天然气的直接转化无法形成经济规模的生产。到目前为止，天然气转化利用主要还是通过间接的途径，即天然气（甲烷为主要成分）首先转化为合成气（CO 和 H₂ 的混合物），然后进一步合成其他化合物如甲醇，甲醛，高碳烃类等。据估算，在绝大多数天然气间接转化过程中，如 F-T 合成，合成甲醇及合成氨，天然气转化制合成气的成本超过了总成本的 60%。因此，有关天然气转化制合成气的新技术研究引起了工业界及学术界的广泛兴趣。甲烷水蒸气重整是天然气转化制合成气的传统工艺。与甲烷水蒸气重整工艺相比，甲烷直接部分氧化为温和的放热反应，同时，生产的合成气的 H₂/CO 比为 2:1，适合后续加工过程的要求。另外，催化剂的使用使得甲烷部分氧化过程所需的反应温度大大降低。因此，甲烷部分氧化工艺引起了广泛的兴趣。与甲烷水蒸气重整工艺相比，采用甲烷部分氧化工艺，能量消耗减少了 10~15%，同时，投资也下降了 25~30%。在过去的 20 多年中，对甲烷部分氧化进行了大量的基础研究及应用技术开发。几乎所有的研究都是基于金属催化剂（如，Rh, Pt, Ni 等）的甲烷部分氧化工艺。然而，由于金属催化甲烷部分氧化遵循“两步反应机理”，即在催化剂床前段，甲烷完全燃烧生成 CO₂ 和 H₂O，在随后的催化剂床中，剩余的甲烷通过 CO₂ 和水蒸气重整水进一步转化为 CO 和 H₂。由于催化剂床前段的强放热反应（ $\Delta H_{298}^{\circ} = -802 \text{ kJ/mol}$ ）造成催化剂床局部过热，产生飞温。同时，金属催化剂在高温及氧化性环境下形成挥发性的金属氧化物而流失，最终导致催化剂失活。正是金属催化剂较差的热稳定性严重阻滞了甲烷部分氧化技术的工业化。与金属催化剂相比，非还原性的（难以还原的）金属氧化物尽管活性及选择性较差，但具有很高的热稳定性。因此，在本论文中，作者对 ZrO₂ 基混合金属氧化物的催化性能进行了较为详细的研究。尤其是，基于 ZrO₂ 基混合金属氧化物的缺陷化学，对其催化反应机理进行了深入的探索。提出了采用双催化剂床部分氧化甲烷制合成气的新工艺。

在第二章中，提出了双催化剂床制合成气的新工艺。通过理论计算及实验结果，将该新工艺与单一金属催化剂工艺进行了对比。Y₂O₃/ZrO₂（YSZ）催化剂可以直接选择性地催化甲烷部分氧化制合成气。四种主要产物 CO，H₂，CO₂ 和 H₂O 都为反应的一次产物。由于大约一半左右的计量氧气转化成了水（该反应不可避免，详见后述），因此，对于化学计量的反应物（CH₄/O₂=2:1），甲烷的转化率总小于 50%。然

而，这种混合金属氧化物在甲烷水蒸气重整及 CO_2 重整的催化性能很差，只有通过金属催化剂补偿其催化重整性能的不足，才能达到甲烷的完全转化及合成气的高选择性。于是，我们提出了双催化剂床的新工艺，在第一反应器中，化学计量比的 CH_4 和 O_2 在非还原性金属氧化物催化剂上，如 YSZ，发生部分氧化反应。在这一催化剂床层中，所有的氧气及大约 50% 的甲烷被转化为 CO , H_2 , CO_2 , 和 H_2O 。在第二个反应器中，装填具有催化重整性能的金属催化剂，如负载的钴或镍等催化剂。在这一催化剂床中，未转化的甲烷与在第一催化剂床中生成的 CO_2 及 H_2O 反应生成 CO 和 H_2 。通过两种催化剂的协同作用，在较高的气体空速下甲烷被氧化成具有平衡组成的合成气。由于在第一催化剂床层上发生的是选择性甲烷部分氧化反应，与深度氧化反应相比，反应生成热大大地减少。这就使得催化剂床层的温度分布较为均匀。更为重要的是，在氧化物催化剂床中，所有的氧气都被完全消耗了，这就排除了第二反应器中金属催化剂在高温下接触氧气的可能性。从而避免了金属氧化物因为形成挥发性的金属氧化物而流失的可能性。这样很好地解决了金属催化剂失活的难题。在这一章中，第一催化剂床的操作温度为 1000°C 。但是，正如在第七章中所讨论的，通过使用高比表面的氧化物催化剂，可以大大地降低这一反应温度。如采用 YSZ14A 催化剂（YSZ, 含 14 wt% Y_2O_3 , 比表面积为 $23 \text{ m}^2/\text{g}$ ）时，所有的氧气在 650°C 下就能在这一催化剂床中被完全消耗。如果这一反应的起始温度能被进一步降低，这种双催化剂床新工艺将具有很好的工业化应用前景。

第二章中的研究表明，基于双催化剂床层工艺， ZrO_2 基混合金属氧化物为具有应用前景的甲烷部分氧化催化剂。为此，对其催化性能进一步研究具有一定的意义。在第三章中，在研究催化剂的表面积，反应温度对其催化性能影响的同时，着重研究了催化剂表面杂质（如 CaO , TiO_2 , 和 HfO_2 ）的影响。采用 XRF, XPS 及 LEIS 对催化剂的体相及表面组成进行了表征。与 ZrO_2 相比，YSZ 具有更高的催化活性及选择性。尽管在这里氧空位对于该氧化反应确切的作用还不清楚，YSZ 优良的催化性能似乎与 YSZ 晶格中存在的大量氧空位有关。YSZ 中 Y_2O_3 的含量（其影响着晶格中氧空位的浓度）对其催化性能的影响被进一步研究。结果表明，YSZ 催化剂的表面组成决定着其催化性能，而其体相组成的影响甚微。有趣的是，当 YSZ 不含有低价态的金属氧化物杂质（如 CaO ）时，高温（ 900°C ）焙烧后的催化剂表面组成与体相组成及焙烧温度无关。由于 Y_2O_3 的偏析及在表面上的富集，其表面总是含有大约 $12\pm 2 \text{ mol}\%$ 的 Y_2O_3 。然而，含有微量碱金属或碱土金属氧化物杂质的 YSZ 显示出很低的催化活性。在体相中检测到的两种主要杂质， TiO_2 和 HfO_2 ，并不存在于 YSZ 表面上。相反，尽管在体相中未检测到的 CaO （微量），却被发现存在于催化剂的表面层中。高温焙烧导致了更高的 CaO 表面覆盖率，从而进一步降低了催化活性。这种富集于表面

的氧化物杂质简单地覆盖了催化剂的活性表面，或者与 YSZ 发生固相反应形成新的固相，而这一新固相具有与 YSZ 完全不同的催化性能。

在这一章中，我们还研究了在高温下可能发生的甲烷水蒸气重整及 CO_2 重整。当反应温度高于 950°C 时，多相催化反应与均相的气相反应同时发挥作用。在如此高温下，甲烷部分氧化，甲烷水蒸气重整，甲烷 CO_2 重整及水气转换反应的逆反应在反应过程中发生竞争。这些反应显著地提高了合成气的选择性。然而，由于 YSZ 对这些后续反应的催化性能很低，即使在很高的温度下，反应也很难达到热力学平衡。

在第四章中，通过原位红外，稳态及动态的实验研究了 YSZ 上的甲烷部分氧化反应。基于实验结果，我们提出了包含多个可能反应步骤的反应网络。 CO 、 H_2 、 CO_2 和 H_2O 的产率与甲烷转化率的线性关系表明这四种产物均为甲烷部分氧化反应的一次反应产物。在稳态实验的反应尾气中，检测到微量的甲醛和甲酸。通过原位红外光谱观察到在 400 到 475°C 之间在 YSZ 催化剂表面上形成了甲酸盐物种。甲醛在 YSZ 上的吸附实验结果表明，即使在室温条件下，甲醛在 YSZ 催化剂表面上能被迅速地转化为表面甲酸盐，而无法观察到吸附态的甲醛。无论表面甲酸盐是通过甲醛吸附转化而成，还是通过甲烷与氧气在 400°C 条件下表面反应而生成，甲酸盐表面物种的程序升温分解（脱附）得到与稳态甲烷部分氧化反应相一致的分解产物 CO 、 CO_2 、 H_2 和 H_2O 。而且，在反应原料气中添加少量甲醛并不影响 CO 、 CO_2 和 H_2 的选择性。这些结果表明甲醛及表面甲酸盐都为甲烷部分氧化反应的中间物种。甲烷首先被氧化成甲醛，同时生成等量的水。 CO 和 H_2 主要通过甲醛的分解而生成。部分甲醛被进一步氧化成表面甲酸盐。甲酸盐分别通过脱氢分解成 CO_2 和 H_2 ，通过脱水分解成 CO 和 H_2O 。整个反应网络包括了甲烷活化成甲醛，甲醛分解，甲醛进一步氧化成甲酸盐，及甲酸盐的分解等关键反应步骤。这些相互竞争的反应步骤的相对反应速度在很大程度上取决于反应温度。

另外，添加于反应原料气中的甲醛与反应物甲烷相互竞争氧气。当反应温度高于 600°C 时，甲烷的转化率随着甲醛添加量的增加而下降，这表明甲烷氧化成甲醛为速度控制步骤。

在第五章中，我们着重研究了 ZrO_2 和 YSZ 上氧气和甲烷的活化中心。通过在反应条件下气态同位素氧与 ZrO_2 和 YSZ 的氧交换及动态脉冲实验，研究了 YSZ 晶格中氧空位在甲烷部分氧化反应中的作用。结果表明 ZrO_2 或 YSZ 催化的甲烷部分氧化反应遵循 Mars-van Krevelen 反应机理。在 YSZ 上， $^{18}\text{O}_2\text{-CH}_4$ 脉冲反应仅仅生成了含 ^{16}O 的氧化产物。这表明甲烷是被 ZrO_2 或 YSZ 上的晶格氧而非吸附态的氧所氧化，尽管表面吸附氧被证明在实验条件下是存在的。基于甲烷脉冲实验结果表明，在 900°C 下， ZrO_2 和 YSZ 外表面层中大约 8% 和 14% 的晶格氧可用于氧化甲烷。这种表面晶格氧被消耗后，在催化剂表面上形成了表面氧空位。然而，对于 ZrO_2 和 YSZ，补充

这种被消耗的晶格氧的途径却大相径庭。对于 ZrO_2 ，气态氧分子在形成的表面晶格氧空位上被直接解离活化，从而填补氧空位。与 ZrO_2 相比，通过在 ZrO_2 掺入少量的 Y_2O_3 ，大量的氧空位存在于 YSZ 的表面和体相。这一特性使得气态分子氧在其表面能迅速解离活化，而且，氧离子在体相中能快速扩散。因此，被消耗的表面晶格氧可以得到更为迅速的补充。这就很好地解释了为什么 YSZ 比 ZrO_2 具有更高的催化活性。

在第六章中，通过催化性能测试及表征 (TPD, SEM, XRD)，研究了 O_2 和 N_2O 在 ZrO_2 和 YSZ 上的活化。着重研究了催化剂结构的影响。催化剂的结构缺陷，（如位于晶体角，棱等处的 Zr 离子）和本征的表面氧空位 ($\text{Zr}'_{\text{Zr}}-\text{V}_{\text{O}}^{\bullet\bullet}-\text{Zr}'_{\text{Zr}}$) 是 N_2O 的活化中心。 N_2O 在这些活性中心上解离，分别形成了两种不同的表面氧物种 ($\alpha\text{-O}$ 和 $\beta\text{-O}$)。与之相反，催化剂的结构缺陷无法活化分子氧。分子氧在催化剂表面活化仅形成 $\beta\text{-O}$ 。而且，这种 $\beta\text{-O}$ 正是能够氧化甲烷的活性晶格氧。在 ZrO_2 掺入 Y_2O_3 显著地降低了催化剂结构缺陷的数量，这主要是由于 Y^{3+} 部分地取代了位于催化剂晶粒边，角等缺陷处的 Zr^{4+} 离子。另外，由于催化剂粒子的长大及表面的规则化，高温焙烧也使得催化剂结构缺陷数量下降。然而，高温焙烧同时也促进了催化剂晶粒表面的重构（重建）形成具有更低表面能的低指数表面。在这种催化剂表面上，Zr 的氧配位数的平均值更低，从而提高了其表面的可还原性，即增加了单位面积上可消耗晶格氧数目。这就使得 YSZ 的催化活性随着焙烧温度的增加而提高。

最后，在第七章中，对主要的研究成果进行了分析与讨论。基于本研究成果，提出了利用液态烃（汽油，柴油）部分氧化制合成气的研究方案。

Chapter 1

General Introduction

Abstract

In this chapter, a general introduction is given on chemical utilization of methane, especially indirect routes via synthesis gas. Three major processes for synthesis gas production, steam reforming, CO₂ reforming and catalytic partial oxidation of methane, are summarized. Especially, catalytic partial oxidation over metal catalysts is briefly reviewed, including catalysts, reaction mechanism, and challenges. Emphasis is put on advantages of catalytic partial oxidation of methane over hardy reducible oxides, such as ZrO₂ and yttrium-stabilized zirconia (YSZ). The structure of YSZ is described. At the end of the chapter the scope of this thesis is presented.

1.1. Introduction

Natural gas, in which methane is the major component, has been the most abundant, clean, and easily extractable energy source since the oil crisis in the 1970s. As shown in Fig. 1, the proven natural resources of methane are enormous. Present estimation indicates that on an oil-equivalent basis, the reserves of natural gas exceed that of oil by about 50%. Moreover, the rate of discovery of new reserves of natural gas outstrips the rate of discovery of oil reserves⁴. Recently natural gas is still mainly used as an energy carrier to home and industry. In the chemical industry the use of natural gas remains limited.

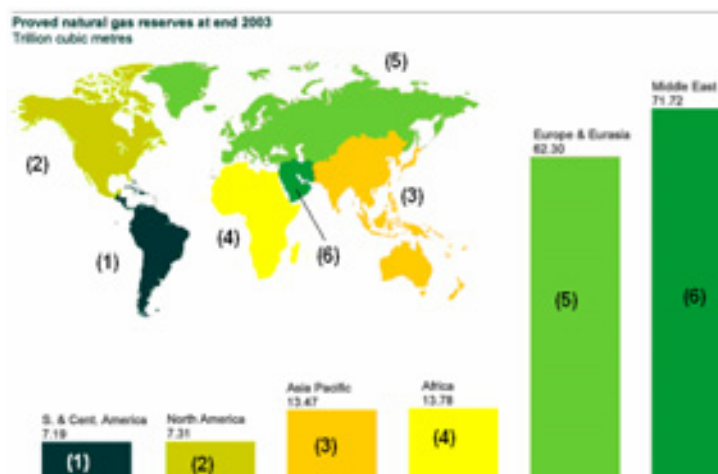


Fig. 1. Proven natural gas reserves up to the end of 2003¹

However, most natural gas is located far away from the consumption sites, and its transportation is expensive and dangerous. It is therefore desirable to convert natural gas into liquid fuels or chemical feedstock for more efficient utilization.

1.2. Methane conversion technologies

Fig. 2 gives a summary of the chemical conversion of synthesis gas to various chemicals. In general, two different types of route for methane conversion to useful products can be distinguished: direct and indirect conversion.

1.2.1. Direct utilization of methane

The direct routes are one-step processes in which the natural gas is directly converted to desired products. Compared with the indirect methods, direct methods are potentially simpler in technology and more economical. However, apart from complete combustion for heating purposes (giving CO₂, and water), all other direct conversion routes have not yet been realized on industrial scale⁵. This is mostly because conversions and/or selectivities are not sufficiently high to be of interest for commercial application. Two major direct conversion routes are oxidative coupling of CH₄ to C₂ hydrocarbons and partial oxidation of CH₄ to formaldehyde and methanol.

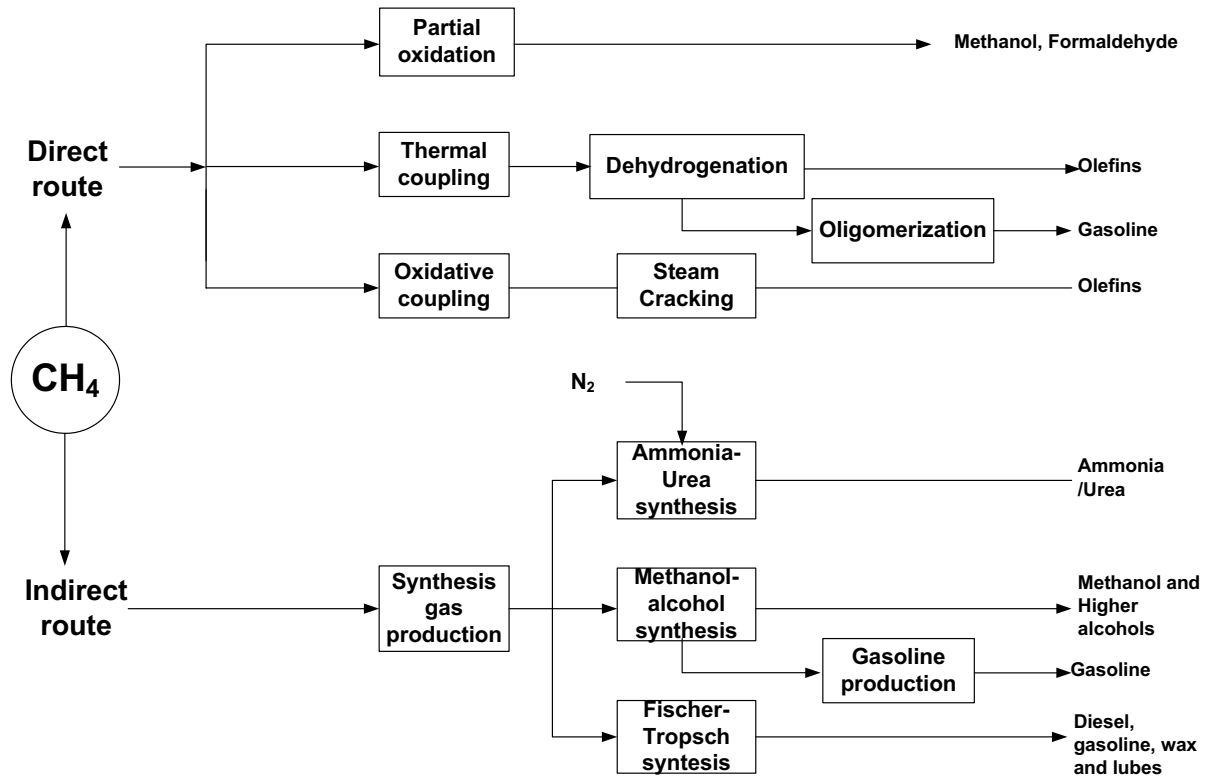


Fig. 2. Conceptual routes for chemical conversion of methane

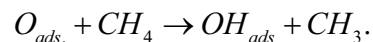
(1) Oxidative coupling of methane to C₂ hydrocarbons (OCM)

In 1982, a paper by Keller and Bhasin⁶ demonstrated that two molecules of methane could be coupled oxidatively (in a cyclic process) over PbO/Al₂O₃ to produce ethane and ethylene.

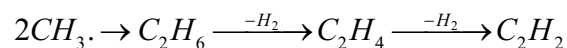


The formation of methyl radicals over OCM catalysts (Li/MgO) was demonstrated experimentally^{7,8}. After investigating the pyrolysis of methane over ThO₂/SiO₂, the authors⁹ proposed a heterogeneous-homogeneous mechanism, including the heterogeneous formation of methyl radicals with their recombination to ethane in the gas phase.

Heterogeneous generation of methyl radicals is postulated in all the models:



In the gas phase the methyl radicals recombine with the formation of ethane, a primary C₂ hydrocarbon, which can be further converted to ethylene (C₂H₄) and ethyne (C₂H₂) via dehydrogenation of C₂H₆.



Work regarding OCM has been reviewed elsewhere¹⁰.

(2) Selective oxidation of methane to formaldehyde and methanol (SOM)



Partial oxidation of methane to methanol may have high selectivity (about 80%) under optimal conditions, but the yield of methanol per pass is still less than 7% due to very low CH₄ conversion for a single pass. This results in requirement for a very big recycle ratio and difficulty in product separation due to low partial pressure of methanol. For comparison, commercial methanol production *via* synthesis gas route has typically a conversion per pass of 50%, and only a recycle ratio of four is required. Selectivity to methanol is above 99%, meaning a yield per pass close to 50%.

1.2.2. Indirect utilization of methane

The indirect route is a two step process whereby natural gas is first converted to synthesis gas (a mixture of H₂, and CO) *via* steam reforming, partial oxidation, CO₂ reforming or combination of two of these reactions. In the second step, synthesis gas is converted to the desired products in downstream processes, e.g. methanol, ammonia synthesis and also Fischer-Tropsch synthesis processes¹¹. Since it is rather difficult to realize OCM and SOM on an economical scale, the indirect route is considered as an alternative strategy for the utilization of natural gas. Two major important processes, which utilize natural gas via synthesis gas, are methanol synthesis and Fischer-Tropsch.

(1) Methanol synthesis

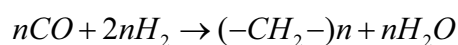
Synthesis gas is used primarily for the production of methanol, a starting point of the route to dimethyl ether (DME), gasoline and ethylene. Thermodynamically, this process is favored by a decrease in temperature, which would shift the equilibrium towards the formation of methanol. Initially zinc-chromium oxide catalysts were used for the synthesis of methanol. Their use requires relatively high temperatures and, consequently, high pressures. More active copper-zinc-aluminum catalysts were then discovered, and this made it possible to conduct the process at lower temperatures and, accordingly, lower pressures. However paradoxically, the process at copper-containing catalysts takes place through the intermediate formation of CO₂ and then reduced to methanol¹². The initial reaction mixture in the “low pressure” process must, therefore, contain a certain amount of CO₂.

Methanol is used in various chemical syntheses and in the production of fuels. A significant part of it is used for the production of a fuel additive, methyl *tert*-butyl ether (MTBE). A promising use of methanol is in the production of dimethyl ether (DME) as an ecologically friendly diesel fuel. The Amoco Corporation, who developed the process for the production of DME in conjunction with Topsoe, has even named DME as the fuel of the twenty first

century¹³. Here the production of DME can be carried out directly from synthesis gas over a composite catalyst, consisting of a methanol catalyst and a catalyst for the dehydration of methanol according to the overall reaction $2\text{CO} + 4\text{H}_2 = (\text{CH}_3)_2\text{O} + \text{H}_2\text{O}$. An important advantage of such a process is the fact that the equilibrium yield of DME is much higher than the equilibrium yield of methanol under the same conditions. Of potential interest is the conversion of methanol into olefins over acidic catalysts. There has also been a trial on the commercial conversion of methanol into gasoline, undertaken by Mobil in New Zealand⁴.

(2) Fischer-Tropsch process

Another important development in the use of synthesis gas is the Fischer-Tropsch (F-T) process, which has a long history^{14;15}. Over Fe, Co, Ru or similar metals, synthesis gas can be converted to paraffinic liquid fuels through F-T reactions:



Current commercial F-T reactors operate in two different temperature ranges. The high temperature F-T operates with iron catalysts at about 340°C and is geared mainly at the production of olefins and gasoline. The low temperature F-T, using either iron or cobalt based catalysts at about 230°C, is geared at the production of diesel and linear waxes.

A leading position in F-T field is taken by Sasol (South Africa), where this process has been realized on a large industrial scale right up to the present time. Recently, the F-T process has again gained interest. The BP-AMOCO Corporation has constructed a large-scale pilot plant in Alaska. The Shell plant for the production of fuel by the F-T reaction continues to operate. The insufficient activity and the selectivity of the F-T catalysts to the required hydrocarbon have been and remain as a bottleneck in the technology of the process. However, the expected future trend towards non-petroleum sources of fuel and, in particular, plenty of methane reserves provide a strong stimulus for the further development of the process on the basis of new fundamental knowledge.

1.3. Synthesis gas production

It has been estimated that in most of applications of natural gas such as methanol, F-T synthesis and ammonia over 60% of the cost of the overall process is associated with synthesis gas generation^{16;17}. Reduction of costs in synthesis gas production would have a large and direct influence on the overall economics of these downstream processes. Therefore, research in synthesis gas production has attracted a lot of attention from both industry and academia. Production of synthesis gas from the natural gas can be realized *via* three reactions, i.e., steaming reforming, CO₂ reforming and partial oxidation. To date, the large-scale process for natural gas conversion is mainly the endothermic reaction known as steam reforming (SR) to synthesis gas, although autothermal reforming (ATR) and partial oxidation are also used.

(1) Steam reforming

Steam reforming has been used for many decades for synthesis gas production since first developed in 1926¹⁸ and over the years much progress has been made in reforming technology.



Steam reforming of methane is highly endothermic and is carried out in fired tubes at temperature above 900°C. Current industrial catalysts are usually based on nickel. The typical scheme is illustrated in Fig. 3.

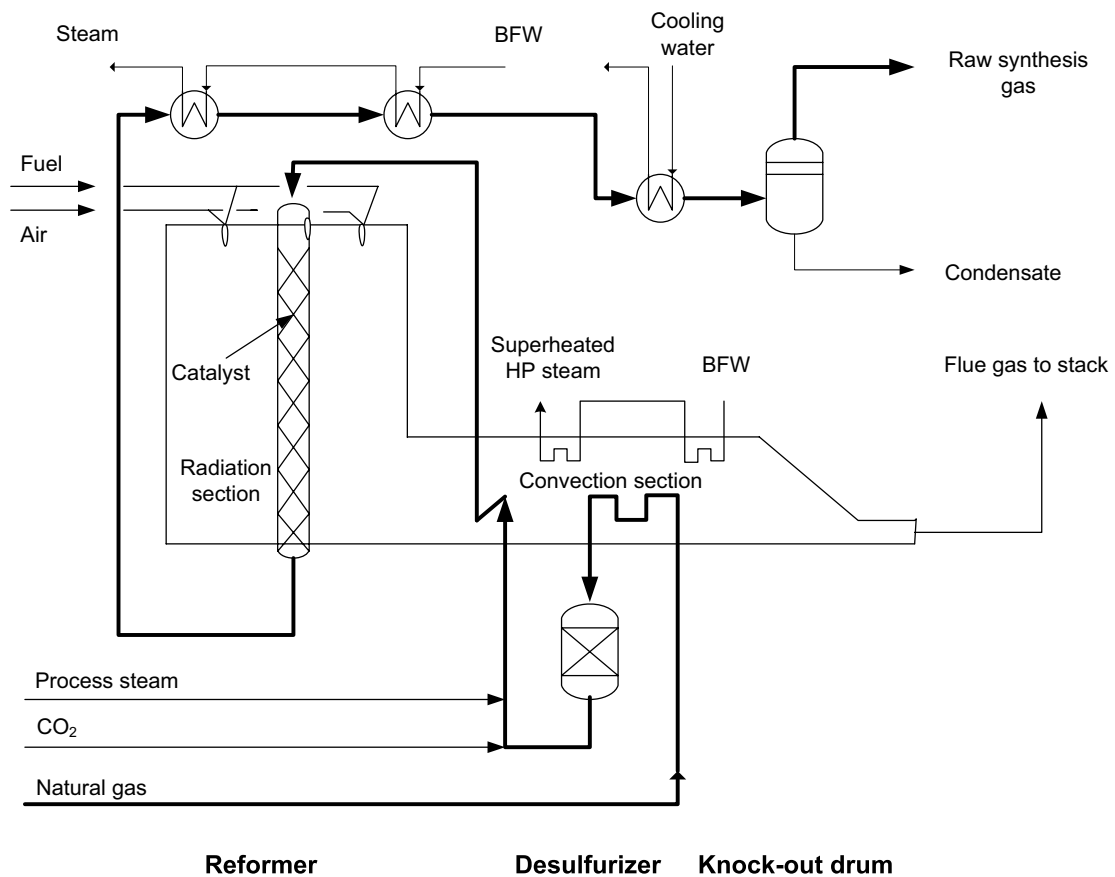


Fig. 3. Typical steam reform process for synthesis gas production.

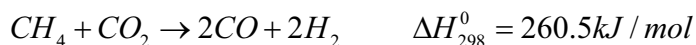
Steam reforming of methane suffers from high endothermicity (intensively energy consuming), catalyst-coking propensity and requirement for operation at high temperatures (>900°C). Supported Ni catalyst is very active for steam reforming of methane to synthesis gas and has been used for many decades. However, Ni catalyst is also very active for decomposition of CH₄ to carbon and hydrogen. At high reaction temperature large amounts of fibrous carbon can be formed, which influences activity and stability of catalyst, and can even damage the reactor¹⁹. To prevent carbon deposition, a high H₂O/CH₄ ratio (2.0~6.0) is required. Excess of water accelerates water-gas shift reaction ($\text{CO} + \text{H}_2\text{O} \rightarrow \text{CO}_2 + \text{H}_2$),

resulting in a high H₂/CO ratio (>3.0), which is not suitable for downstream processes, e.g. methanol synthesis.

Based on the conventional steam reforming technology, autothermal reforming (ATR) was first developed in the late 1970s with the aim of carrying out reforming in a single reactor¹⁸. In the first part of the autothermal reforming reactor, homogeneous oxidation of methane is carried out with O₂ in a flame. The final steam reforming and equilibration take place in the catalyst bed in the second part of the reactor. For normal operation, the autothermal reforming operates at high temperatures around 2000°C in the combustion zone and 1000-1200°C in the catalytic zone. The product gas composition can be adjusted by varying the H₂O/CH₄ in the feed.

(2) CO₂ reforming

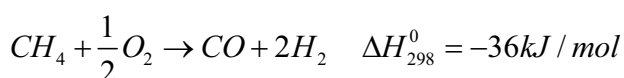
Carbon dioxide reforming is also highly endothermic requiring large heat input, even higher than for steam reforming.



Despite this drawback, a resurgence of interest in CO₂/CH₄ reforming has occurred mainly due to the realization of a possible positive impact of large-scale application of the process on the global CO₂ emissions. Another advantage of this process is its product, synthesis gas with 1:1 ratio of hydrogen to carbon monoxide. It is low as compared with those obtained by other routes for synthesis gas production, as the steam reforming (H₂/CO=3) or the partial oxidation of methane (H₂/CO=2). The lower H₂/CO ratio is desirable for direct using synthesis gas as feedstock for different Fischer-Tropsch synthesis processes and also for carbonylation (e.g. R-H+CO → R-CHO) and hydroformylation (e.g. R-HC=CH₂+CO+H₂ → R-CH₂-CH₂-CHO) processes. This reaction also has important environmental application as two greenhouse gases, CO₂ and CH₄, are converted into a valuable feedstock.

(3) Partial oxidation

The catalytic partial oxidation of methane to synthesis gas is not a new idea. Because of the considerable expense associated with maintaining the reaction conditions needed for conventional steam reforming, the direct partial oxidation of methane to synthesis gas has obtained a renewed interest, since 1990.



The direct partial oxidation reaction is slightly exothermic, a reactor based on this reaction would be much more energy efficient than the energy intensive steam- and CO₂-reforming processes. Compared with reforming reactions, oxidation reactions are much faster. Moreover, this process directly produces the desired 2:1 ratio required for the downstream processes, e.g. methanol or Fischer-Tropsch synthesis in a single stage. In contrast, the synthesis gas produced *via* either CO₂- or steam- reforming needs to be adjusted to a suitable H₂/CO ratio

before used in the downstream processes. This suggests that a single stage process for the production of synthesis gas would be a viable alternative to steam or CO₂ reforming and also results in smaller reactor and higher throughput, which even makes it possible to apply this process to produce H₂ for fuel cells.

Non-catalytic homogeneous partial oxidation for synthesis gas production is well established. For example, in Sarawak, Malaysia, Shell has been successfully operating a highly selective process for production of synthesis gas at high temperatures, typically higher than 1400K, and pressures of around 50~70 atm as a part of the middle distillate synthesis process (SMDS)²⁰. The operation temperature required for the reaction could be significantly reduced if a catalyst would be used, which would make the partial oxidation process even more economically attractive. An estimated 10-15% reduction in the energy requirement and 25-30% lower capital investment are expected for catalytic partial oxidation compared to the typical steam reforming processes¹⁶. It was concluded by Schmidt *et. al.*¹⁶ that with renewed interest in inexpensive routes from natural gas to liquid fuels, direct catalytic oxidation is almost certainly the process of choice for future natural gas utilization. Therefore, current research on catalytic partial oxidation of natural gas to synthesis gas, the subject of this thesis, will be briefly reviewed in next section.

1.4. Catalytic partial oxidation of methane to synthesis

1.4.1. Thermodynamic analysis of methane partial oxidation

Fig. 4 shows a scheme of the thermodynamics of the partial oxidation of methane. This process is likely to become more important for methane conversion in the future due to the thermodynamic advantages over steam reforming.

As shown in Fig. 5, reaction conditions, e.g. reaction temperature, total pressure and ratio of CH₄/O₂, influence significantly the thermodynamic product distribution

of CPOM. Thermodynamic calculations were performed using HSC package (HSC Chemistry ver. 4.1, Outokumpu Research Oy, Pori, Finland) for feedstocks with different CH₄/O₂ ratios and assuming no carbon formation. The calculations suggest that a high reaction temperature is advantageous for high methane conversion and high selectivity to CO and H₂. Lowering ratio of CH₄/O₂ (<2) decreases selectivity to CO and H₂ significantly, although methane conversion at the same temperature decreases. However, as shown in Fig. 5(e), increasing the reaction pressure is unfavorable for both CH₄ conversion and selectivity to CO

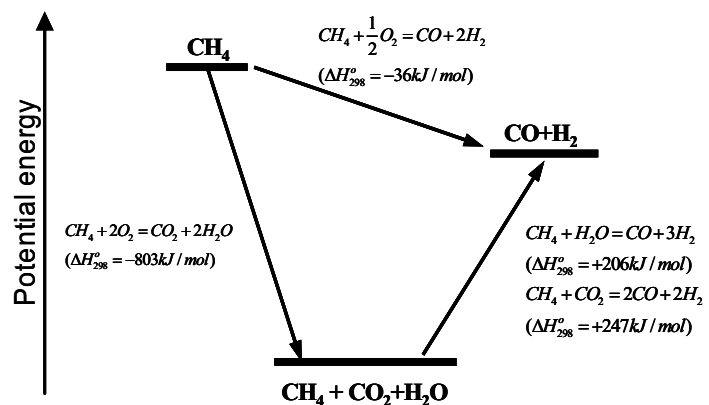


Fig. 4. Thermodynamic representation of the partial oxidation of methane to synthesis gas

and H_2 . Apparently, under 1 bar and at 1000°C , CH_4 conversion and selectivity to CO and H_2 can theoretically reach 98.9% and 99.6% respectively.

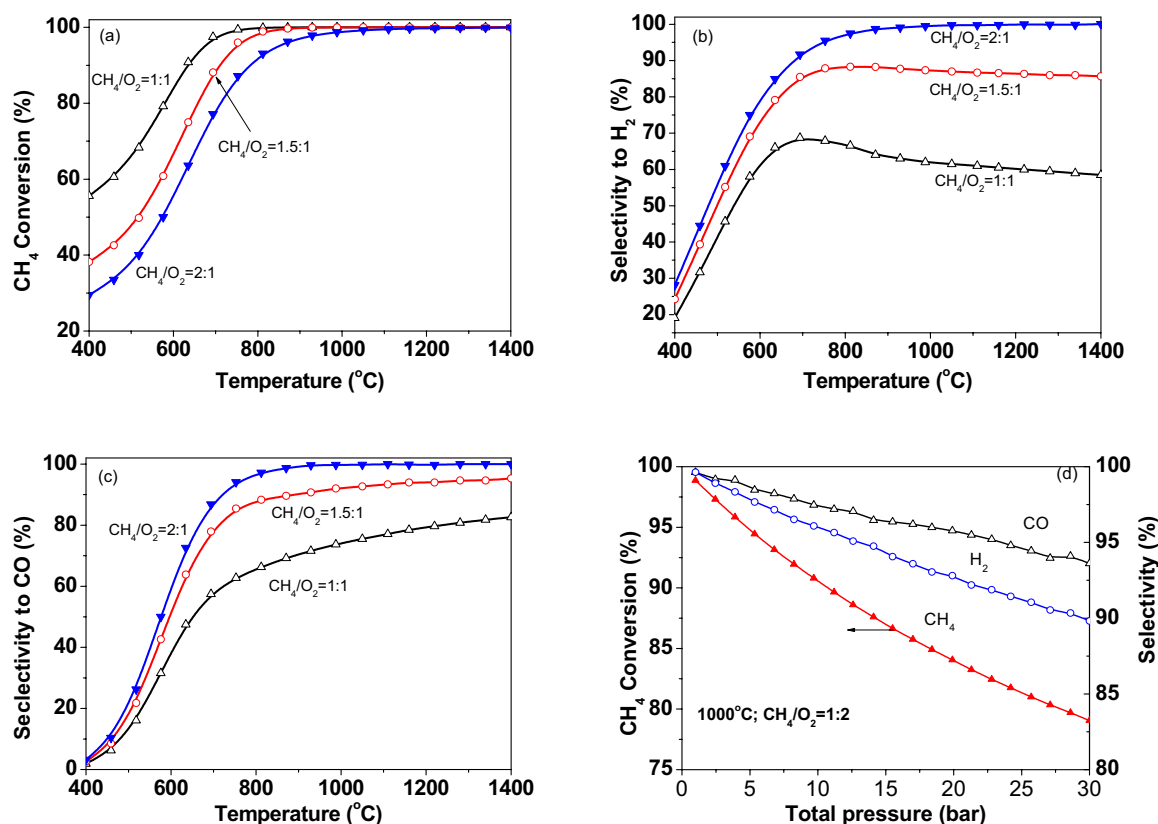


Fig. 5. Thermodynamic equilibrium calculations of (a) Methane conversion (b) Selectivity to H_2 , and (c) Selectivity to CO at different conditions, and (d) effect of reaction pressure.

1.4.2. CPOM over metallic catalysts

1.4.2.1. Metallic catalysts

Study on the partial oxidation of CH_4 to synthesis gas began as early as 1946²¹. High yields of synthesis gas were only obtained at temperatures in excess of 850°C . The latter studies showed that a non-equilibrium product distribution was observed at temperatures below 850°C . Because of these factors, as well as the success of the steam reforming process, not much was done on partial oxidation reaction over the next 25 years. Before the middle of 1980s, only Ni catalysts, which are typically used for steam reforming, were the subject of most early investigations in the catalytic partial oxidation of methane. At the beginning of 1990s, a significant contribution to CPOM has been made by Ashcroft and coworkers²²⁻²⁶. In a series of five publications, they reported evaluation of a large number of catalysts for synthesis gas production.

Recently, CPOM over metallic catalysts has been briefly reviewed by Green *et al.*²⁷ The catalysts studied for CPOM can be classified into (1) supported nickel, cobalt or iron catalysts, (2) supported noble metal catalysts (Pt, Rh and Pd), and (3) transition metal carbide catalysts.

(1) Supported Ni, Co or Fe catalysts

Co and Fe catalysts have a much lower performance for CPOM as compared with Ni, because CoO and Fe₂O₃ have higher activity for complete oxidation of methane. Nickel-based catalysts emerged as the most suitable because of their fast turnover rates and low cost. Lunsford and co-workers studied supported Ni catalysts for CPOM in the temperature range 450~900°C. At about 700°C complete methane conversion with about 95% of selectivity to CO and H₂ could be achieved. They also found that three regions exist in the catalyst bed with different states of the catalyst, NiAl₂O₄, NiO/Al₂O₃ and supported nickel metal particles²⁸. Obviously, NiAl₂O₄ and NiO/Al₂O₃ are only active for deep oxidation of methane. High selectivity to synthesis gas over this catalyst bed suggests that CPOM over supported Ni catalysts proceeds *via* combustion followed by steam-and CO₂ reforming.

However, the major technical problem for the nickel-based catalysts is carbon deposition on the catalyst, which causes break up of the nickel metal particles or support over the catalyst, and deactivates the catalyst by covering the nickel surface. To solve this problem, much work has been done. (i) Effects of different oxide supports, e.g. CaO, TiO₂, Y₂O₃, ZrO₂, ThO₂ and UO₂²⁹⁻³¹, perovskite (Ca_{0.8}Sr_{0.2}TiO₃)³² on the catalytic performance have been studied; (ii) It was reported that formation of a solid solution in the Ni-MgO system and the weak basicity of MgO suppresses somewhat carbon deposition^{33;34}. Rare earth metal oxides or alkaline metal oxides as supports can restrict carbon formation of the supported Ni catalysts³⁵⁻³⁷. This promotion is attributed to the capability for oxygen storage of these rare earth metal and alkaline metal oxides, which help by oxidizing the surface carbon deposited³⁶. Despite that lot of efforts towards modification of the Ni catalysts, carbon deposition still can not be completely avoided. To suppress carbon formation is still a subject of many studies today.

(2) Supported noble metal catalysts

Noble metal catalysts have attracted great attention and have been widely studied in the last three decades. Schmidt *et al.*³⁸⁻⁴⁰ and Poirier *et al.*⁴¹ studied CPOM over Rh catalysts and Pt-Pd catalysts at extremely high flow rates, respectively. It was reported that these noble metal catalysts, even with very low metal loadings, were much more active than Ni catalysts. It was shown by Green *et al.*^{42;43} that high yields of synthesis gas can be obtained over nearly all noble metals. Preparation method and support properties also influence the catalytic performance of noble metal catalysts. The effect of the support on the performance of Rh-based catalyst in the partial oxidation of methane to synthesis gas was investigated by Ruckenstein *et al.*⁴⁴. It was concluded that in general noble metal supported on reducible oxide (e.g., CeO₂, Nb₂O₅, Ta₂O₅, TiO₂ and ZrO₂) is much less active and selective to CO and

H₂ than noble metal supported on irreducible oxides (e.g., γ -Al₂O₃, La₂O₃, MgO, SiO₂ and Y₂O₃). Among the irreducible oxide supports, γ -Al₂O₃, La₂O₃ and MgO supported Rh₂O₃ catalysts provided stable catalytic performance. This high stability was attributed to formation of MgRh₂O₄ due to the strong interaction between Rh and MgO. Guerrero-Ruiz *et al.*⁴⁵ studied CPOM and CO₂ reforming of methane over Ru/Al₂O₃ and Ru/SiO₂ using isotopic tracing technique. It was reported that the support was also involved in reactions, somewhat modifying the catalytic behavior. To realize CPOM over noble catalysts at extremely short contact time (in the order of milliseconds), monolith-supported noble metal catalysts have been also studied⁴⁶. At a contact time of 10⁻³ second, more than 90% of methane and complete oxygen (CH₄/O₂=2:1) can be converted over Rh-coated ceramic monoliths to synthesis gas with a selectivity of 90%.

Much less carbon deposition was observed for the noble catalysts as compared with non noble metal catalysts. The relative order of carbon formation decreases in the order: Ni>Pd>>Rh, Ru, Ir, Pt⁴⁷.

1.4.2.2. Reaction mechanisms for CPOM over metal catalysts

Two different mechanisms have been proposed for CPOM over metallic catalysts. One is so-called “two-step reaction mechanism”, which is mainly proposed for CPOM over non noble metal catalysts, e.g. Ni, Co and CPOM over noble catalysts (Pt and Rh) at relatively low temperatures (<800°C). The other is “direct partial oxidation mechanism”, which is mainly proposed for CPOM over noble catalysts e.g. Pt and Rh, especially at very high temperatures (>1000°C) and with an extremely short contact time (in the order of milliseconds).

(1) Two-step reaction mechanism

Ashcroft and coworkers²²⁻²⁶ reported that synthesis gas can only be produced when part of the metal oxide catalyst is reduced to metal, although methane can be oxidized over metal oxides. They also studied the effect of contact time, and found that with a decrease in contact time the conversion and selectivity decrease. Therefore, they suggested that the reaction pathway may involve initial deep oxidation of some CH₄ to CO₂ and H₂O, followed by a sequence of steam- and CO₂-reforming of unconverted CH₄ to synthesis gas and reverse water gas shift reactions to give equilibrium product yields.

By carefully measuring the temperature gradients in Ni-based catalyst bed, Vermeiren *et al.*⁴⁸ observed pronounced exothermic reactions near the inlet of the catalyst bed and endothermic reactions in the latter half of the bed. Their results further confirmed that CPOM proceeds *via* a sequential reaction mechanism.

(2) Direct partial oxidation mechanism

In contrast to previous proposal of the generation of synthesis gas via a sequence of total oxidation followed by reforming, Schmidt *et al.*³⁹ demonstrated that both H₂ and CO are

primary products of the direct oxidation of methane at high temperatures and an extremely short contact time (in the order of milliseconds). The direct partial oxidation mechanism is illustrated in Fig. 6. It was suggested that the mechanism involved direct formation of H_2 initiated by CH_4 pyrolysis on the surface of noble catalysts to give surface C and H species.

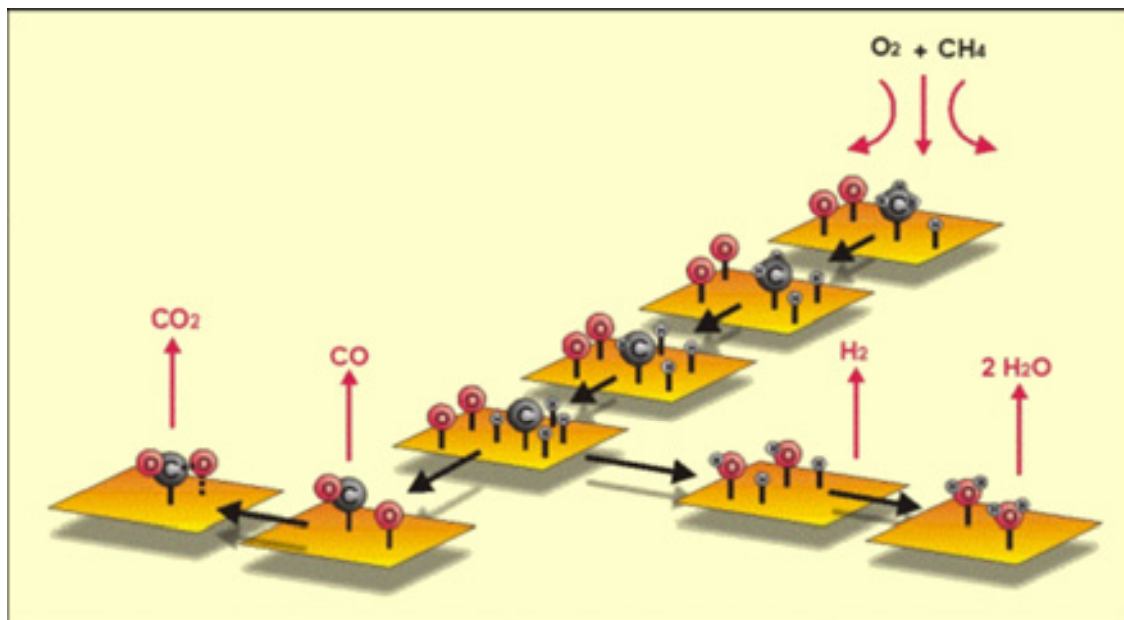


Fig. 6. Schematic mechanism of direct partial oxidation of methane to synthesis gas.

The H adatoms dimerize and desorb as H_2 , while the surface C atoms react with adsorbed O atoms and desorb as CO.

They also modeled CH_4 oxidation in an plug flow reactor using the CH_4 pyrolysis mechanism⁴⁰. Their model agreed well with the experiments, confirming that direct oxidation was the mechanism for oxidation over Rh coated monolith catalyst. However, it still can not be completely excluded that both deep oxidation and consecutive reforming reactions occur, because both reaction zones could be too close to be distinguishable under the extreme conditions (very high temperatures and very short contact time).

1.4.2.3. Problems with metal catalysts

CPOM is normally carried out at high reaction temperatures to reach high methane conversion and high selectivity to CO and H_2 . Moreover, according to the “two-step reaction mechanism”⁴³, CPOM over metal catalysts proceeds *via* deep oxidation followed by steam- and CO_2 -reforming as consecutive reactions. High exothermicity of the deep oxidation results in a temperature gradient in the catalyst bed amounting to more than $1000^\circ C$ above set point at the top of the catalyst bed. In the second part of the reactor bed the endothermic reforming reactions lead to lower temperatures. Over noble metal catalysts e. g. Rh, synthesis gas seems to be produced by directly partial oxidation of CH_4 at very high temperature ($>1000^\circ C$) and with a very short contact time³⁹. However, the catalyst still suffers from extremely high

temperatures, although this provides an elegant solution to the temperature gradients over the reactor.

The volatility of support materials or that of the active catalytic components is usually not considered as a problem. However, in the case of catalytic oxidation at these high temperatures volatilization of the active phase must be considered as an important factor for deactivation of the catalyst. As illustrated in Fig. 7, significant loss of Pt *via* formation of volatile oxides is observed at 1000°C in the presence of oxygen. Hermans *et al.*⁴⁹ studied platinum volatilization from supported Pt catalysts at temperatures above 600°C. It was found that PtO₂ is the most dominant volatile species and high dispersion of Pt on the support results in even higher volatilization of PtO₂ than expected from thermodynamic equilibrium. Metal loss in the form of volatile oxide, which contributes to deactivation of the catalyst, is also a serious problem in the ammonia oxidation process over Pt-Rh gauzes operated at similar conditions as CPOM⁵⁰. Moreover, very high operation

temperature also results in deactivation of the catalyst due to extensive sintering of both metal and oxide support. Fig. 8 shows that surface areas of oxide supports decrease significantly with increasing operation temperature. Vaccari *et al.*⁵¹ studied deactivation of a Pt/ γ -Al₂O₃ catalyst used for CPOM causing at 900°C. Significant sintering of both Pt and γ -Al₂O₃ was observed, which results in deactivation of the catalyst.

1.4.3. Oxide catalysts

1.4.3.1. CPOM over oxides

Compared to metal catalysts, oxide catalysts have almost not been studied for CPOM. However, CPOM has been often mentioned as a major side reaction in both oxidative coupling of methane over rare oxides⁵² and partial oxidation of methane to formaldehyde on TiO₂⁵³. CPOM over some irreducible or hardly reducible metal oxides such as TiO₂, La₂O₃,

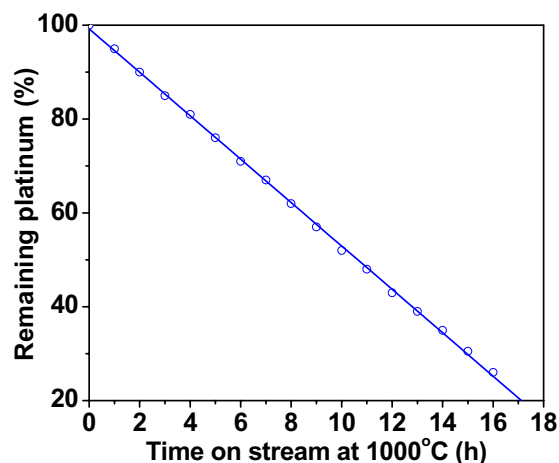


Fig. 7. Loss of Pt from 1% Pt monolith catalyst at 1000°C in moist air².

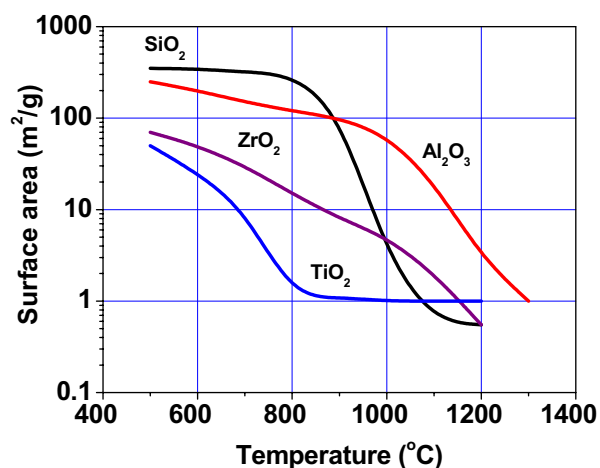


Fig. 8. Loss of surface area of oxide support due to sintering².

and ZrO_2 -based mixed oxides was studied by Steghuis *et al.*^{54;55} and Stobbe *et al.*⁵⁶. Yttrium-stabilized zirconia (YSZ) showed the best catalytic performance among these oxide catalysts. Stobbe concluded, based on the relation between methane conversion and selectivities over ZrO_2 , that CO and H_2 are primary products of CPOM over ZrO_2 , whereas CO_2 is formed by water-gas shift and oxidation of CO . Steghuis proposed a reaction mechanism of CPOM over YSZ, including homolitic dissociation of methane over $\text{O}^{\cdot}_{(s)}$ sites followed by conversion to CO , H_2 and H_2O *via* the formation and decomposition of formaldehyde as an intermediate. CO_2 is produced by further oxidation of the reaction intermediate.

As reported by Steghuis *et al.*⁵⁴, YSZ catalyzes direct partial oxidation of methane to synthesis gas with a reasonable activity and selectivity, although they are still as compared with metal catalysts. Moreover, YSZ is much more thermally stable as compared with metals under CPOM conditions (in the presence of oxygen at high temperature). These features make YSZ a very interesting catalyst for CPOM. However, the details of catalysis of YSZ during CPOM are not fully understood yet. The defective structure of YSZ seems to play an important role in CPOM. Besides for CPOM, the role of defects in the activation of both oxygen and alkanes over oxide catalysts is also an interesting concept, which is under study in *the group of catalytic processes and materials* (University of Twente, the Netherlands), for both methane coupling to C_2 hydrocarbons over Li/MgO ⁵⁷ and oxidative dehydrogenation of alkanes to olefins, e.g. C_3H_8 to C_3H_6 over Li/MgO ⁵⁸. The following section describes the structure and defect chemistry of ZrO_2 and YSZ.

1.4.3.2. Yttrium-stabilized zirconia (YSZ)

During recent years zirconium oxide has attracted much attention from researchers in the field of heterogeneous catalysis. In addition to being used as catalyst support in numerous applications, ZrO_2 -based oxides are also used as active catalysts, e.g. for CO_2 hydrogenation⁵⁹, nitrous oxide decomposition⁶⁰, and CO oxidation⁶¹. The monoclinic single phase of pure zirconia (ZrO_2) is stable at temperatures below 1200°C ; upon increasing temperature the material transforms to tetragonal (*t*) ($1200\sim 2280^\circ\text{C}$) and then to a cubic (*c*) fluorite structure ($>2280^\circ\text{C}$), respectively⁶². Structures of these three different phases are schematically

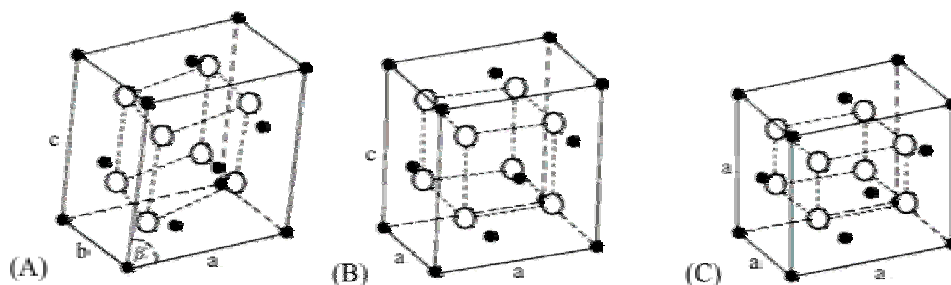


Fig. 9. Three different phases of ZrO_2 : (A) monoclinic, (B) Tetragonal, and (C) cubic. Small solid circles indicate Zr atoms and big open circles represent oxygen atoms.

illustrated in Fig. 9. These phase transitions induce large volume changes and make the pure material unsuitable for applications in catalysis, fuel cells, oxygen sensors and artificial diamonds. Therefore, stabilized zirconia is a material of significant technological importance. By doping ZrO_2 with lower-valence oxides, e.g. CaO , MgO , or Y_2O_3 , ZrO_2 can be stabilized in the tetragonal and cubic phase, depending on the dopant concentration⁶³. Cubic yttrium-stabilized zirconia (YSZ) is obtained when the Y_2O_3 concentration in ZrO_2 is not less 8 mol%⁶⁴. Charge neutrality in YSZ is maintained by the formation of oxygen vacancies. The local atomic environments in YSZ, i.e. the arrangement of neighboring ions, are very different between the corresponding stoichiometric (*t* and *c*) phases. The structure of cubic YSZ is illustrated in Fig. 10.

The high ionic conduction and oxygen diffusion in YSZ are related to the presence of oxygen vacancies. Ionic conduction and diffusion occur by migration of oxygen ions *via* the vacancies, which are highly mobile at high temperatures. The conductivity increases with increasing Y_2O_3 content, because of the increasing concentration of oxygen vacancies, until it reaches a maximum (at about 10 mol% Y_2O_3), followed by a decrease at higher concentrations of Y_2O_3 . The origin of this decrease in conductivity is not yet cleared up in detail. Currently, it is generally believed that defect interactions, clustering effects and/or the tendency for ordering of oxygen vacancies play a role⁶⁵.

In general, it is known that defect sites, the most common being oxygen vacancies, are important in the surface chemistry and catalysis of metal oxides. The electronic structure of the metal cation at these sites is significantly altered. Ekerdt and co-workers⁶⁶⁻⁶⁸ reported that the active site for CO hydrogenation over YSZ and CaO -stabilized ZrO_2 is an oxygen vacancy. They further pointed out that both a higher selectivity to C_4 products and a high reaction rate are realized with higher a mobility of the oxygen vacancies.

The surface properties of YSZ are of importance for its application, especially in catalysis. However, only few studies have been devoted to the surface of cubic YSZ, and most of these are only for the (100) face⁶⁹, while a great deal of both experimental and theoretical data has been reported for the surface properties of the monoclinic phase of pure ZrO_2 and for tetragonal zirconia (with very low Y_2O_3 content)^{70;71}.

Three main surfaces of cubic YSZ are illustrated in Fig. 11. Surfaces of cubic YSZ were studied by Ballabio *et al.*⁷² using first-principle calculations. Due to the electrostatic attraction of oxygen vacancies, the surface relaxation with respect to the ideal fluorite structure occurs to a certain extent. Both (111) and (110) faces are neutral. Compared with

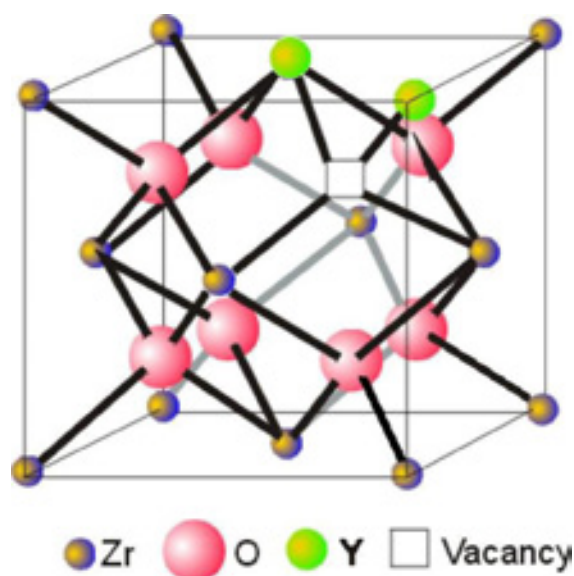


Fig. 10. Formation of oxygen vacancy in YSZ

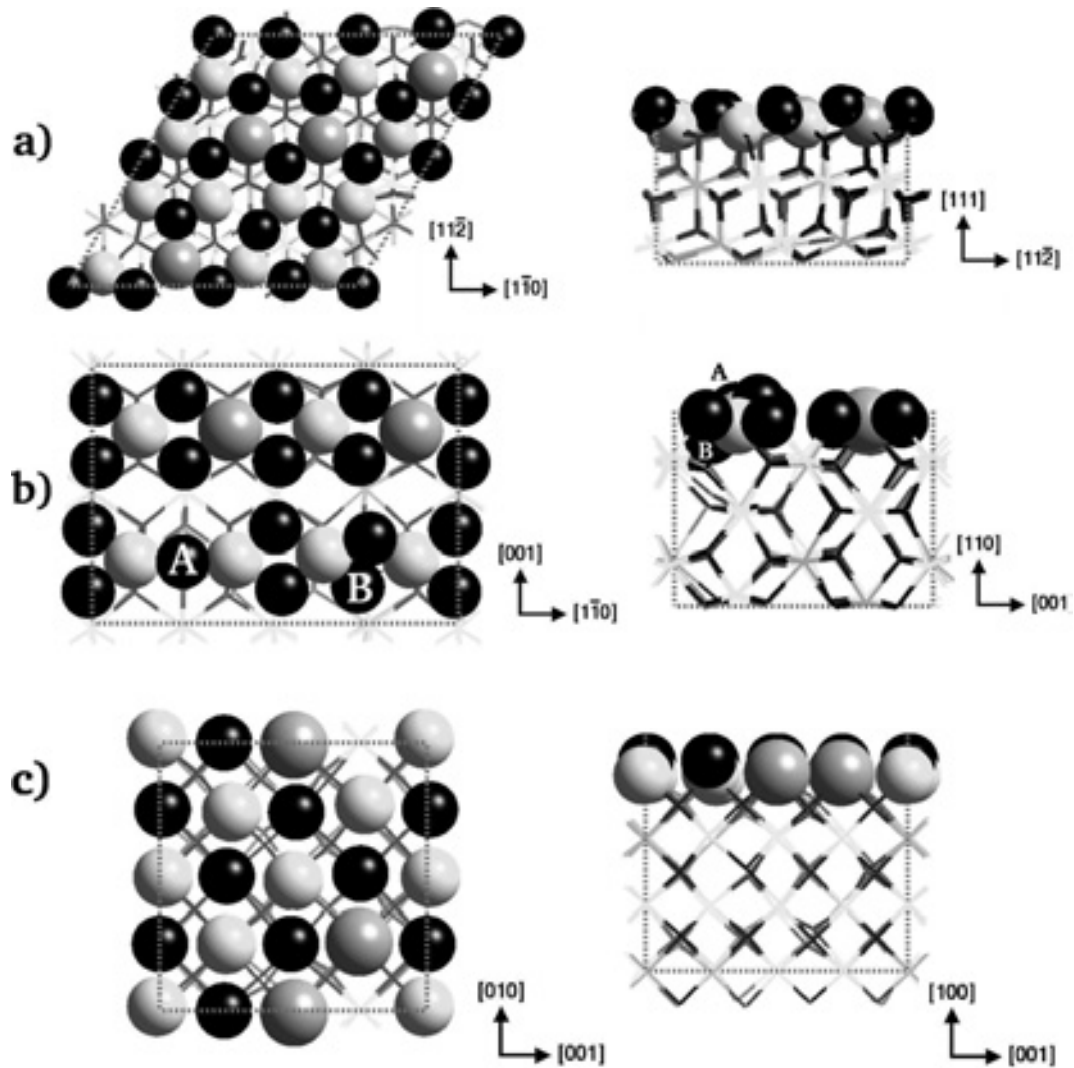


Fig. 11. Top (right) and side (left) view of (a) the (111), (b) the (110) and (c) ideal (100) surfaces of cubic YSZ. Light gray, dark gray and black spheres denote zirconium, yttrium and oxygen ions, respectively. Oxygen atoms labeled with A and B in (b) are surface atoms nearest neighbor to oxygen vacancies. Adopted from ref.³

other two main faces, the (111) surface undergoes minor relaxations. On average, the outermost oxygen ions relax inward by only $\sim 0.01\text{\AA}$. In contrast, the oxygen sublattice is strongly distorted with respect to the ideal fluorite structure both at the surface and in the bulk. As a consequence the surface Zr-O plane is buckled, the oxygen atoms on the first layer move outward by 0.08\AA with respect to the ideal truncation of the YSZ bulk. Moreover, some surface oxygen atoms that are nearest neighbor to vacancies move much more and up to 0.7\AA , as shown in Fig. 11 (b). The oxygen atom labeled with A in this figure initially is the nearest neighbor to a vacancy along the $[110]$ direction. It relaxes and moves outwards above the nearest metal ions. Similarly, the oxygen ion labeled with B is nearest neighbor to an oxygen vacancy in the layer underneath and moves inwards. The real (100) face is polar. In order to be neutral, half of the oxygen atoms in the outermost layer need to be removed. Therefore, the

(100) face could be the most disordered surface, although geometry of an ideal (100) face is illustrated in Fig. 11 (c).

The surface energy is estimated for these three relaxed faces, 65 meV/Å² for the (111) face, which is much lower than those for the (110) face (90 meV/Å²) and the (100) face (109 meV/Å²). For YSZ with a cubic fluorite structure, coordination numbers of Zr and oxygen are 8 and 4 in the bulk. Whereas, the coordination numbers of Zr and oxygen atoms are respectively, 7 and 3 on the (111) surface, 6 and 3 on the (110) surface, and 6 and 2 on the ideal neutralized (100) face, respectively. As one would have envisaged by counting the number of bonds broken by cleavage, or equivalently the change in the coordination number of surface atoms with respect to the bulk values, the (111) face has the lowest surface energy.

1.5. Scope of this thesis

ZrO₂-based oxides are promising in CPOM because of both superior stability and reasonable catalytic performance, although their activity and selectivity are lower as compared with metal catalysts. In order to further improve their catalytic performance, a better understanding of the reaction mechanism of CPOM is essential. Therefore, the objective of this thesis is to gain more insight in the reaction mechanism of CPOM over ZrO₂ and YSZ catalysts, and to understand the role of the structure of these oxides in activation of both oxygen and methane.

In chapter 2, taking advantages of both superior stability of oxide catalyst and good activity of metal catalyst, a dual catalyst bed concept, which consists of two catalyst beds instead of one single metal catalyst bed, is proposed for CPOM. The viability of this concept is demonstrated on a lab scale. The advantages of the concept are discussed based on concentration profiles as well as estimations of temperature profiles through the reactor. **In chapter 3**, to further improve activity and selectivity of the catalyst, the influence of calcination temperature, Y₂O₃ content and especially impurities such as CaO, TiO₂, Na₂O on catalytic performance of YSZ are investigated. The roles of consecutive steam- and CO₂-reforming reactions are studied as well. **In chapter 4**, CPOM over YSZ catalyst is studied with *in-situ* FTIR and catalytic experiments with methane and/or formaldehyde in both steady state experiments and transient experiments. Based on the obtained results, a reaction scheme is proposed, including all significant reaction pathways. This information is essential to define a research strategy to achieve higher selectivity with YSZ-based catalysts. **In chapter 5**, isotopic oxygen ¹⁸O₂ exchange with the catalysts is studied both in the absence of and in the presence of methane and under reaction conditions for CPOM. Based on the results obtained, active sites for activation of both oxygen and methane on the surfaces of YSZ and ZrO₂ are identified. **In chapter 6**, effects of defects, including structural defects, e.g. corners, edges, kinks and steps of the crystallites, intrinsic oxygen vacancies formed by partial reduction of the surface of ZrO₂ or YSZ, and extrinsic defects generated by doping ZrO₂ with Y₂O₃, on the activation of both O₂ and N₂O are studied. Finally, the thesis ends with a general discussion and recommendations for future work **in chapter 7**.

References

1. Proved natural gas reserves up to the end of 2003.
<http://www.bp.com/genericarticle.do?categoryId=112&contentId=2008083> .
2. R.A.D.Betta, *Catal.Today* 35, 129 (1997).
3. G.Ballabio, M.Bernasconi, F.Pietrucci, S.Serra, *Phys.Rev.B* 70, 075417 (2004).
4. J.H.Lunsford, *Catal.Today* 63, 165 (2000).
5. YU.I.Pyatnitskii, *Theoretical and experimental chemistry* 39, 201 (2003).
6. G.E.Keller and M.M.Bhasin, *J.Catal.* 73, 9 (1982).
7. Y.Feng and D.Gutman, *J.Phys.Chem.* 95, 6556 (1991).
8. K.D.Campbell and J.H.Lunsford, *J.Phys.Chem.* 92, 5792 (1988).
9. T.Fang and J.Yeh, *J.Catal.* 69, 227 (1981).
10. M.Baerns and J.R.H.Ross, in *Perspectives in Catalysis*, J.M.Thomas and K.I.Zamaraev, Eds. (Blackwell, Oxford, 1992).
11. V.A.Tsipouriari and X.E.Verykios, *J.Catal.* 179, 292 (1998).
12. Y.B.Kagan, A.Y.Rozovskii, L.G.Liberov, *Dokl.Akad.Nauk.SSSR* 224, 1081 (1975).
13. T.H.Fleisch, A.Basu, M.J.Gradassi, *Stud.Surf.Sci.Catal.* 107, 117 (1997).
14. M.E.Dry, *Catal.Today* 71, 227 (2002).
15. H.Schulz, *Appl.Catal.A* 186, 3 (1999).
16. S.S.Bharadwaj and L.D.Schmidt, *Fuel Processing Tech.* 42, 109 (1995).
17. M.E.Dry, *Encyclopaedia of Catalysis* (Wiley, New York, 2003), p. 347.
18. Haldor Topsoe A/S and Soc.Belge de l'Azote, *Hydrocarbon Process* 67, 77 (1988).
19. K.G.Marnasidou, S.S.Voutetakis, G.J.Tjatjopoulos, I.A.Vasalos, *Chem.Eng.Sci.* 54, 3691 (1999).
20. J.Eilers, S.A.Posthuma, S.T.Sie, *Catal.Lett.* 7, 253 (1990).
21. M.Prettre, C.Eichner, M.Perrin, *Trans.Faraday Soc.* 43, 335 (1946).
22. R.H.Jones, A.T.Ashcroft, D.Waller, A.K.Cheetham, J.M.Thomas, *Catal.Lett.* 8, 169 (1991).
23. P.D.F.Vernon, M.L.H.Green, A.K.Cheetham, A.T.Ashcroft, *Catal.Today* 13, 417 (1992).

-
24. P.D.F.Vernon, M.L.H.Green, A.K.Cheetham, A.T.Ashcroft, *Catal.Lett.* 6, 181 (1990).
 25. A.T.Ashcroft, A.K.Cheetham, M.L.H.Green, P.D.F.Vernon, *Nature* 352, 225 (1991).
 26. A.T.Ashcroft et al., *Nature* 344, 319 (1990).
 27. A.P.E.York, T.Xiao, M.L.H.Green, *Topics Catal.* 22, 345 (2003).
 28. D.Dissanyake, M.P.Rosynek, K.C.C.Kharas, J.H.Lunsford, *J.Catal.* 132, 117 (1991).
 29. V.R.Choudhary, V.H.Rane, A.M.Rajput, *Appl.Catal.A* 162, 235 (1997).
 30. V.R.Choudhary, A.M.Rajput, B.Prabhakar, *Catal.Lett.* 15, 363 (1992).
 31. V.R.Choudhary, R.M.Ramarjeet, V.H.Rane, *J.Phys.Chem.* 96, 8686 (1992).
 32. B.L.Basini et al., *J.Catal.* 173, 247 (1998).
 33. S.Tang, J.Lin, K.L.Tan, *Catal.Lett.* 51, 169 (1998).
 34. V.R.Choudhary and A.S.Mammam, *Appl.Energy* 66, 161 (2000).
 35. A.Slagtern and U.Olsbye, *Appl.Catal.A* 110, 99 (1994).
 36. S.Liu et al., *Stud.Surf.Sci.Catal.* 130D, 3567 (2000).
 37. W.Chu et al., *Stud.Surf.Sci.Catal.* 1998, 119 (1998).
 38. D.A.Hickman, E.A.Hauptfear, L.D.Schmidt, *Catal.Lett.* 17, 223 (1993).
 39. D.A.Hickman and L.D.Schmidt, *Science* 259, 343 (1993).
 40. D.A.Hickman and L.D.Schmidt, *AIChE J.* 39, 1164 (1993).
 41. M.G.Poirier, J.Trudel, D.Guay, *Catal.Lett.* 21, 99 (1993).
 42. S.C.Tsang, M. L. H. G. J.B.Claridge, M.L.H.Green, *Catal.Today* 23, 3 (1995).
 43. A.T.Ashcroft et al., *Nature* 344, 319 (1990).
 44. E.Ruchenstein and H.Y.Wang, *J.Catal.* 187, 151 (1999).
 45. A.Guerrero-Ruiz, P.Ferreira-Aparicio, M.B.Bachiller-Baeza, I.Rodriguez-Ramos, *Catal.Today* 46, 99 (1998).
 46. L.D.Schmidt and M.Huff, *Catal.Today* 21, 443 (1994).
 47. M. L. H. G. J.B.Claridge, S.C.Tsang, A.P.E.York, A.T.Ashcroft, P.D.Battle, *Catal.Lett.* 22, 299 (1993).
 48. W.J.M.Vermeiren, E.Blomsma, P.A.Jacobs, *Catal.Today* 13, 427 (1992).

49. P.M.J.A.Hermans, *Ph.D thesis, Technic university of Delft, The Netherlands* (2004).
50. M.M.Karavayev, A.P.Zasorin, N.F.Kleshchev, *Catalytic oxidation of ammonia, Khimia, Moscow* (1983).
51. S.Albertazzi et al., *Appl.Catal.A* 247, 1 (2003).
52. K.D.Campbell, H.Zhang, J.H.Lunsford, *J.Phys.Chem.* 92, 750 (1988).
53. A.Parmaliana and F.Arena, *J.Catal.* 167, 57 (1997).
54. A.G.Steghuis, *Ph.D thesis, University of Twente, The Netherlands* (1998).
55. A.G.Steghuis, J.G.van Ommen, J.A.Lercher, *Catal.Today* 46, 91 (1998).
56. E.R.Stobbe, *Ph.D thesis, University of Utrecht, The Netherlands* (1999).
57. M.A.Johnson, E.V.Stefanovich, T.N.Truong, *J.Phys.Chem.B* 101, 3196 (1997).
58. L.Leveles, *Ph.D thesis, University of Twente, The Netherlands* (2002).
59. J.H.Bitter, K.Seshan, J.A.Lercher, *J.Catal.* 171, 279 (1997).
60. T.M.Miller and V.H.Grassian, *J.Am.Chem.Soc.* 117, 10969 (1995).
61. W.P.Dow and T.J.Huang, *J.Catal.* 147, 322 (1994).
62. P.Aldebert and J.P.Traverse, *J.Am.Ceram.Soc.* 68, 34 (1985).
63. E.C.Subbarao, in *Science and Technology of Zirconia, Vol. 3*, A.H.Heuer and L.W.Hobbs, Eds. (The American Ceramic society, Columbus, OH, USA, 1981).
64. J.P.Goff, W.Hayes, S.Hull, M.T.Hutchings, K.N.Clausen, *Phys.Rev.B* 59, 14202 (1999).
65. M.Weller et al., *Solid State Ionics* 175, 409 (2004).
66. N.B.Jackson and J.G.Ekerdt, *J.Catal.* 126, 46 (1990).
67. N.B.Jackson and J.G.Ekerdt, *J.Catal.* 126, 31 (1990).
68. R.G.Silver, C.J.Hou, J.G.Ekerdt, *J.Catal.* 118, 400 (1989).
69. T.Nishimura, H.Toi, Y.Hoshino, E.Toyoda, Y.Kido, *Phys.Rev.B.* 64, 073404 (2001).
70. A.Hoffman, S.J.Clark, M.Oppen, I.Hahndorf, *Phys.Chem.Chem.Phys.* 4, 3500 (2002).
71. K.Meinel, K.M.Schindler, H.Neddermeyer, *Surf.Sci.* 532, 420 (2003).
72. G.Ballabio, M.bernasconi, F.Pietrucci, S.Serra, *Phys.Rev.B.* 70, 075417 (2004).

Chapter 2

Dual Catalyst Bed Concept for Catalytic Partial Oxidation of Methane to Synthesis Gas

Abstract

A system with two catalyst beds instead of one single metal catalyst bed is proposed for partial oxidation of methane to synthesis gas (CPOM). In this dual catalyst bed system, an irreducible stable oxide, such as yttrium-stabilized zirconia (YSZ), is used in the first catalyst bed to obtain selective oxidation to synthesis gas with significant highly exothermic deep oxidation occurring as well. This feature results in milder temperature profiles in the reactor because less heat is liberated compared to initial deep oxidation as occurred, e.g. on metal catalysts. More importantly, all oxygen is completely consumed in the oxide catalyst bed. The second bed comprises a metal catalyst, e.g. Co-based, for reforming methane with H_2O and CO_2 exclusively. In this way the catalysts are exposed to less extreme temperatures and, exposure of metallic catalysts to oxygen at high temperatures is prevented. Therefore catalyst deactivation via evaporation of precious metal oxides is circumvented. Finally, synthesis gas with an equilibrium composition (almost 100% CO and H_2 yields) is produced

Key words: *Partial oxidation of methane, Yttrium-stabilized zirconia, $LaCoO_3$, Dual catalyst beds*

2.1. Introduction

Steam reforming of methane, a traditional process for synthesis gas production, suffers mainly from high energy consumption, high investment cost and H_2/CO ratios (≥ 3) that do not suit all important downstream processes. Recently more attention¹⁻⁴ has been paid to catalytic partial oxidation of methane (CPOM), a mildly exothermic process with a H_2/CO ratio of about 2, which is appropriate for e.g. methanol synthesis and Fischer-Tropsch synthesis.

CPOM over metal catalysts was studied intensively. Nickel⁵⁻⁷, cobalt⁷⁻⁹ and noble metal based catalysts¹⁰⁻¹² showed high activities in CPOM. It is widely accepted¹⁰⁻¹² that metal catalysts first oxidize methane to CO_2 and water in the first part of the catalyst-bed until oxygen is exhausted, followed by reforming of the remaining methane with the CO_2 and water formed initially (two-step mechanism). However, at extremely high temperatures and very short contact time in the order of milliseconds, it is still possible that synthesis gas is formed directly¹³⁻¹⁵.

A sharp temperature profile over the reactor will always be present because deep oxidation is strongly exothermic whereas the reforming reactions are endothermic. Moreover the formation of hotspots may also occur affecting both stability and safety of the process. The resulting high temperature of operation is a major threat to the stability of supported metal catalyst: the catalyst may sinter, lose activity and, most importantly, the exposure of metals to oxygen at these temperatures will form volatile oxides resulting in metal loss.

Many efforts have been made to solve these problems. Coupling partial oxidation of methane with steam reforming of methane and/or CO_2 reforming of methane has been reported as a possible solution¹⁶⁻¹⁹, since reforming reactions are highly endothermic. However, the H_2/CO ratio of final synthesis gas will vary with composition of the feed. Therefore, it is much more attractive to find a stable catalyst for direct partial oxidation of methane. Compared with metal catalysts, metal oxide catalysts showed excellent stability at the expense of low activity for CPOM. Methane can be directly converted according to the reaction: $CH_4 + O_2 \rightarrow CO + H_2 + H_2O$ over ZrO_2 -based catalysts at temperature around $900^\circ C$ as Steghuis et al.^{20,21} reported. Methane can thus be converted to synthesis gas with significant selectivity, though deep oxidation can not be completely avoided.

Taking advantages of both stability of oxide catalyst and good activity of metal catalyst, we propose here a dual catalyst bed concept. In this concept, an oxide catalyst is used in the first catalyst bed to carry out partial oxidation though with incomplete selectivity and methane conversion, but with 100% oxygen conversion. A metal catalyst is used in the second catalyst bed to compensate the shortcomings of the oxide catalyst in the first bed by CO_2 and steam reforming of unconverted methane. In this system, exothermic reactions occur only on the stable oxide catalyst, followed by endothermic reforming reactions on the metal catalyst. Synthesis gas with H_2/CO ratio of 2 is produced because the ratio of CH_4/O_2 in the feed gases is not changed.

In this work we demonstrate the viability of the concept on a lab scale with diluted as well as undiluted methane/oxygen mixtures. The advantages of the concept will be discussed based on the concentration profiles as well as estimations of the temperature profiles through the reactor.

2.2. Experimental

2.2.1. Catalyst preparation

Yttrium-stabilized zirconia (YSZ) (Gimex, The Netherlands), which consists of 12 wt.% yttria in zirconia, was calcined at 1100°C for 15 h. After calcination, the powder with BET surface area of 4.5 m²/g was pressed, crushed and sieved to 0.3-0.6 mm particles. We refer to this catalyst as YSZ12C. LaCoO₃ perovskite was prepared *via* the auto-combustion method, as described elsewhere^{1,2}. BET surface area of the LaCoO₃ sample was 1.8 m²/g after calcination at 950°C in air for 5 h. XRD showed the presence of the perovskite structure exclusively.

2.2.2. Catalytic reaction

The CPOM over the single catalyst bed was carried out in a conventional flow system at atmospheric pressure. Experiments were performed with 0.3 g catalyst diluted with 0.3 g α -Al₂O₃.

Dual-bed experiments were done with two α -Al₂O₃ tubular reactors that can be operated consecutively or separately (similar to that shown in Fig. 5(a)). The effluent gas from the first bed was introduced directly to the second reactor. The first reactor was operated with 0.3 g YSZ12C, the second reactor contained 0.3 g LaCoO₃ perovskite.

The temperature was varied and the system was allowed reach steady-state within two hours. Experiments with diluted CH₄ and O₂ (CH₄:O₂:He=2:1:14) were performed with 170 ml/min (STP) total gas flow. Experiments with undiluted CH₄ and O₂ (2:1 v/v) were done with 150 ml/min (STP) total gas flow rate. On-line gas chromatography with Carboxan 1000 and Haysep N columns was used to analyze the effluent gases from both reactors. N₂ was used as an internal standard. Conversions (X) and yields (Y) were calculated according to:

$$X_{CH_4} = \frac{CH_4^{in} - CH_4^{out}}{CH_4^{in}}; X_{O_2} = \frac{O_2^{in} - O_2^{out}}{O_2^{in}}; Y_{CO} = \frac{CO^{out}}{CH_4^{in}}; Y_{CO_2} = \frac{CO_2^{out}}{CH_4^{in}}; Y_{H_2} = \frac{H_2^{out}}{2CH_4^{in}}; Y_{H_2O} = \frac{H_2O^{out}}{2CH_4^{in}}$$

2.3. Results and Discussion

2.3.1. CPOM in a single catalyst bed

The catalytic performance of YSZ12C is shown in Fig. 1a with diluted feed. CPOM reaction starts at about 550°C. Conversions and yields increased with increasing reaction temperature. Complete conversion of oxygen was reached at about 950°C with 42% methane conversion. When increasing temperature further, yields of CO and H₂ increased dramatically at the

expense of CO_2 , H_2O and methane. This indicates that carbon dioxide and steam reforming reactions might take place at higher temperatures ($>950^\circ\text{C}$).

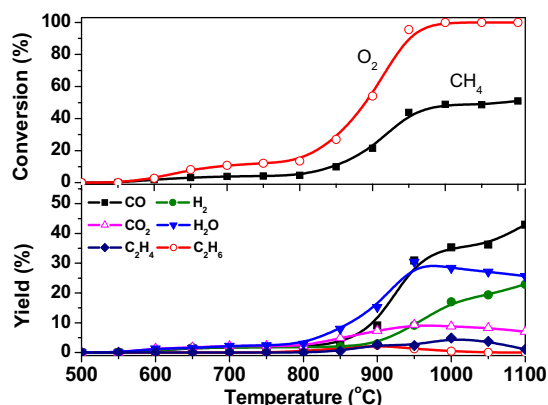


Fig. 1a. Conversion and yields for CPOM over 0.3 g YSZ12C with diluted feed gases as a function of reaction temperature. $\text{CH}_4/\text{O}_2/\text{He} = 2:1:14$, 170 ml/min (STP) total flow rate.

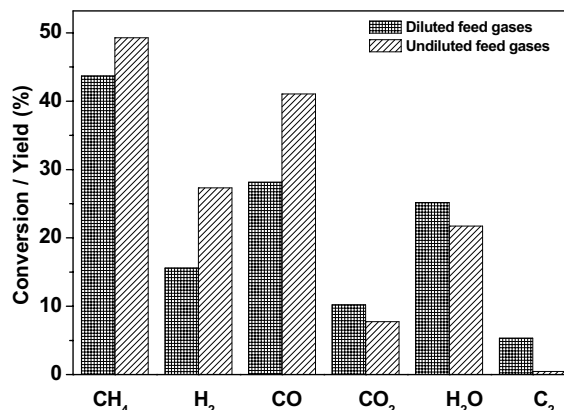


Fig. 1b. Comparison of COPM results on YSZ12C at 1000°C with diluted and undiluted feed gases.

Fig. 1b shows that the selectivity at 1000°C is even higher when CH_4 and O_2 are not diluted and consequently methane conversion also increases as O_2 is exhausted. We suggest that this effect is caused by actual higher temperatures of the catalyst when operated without dilution because of the heat of reaction. We will report more details on the properties of YSZ catalyst in a future publication.

Conversion and yields over LaCoO_3 for CPOM at different reaction temperatures are shown in Fig. 2. As expected, LaCoO_3 perovskite is a very active catalyst for combustion at lower temperatures (starting from 350°C). At 600°C , oxygen was converted completely with 25% methane conversion. CO_2 and H_2O were produced exclusively in a wide temperature window ($350\sim 750^\circ\text{C}$). Yields of CO and H_2 increased dramatically with increasing temperature above 750°C . Complete conversion of CH_4 and 100% selectivity to synthesis gas was obtained at about 950°C . Similar catalytic performances were also observed by Slagtern *et. al.*²² This indicates that LaCoO_3 , although a good combustion catalyst in temperature window $350\sim 750^\circ\text{C}$, is not active for steam-reforming and CO_2 -reforming reactions. However, after prolonged

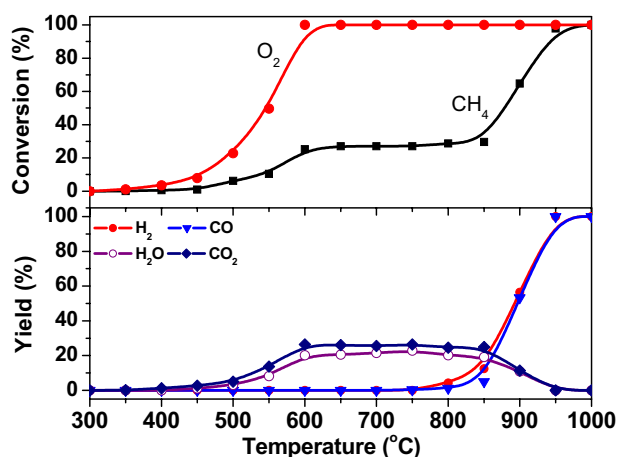


Fig. 2. Conversion and yields for CPOM over 0.3 g LaCoO_3 with diluted feed gases as a function of reaction temperature. $\text{CH}_4/\text{O}_2/\text{He} = 2:1:14$, 170 ml/min (STP) total flow rate.

exposure to methane, steam and carbon dioxide at higher temperature ($>750^{\circ}\text{C}$), LaCoO_3 can be reduced to metallic cobalt, which is known to be active for reforming reactions. Cobalt particles in reduced LaCoO_3 are responsible for 100% yield of synthesis gas at higher temperatures²³. In this work, LaCoO_3 was used as a precursor of a supported cobalt metal catalyst in the second reactor of the dual catalyst bed system to carry out reforming reactions, by reducing the perovskite phase *in-situ* at 950°C for 1.0 hour till 100% yield of synthesis gas was obtained.

2.3.2. CPOM in the dual catalyst bed system

To demonstrate the dual-bed concept, the product mixture of the first reactor with YSZ12C at 1000°C was introduced directly into the second reactor with Co catalyst. The composition of this product mixture with diluted feed was 3.5% H_2 , 3.2% CO , 1.2% CO_2 , 5.7% H_2O , 6.4% unreacted methane and traces of hydrocarbons (0.06% C_2H_2 , 0.22% C_2H_4 , 0.02% C_2H_6) with He balance. Undiluted feed resulted in a mixture fed to the second reactor containing 27.5% H_2 , 20.7% CO , 3.9% CO_2 , 21.9% H_2O , 0.46% C_2 -hydrocarbon and 25.6% CH_4 .

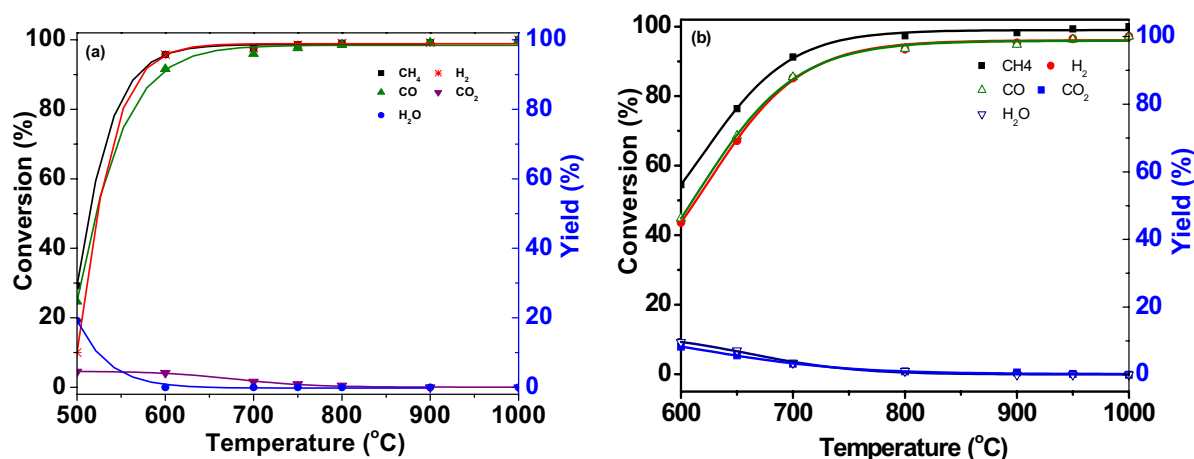


Fig. 3. Final conversion and yields as a function of temperature of the second reactor in dual catalyst bed system. (a) diluted feed gases, $\text{CH}_4/\text{O}_2/\text{He} = 2:1:14$, 170 ml/min (STP) total flow rate (b) undiluted feed gases $\text{CH}_4/\text{O}_2 = 2:1$, 150 ml/min (STP) total flow rate. When undiluted feed gases were used, H_2 yield was calculated based on hydrogen balance.

CO_2 and H_2O produced in the first reactor reacted with unconverted methane over cobalt catalyst in the second reactor. The influence of the temperature of the second reactor on total conversion and yields is shown in Fig. 3 for both diluted and undiluted feed. In both cases complete conversion to CO and H_2 was achieved, although a higher temperature for the second reactor is needed for the undiluted feed. The reason for this obviously is the higher gas hourly space velocity (GHSV) with the undiluted feed $2 \times 10^4 \text{ h}^{-1}$ versus $4 \times 10^3 \text{ h}^{-1}$ for the diluted feed. Gas hourly space velocity (GHSV) is defined as the ratio of the volumetric flow of reactants at standard conditions (25°C , and 1 bar) to the total catalyst volume.

2.3.3. Adiabatic temperature changes

The maximum temperature in the dual-bed concept is located at the exit of the first reactor when oxygen is exhausted. The small-scale lab reactor used in this study is far from adiabatic and therefore we choose to calculate theoretical temperature profiles based on the conversion observed and assuming ideal adiabatic operation. In the first catalyst bed the following reactions proceed:

Partial oxidation on YSZ12C²¹:



Combustion:



In the second catalyst bed reforming reactions take place:

Dry reforming:



Steam reforming:



In the first reactor with YSZ12C catalyst only about 10% methane is combusted and 30% of methane is partially oxidized to CO, H₂ and H₂O (eq.(1)). The remaining CH₄ is converted to synthesis gas by reforming reactions (eq.(3) and (4)) in the second reactor. The thermal behavior of the dual-bed concept will be compared to operation with a single metal catalyst, assuming first complete deep oxidation followed by extensive reforming reactions¹⁰⁻¹².

The adiabatic temperature change at each reaction step was calculated respectively using the HSC chemistry package²⁴. The difference in the adiabatic temperature rise between the combustion zone of the single metal catalyst bed and the oxide catalyst bed in the dual catalyst bed system is shown in Fig. 4. For a single metal catalyst the deep oxidation causes an adiabatic temperature rise of 817°C with the diluted feed gases and 1817°C with the undiluted feed gases respectively. The oxide catalyst bed of the dual catalyst bed system results in adiabatic temperature rises of 689°C and 1344°C for diluted and undiluted operation respectively. Clearly, the amount of heat released is decreased in the order of 25%, which implies that actual temperature gradients will be smaller and process control will be simplified. It was claimed¹³ that partial oxidation of methane at very short contact time proceeds via a direct mechanism. In that case, the temperature rise will be lower obviously. However, this type of operation is only possible at high operation temperatures and very short contact time. Independent of this, the metal catalyst is always exposed to oxygen at high temperature, causing the formation of volatile metal oxides, resulting in metal loss.

The dual-bed concept is able to prevent the exposure of the metallic reforming catalyst to oxygen at high temperatures, so that evaporation of volatile metal-oxides is completely prevented. Therefore this system is expected to show improved stability with time on stream.

We never observed any deactivation although we are not equipped to run experiments longer than 250 hours.

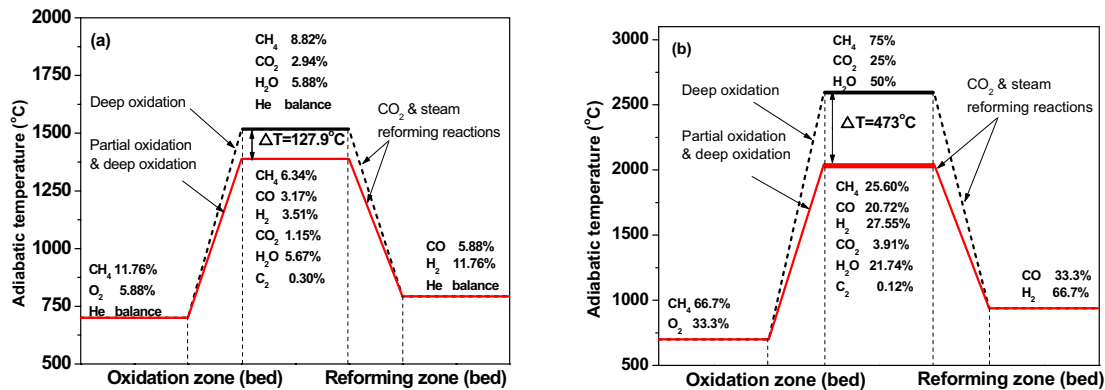


Fig. 4. Adiabatic temperature changes in the single metal catalyst bed (dot line) and in the dual catalyst bed system (solid line) with the diluted feed gases (a) and the undiluted feed gases (b) respectively. Feed gases were preheated to 700°C.

2.3.4. Productivity and reactor concepts

The results of this work show that the dual bed concept can be operated with complete conversion at GHSV of $2 \times 10^4 \text{ h}^{-1}$ under the conditions reported here. The range of GHSV is not significantly different from typical values reported for metal catalysts. Aschcroft and coworkers²⁵ studied CPOM on supported Rh catalyst. A 90% CH₄ conversion with 94% selectivity to synthesis gas was reached at GHSV of 10^4 h^{-1} . However, a lower conversion and a lower selectivity were resulted from a higher GHSV of 10^5 h^{-1} . Witt and Schmidt²⁶ studied the effect of flow rate on CPOM over Rh coated monolith catalyst. They reported that CH₄ conversion dropped from 90% at GHSV of $5 \times 10^4 \text{ h}^{-1}$ to 20% at $1 \times 10^6 \text{ h}^{-1}$. The level of productivity is therefore in the same order of magnitude. The remaining question is to which level the temperature of especially the first reactor may be decreased without affecting the performance of the dual-bed system. Work described in Chapter 3 provides more details on the effects of temperature, surface composition, Y₂O₃ contents and contaminations on the performance of the Y₂O₃ doped ZrO₂ catalysts.

Naturally, many other metal catalysts such as Pt, Rh, Ni with good activities in steam and CO₂ reforming reactions can be used

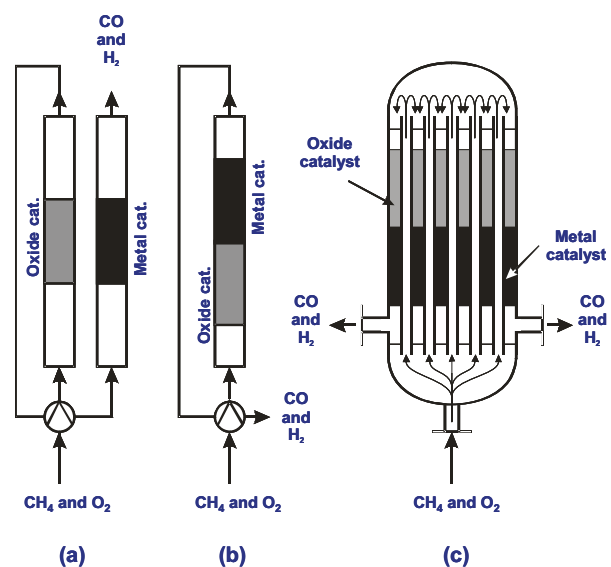


Fig. 5. Optional configurations of the dual catalyst bed reactor for CPOM.

in the second catalyst bed instead of Co. In the present work, two consecutive reactors demonstrate the dual catalyst bed concept as shown in Fig. 5(a). There are, however, many other options to realize this concept, such as two catalyst beds in a single tubular reactor (Fig. 5(b)) and heat exchanger-type reactor (Fig. 5(c)). Considering efficient utilization of reaction heat, the heat exchanger-type reactor may be a better option.

2.4. Conclusion

The present results demonstrate that the dual-catalyst bed concept which uses YSZ for partially selective oxidation of CH₄ and consecutively a metal catalyst (e.g. Co) for reforming of the remaining CH₄ results in complete conversion to synthesis gas at high GHSV. The partially selective oxidation in the first bed decreases significantly (~25%) the amount of heat generated in the first bed compared to the first part of a single metal catalyst bed for CPOM. Temperature profiles are therefore flattened out. The most important advantage of this approach, however, is the prevention of any contact between oxygen and the metal catalyst, because O₂ is completely converted on the YSZ catalyst. Therefore, metal loss *via* evaporation of oxides can be excluded. This feature suggests that the concept of this dual catalyst bed system is an interesting candidate for application in synthesis gas production by partial oxidation of methane.

Acknowledgements

This work was performed under the auspices of the Netherlands Institute for Catalysis Research (NIOK) and Institute of Mechanics, Processes And Control Twente (IMPACT). The financial support from STW under project number UPC-5037 is gratefully acknowledged.

References

1. C.T.Au and H.Y.Wang, *J.Catal.* 167, 154 (1997).
2. A.T.Aschcroft et al., *Nature* 344, 319 (1990).
3. A.M.Diskin and R.M.Ormerod, *Stud.Surf.Sci.Catal.* 130, 3519 (2000).
4. D.A.Hichman and L.D.Schmidt, *J.Catal.* 138, 267 (1992).
5. V.R.Choudhary, V.H.Rane, A.M.Rajout, *Appl.Catal.A* 162, 235 (1997).
6. V.R.Choudhary, V.H.Rane, A.M.Rajout, *Catal.Lett.* 22, 289 (1993).
7. V.R.Choudhary, A.M.Rajout, B.Prabhakar, *Catal.Lett.* 15, 363 (1992).
8. V.R.Choudhary, S.D.Sansare, A.S.Mamman, *Appl.Catal.A* 90, L1 (1992).

9. V.R.Choudhary, A.M.Rajout, V.H.Rane, *Catal.Lett* 16, 269 (1992).
10. A.T.Ashcroft, P.D.F.Vernon, M.L.H.Green, *Nature* 344, 319 (1990).
11. W.J.M.Vermeriren, E.Blomsma, P.A.Jacobs, *Catal.Today* 13, 427 (1992).
12. D.Dissanayake, M.P.Rosynek, K.C.Kharas, J.H.Lunsfort, *J.Catal.* 132, 117 (1991).
13. D.A.Hickman and L.D.Schmidt, *Science* 259, 343 (1993).
14. L.D.Schmidt and M.Huff, *Catal.Today* 21, 443 (1994).
15. D.A.Hickman and L.D.Schmidt, *Catal.Lett* 17, 223 (1993).
16. P.D.F.Vernon, M.H.L.Green, A.K.Cheetham, A.T.Ashcroft, *Catal.Today* 14, 417 (1992).
17. A.M.O'Connor and J.R.H.Ross, *Catal.Today* 46, 203 (1998).
18. T.Innui, K.Saigo, Y.Fujioka, *Catal.Today* 26, 295 (1995).
19. S.Liu, G.Xiong, H.Dong, W.Yang, *Appl.Catal.A* 202, 141 (2000).
20. A.G.Steghuis, J.G.van Ommen, K.Seshan, J.A.Lercher, *Stud.Surf.Sci.Catal.* 107, 403 (1997).
21. A.G.Steghuis, J.G.van Ommen, J.A.Lercher, *Catal.Today* 46, 96 (1998).
22. A.Slagtern and U.Olsbye, *Appl.Catal.A* 110, 99 (1994).
23. J.Zhu, M.S.M.M.Rahuman, J.G.van Ommen, L.Lefferts, *Stud.Surf.Sci.Catal.* 147, 205 (2004).
24. *HSC Chemistry 4.1, Outokumpu Research Oy, Finland* (2002).
25. P.D.F.Vernon, M.L.H.Green, A.K.Cheetham, A.T.Ashcroft, *Catal.Lett* 6, 181 (1990).
26. P.M.Witt and L.D.Schmidt, *J.Catal.* 163, 465 (1996).

Chapter 3

Effect of Surface Composition of Yttrium-stabilized Zirconia on Partial Oxidation of Methane to Synthesis Gas

Abstract

Catalytic partial oxidation of methane to synthesis gas (CPOM) over yttrium-stabilized zirconia (YSZ) was studied within a wide temperature window (500~1100°C). The catalysts were characterized by X-ray fluorescence (XRF) and low-energy ion scattering (LEIS). The influence of calcination temperature, Y₂O₃ content and especially impurities such as CaO, TiO₂, Na₂O on catalytic performance was investigated. Creation of active sites by doping with Y₂O₃ improves the catalytic performance of ZrO₂ significantly. The surface composition rather than the bulk composition determines the catalytic performance of the catalysts in CPOM. As long as the YSZ catalyst is not contaminated, the composition of the outermost surface of calcined YSZ is independent of both the concentration of Y₂O₃ in the bulk and calcination temperature; the surface always contains 12±2 mol% Y₂O₃ due to segregation of Y₂O₃. Calcination at higher temperatures creates more active sites per m², while the catalyst loses surface area via sintering. The same sintering treatment causes decrease of the activity of YSZ containing trace of (earth) alkali oxides. The effect is probably due to segregation of the impurities to the surface, which either blocks active surface of the YSZ catalyst or forms new phases with different catalytic properties. However, it cannot be ruled out that enhanced segregation of Y₂O₃ contributes to this effect as well.

Heterogeneous reactions occur concurrently with homogeneous reactions at temperatures above 950°C during CPOM over YSZ. At such high temperatures, CPOM, steam- and CO₂ reforming, as well as reverse water-gas shift, compete with each other during CPOM. These reforming reactions of methane result in a significant increase of selectivity to synthesis gas, although the catalyst activity is still too low to reach thermodynamic equilibrium.

Key words: *Partial oxidation of methane; Synthesis gas; Yttrium-stabilized zirconia; Contamination; LEIS.*

3.1. Introduction

There has been a growing interest in the direct conversion of natural gas to CO and H₂ as a potential alternative to steam reforming of methane. The H₂/CO ratio of synthesis gas obtained by direct oxidation, $\text{CH}_4 + 1/2\text{O}_2 \rightarrow \text{CO} + 2\text{H}_2$ ($\Delta H = -22.2$ kJ/mol, 1000K) is more favorable for methanol synthesis and the Fischer-Tropsch process. Moreover, direct partial oxidation of methane to synthesis gas is mildly exothermic, whereas the steam reforming reaction is extremely endothermic.

The catalytic partial oxidation of methane (CPOM) to synthesis gas has been studied intensively for about two decades¹⁻⁵. The first row of transition metals (Ni, Co) and noble metals (Ru, Rh, Pd, Pt, and Ir) have been reported as active catalysts for CPOM. However, these metal catalysts are also good catalysts for CH₄ decomposition to carbon and H₂. The problem of carbon deposition on these catalysts remains to be solved. Recent studies have focused on developing a highly active and stable catalyst for CPOM. Mixed metal oxides NiO-MgO solid solution⁶, Ni-BaTiO₃⁷, Ni-Mg-Cr-La-O⁸ and Ca_{0.8}Sr_{0.2}Ti_{0.2}Ni_{0.2}⁹ were reported to be highly active and selective catalysts at high space velocities (10²-10³ m³/kg.h) and high temperatures (>700°C) with improved carbon resistance. A significant temperature gradient is observed in the catalyst bed due to highly exothermic combustion of methane at the entrance, followed by reforming reactions in the rest of the catalyst bed (indirect mechanism). On the other hand, direct partial oxidation of methane to synthesis gas was claimed under very short contact time in the order of a millisecond at extremely high temperatures (>1000°C) by Schmidt and co-workers¹⁻³. Evaporation of metal in the form of volatile metal oxides formed at high temperatures, especially in presence of oxygen, causes deactivation of the metal catalysts. Metal loss in the form of volatile oxide, which results in deactivation of the catalyst, is also a serious problem in the ammonia oxidation process operated under almost the same conditions^{10;11}.

Selectively partial oxidation of methane to synthesis gas over oxide catalysts has been often mentioned as a major side reaction in both oxidative coupling of methane over rare oxides¹² and partial oxidation of methane to formaldehyde on titania¹³. In our laboratory, CPOM over some irreducible metal oxides such as TiO₂, La₂O₃, and ZrO₂-based mixed oxides was studied by Steghuis *et al.*^{14;15} Yttrium-stabilized zirconia (YSZ) showed the best catalytic performance among these oxide catalysts. Compared with metal catalysts, the activity and selectivity are lower for YSZ. However, the stability is superior and the lower selectivity can be dealt with by introducing a second metal-based reforming catalyst that can be kept stable because contact with oxygen at high temperatures is avoided, as described in Chapter 2 and our previous publication¹⁶.

The objective of the present work is to determine whether the catalytic performance of YSZ can be further improved in terms of selectivity and activity by increasing the operation temperature or by changing the catalyst surface area. The roles of consecutive steam- and

CO₂- reforming reactions are investigated as well. The influence of the catalyst surface area as well as the surface composition is studied in detail.

3.2. Experimental

3.2.1. Catalysts

All catalysts were made of ZrO₂-based powder stabilized with different amounts of Y₂O₃, which were provided by TOSOH (Japan) and GIMEX (The Netherlands). Except pure ZrO₂ which was calcined at 900°C, YSZ samples were calcined at different temperatures (900°C, 1000°C or 1100°C) in air for 15 h. After calcination, the powder was pressed, crushed and sieved to 0.3-0.6 mm particles. According to the Y₂O₃ content in weight percentage and calcination temperature, the catalysts are referred as YSZ5A, YSZ9A, YSZ12A, YSZ12B, YSZ12C, YSZ14A, YSZ14B, and YSZ14C. In the sample code, YSZ means yttrium-stabilized zirconia, the number refers to weight percent of Y₂O₃ in the sample, and A, B and C represent the different calcination temperatures, 900°C, 1000°C and 1100°C respectively. Table 1 gives the details for all catalysts used in the present work.

3.2.2. Catalyst characterization

The BET surface area was determined by nitrogen adsorption at 77 K with a Micromeritics ASAP 2000 instrument. Prior to each measurement the sample was degassed at 300°C for 2 h under 0.1 Pa.

Chemical composition was measured by X-ray fluorescence (XRF) with a PW1480 (Philips) apparatus.

Surface composition of fresh samples was measured by low-energy ion scattering (LEIS) with the Calipso setup¹⁷, which has a double toroidal electrostatic energy analyzer. This gives a factor of 1000 higher sensitivity than the cylindrical mirror analyzer used in the past¹⁸. Another advantage of this setup is that the signals are virtually independent of the specific surface area of the catalyst¹⁹. As described in Ref.²⁰, before surface analysis, contaminations such as water and hydrocarbons were removed from the sample surface by annealing to 300°C and oxidation with atomic oxygen (Oxford Applied Research Atom/Radical Beam source MPD21). This treatment results in a clean YSZ surface without changing its inherent composition and structure²⁰. The LEIS measurements were done at room temperature with 3 keV ⁴He⁺ ions to determine concentrations of the impurities on the surface. Since Y and Zr are neighbors in the periodic system, it is impossible to separate them with He ion scattering. The Y₂O₃ content is, therefore, determined with 5 keV ²⁰Ne⁺ ions. Both pure ZrO₂ (Alfa, 99.9%) and Y₂O₃ (Alfa, 99.999%) were used as references. The Y₂O₃ concentration on the surface was estimated by fitting LEIS spectra of YSZ samples.

3.2.3. Catalytic measurement

The catalytic reactions were carried out using a fixed-bed reactor operated at atmospheric pressure. The catalyst (ca. 0.3 g) diluted with the same amount of α -Al₂O₃ was held by quartz wool. It was pretreated in an alumina reactor (inner diameter 4 mm) with a gas flow containing He (50 ml/min.) and O₂ (30 ml/min.) at 800°C for 1h, subsequently cooled down to reaction temperature in the flow of helium. In order to minimize the contribution of gas-phase reactions, two thin alumina sleeves were put in front of and behind the catalyst bed, which were used as thermocouple-wells as well. The blank experiments were performed either with 0.6 g α -Al₂O₃ or in the empty reactor. The typical reaction conditions were as following, unless specified otherwise: P_{CH₄} = 0.118 bar, P_{O₂} = 0.059 bar, balance with helium, total flow rate was kept at 170 ml/min.(STP). The temperature gradient of the catalyst bed caused by the reaction is about 2°C at 800°C when diluted CH₄ and O₂ are converted for 40% and 100% respectively. For the purpose of adding steam to the reaction, the reactant mixture can pass through a steam saturator by switching a four-port valve. Partial pressure of steam was determined by temperature of the saturator. Reaction temperature was varied and the system was kept at steady-state for two hours for analysis. On-line gas chromatography with Carboxan 1000 and Haysep N columns was used to analyze the effluent gases from the reactor. N₂ was used as an internal standard. Conversions (X) and yields (Y) were calculated according to:

$$X_{CH_4} = \frac{CH_4^{in} - CH_4^{out}}{CH_4^{in}}; \quad X_{O_2} = \frac{O_2^{in} - O_2^{out}}{O_2^{in}}; \quad Y_{CO} = \frac{CO^{out}}{CH_4^{in} + CO_2^{in}};$$

$$Y_{CO_2} = \frac{CO_2^{out} - CO_2^{in}}{CH_4^{in}}; \quad Y_{H_2} = \frac{H_2^{out}}{2CH_4^{in} + H_2O^{in}}; \quad Y_{H_2O} = \frac{H_2O^{out} - H_2O^{in}}{2CH_4^{in}}$$

3.3. Results

3.3.1. Surface composition

All samples studied in the present work are listed in table 1. The major contaminations detected by XRF are TiO₂ and HfO₂, which were found in all samples. However, compared with the samples provided by TOSOH (Japan), more TiO₂ is found in YSZ12A, YSZ12B and YSZ12C, which are provided by GIMEX (The Netherlands). The surface composition was measured with LEIS. All YSZ catalysts from TOSOH show identical surface Y₂O₃ concentrations within experimental error, independent of the Y₂O₃ content in bulk of the catalyst and of the calcination temperature. In contrast, high Y₂O₃ concentrations were detected in the outermost layer of YSZ samples provided by GIMEX. Moreover, it is also observed in these samples that more Y₂O₃ segregates to the outermost surface when the sample is calcined at higher temperatures.

Fig. 1 shows LEIS spectra of YSZ12C sputtered with different ⁴He⁺ ion intensities. A weak signal due to Y and/or Zr, which cannot be separated, is observed in the spectrum of YSZ12C

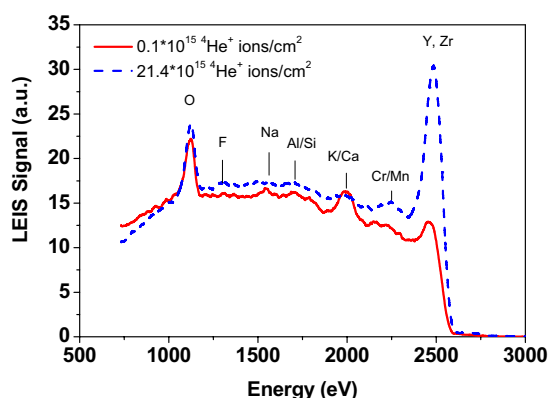


Fig. 1. LEIS spectra (3 keV, $^4\text{He}^+$) of fresh YSZ12C with different $^4\text{He}^+$ ion doses

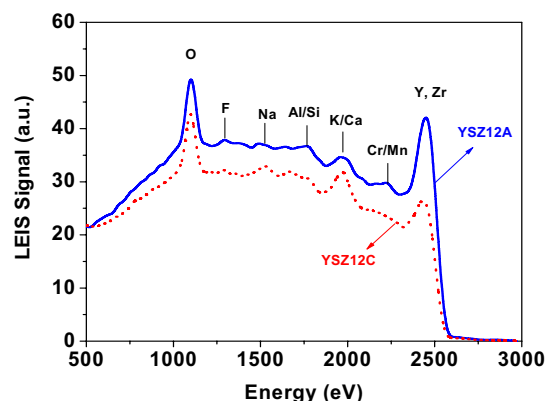


Fig. 2. LEIS spectra (3 keV, $^4\text{He}^+$) of fresh YSZ12A and YSZ12C

after sputtering with a low $^4\text{He}^+$ ion dose (0.1×10^{15} ions/cm²). Contaminating elements, such as F, Na, Al/Si, K/Ca, and Cr/Mn are detected on the outermost surface of YSZ12C. After extended sputtering (21.4×10^{15} ions/cm²), intensities of the impurities decrease significantly, though they are still detectable, and at the same time, the intensity of the Y-Zr LEIS signal increases by a factor of 2.4. So, it is roughly estimated that more than half of the outermost surface of YSZ12C is covered with impurities in the form of oxides. In contrast with YSZ12C (calcined at 1100°C), the spectrum of YSZ12A (calcined at 900°C), as shown in Fig. 2, shows less impurities on its outermost surface and the shielding of Y and Zr is much weaker.

LEIS spectra of YSZ14A (calcined at 900°C) and YSZ14C (calcined at 1100°C) are shown in Fig. 3. Unlike the surfaces of YSZ12A and YSZ12C, hardly any impurities were detected on the surfaces of YSZ14A and YSZ14C. The high purity of YSZ14 samples is confirmed by the fact that removal of impurities *via* sputtering causes only a modest increase in the Y-Zr signal as shown in Fig. 4. This effect is much smaller than that observed in Figs. 1 and 2. Comparable results were obtained for YSZ5A as well.

The major bulk impurities TiO_2 and HfO_2 , detected by XRF, are not observed on the outermost surface of any of the samples with LEIS.

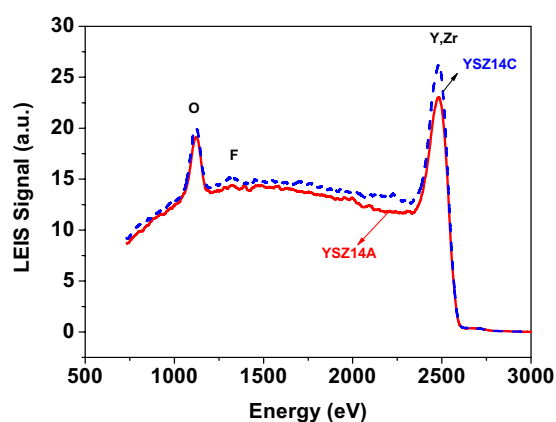


Fig. 3. LEIS spectra (3 KeV, $^4\text{He}^+$) of fresh YSZ14A and YSZ14C

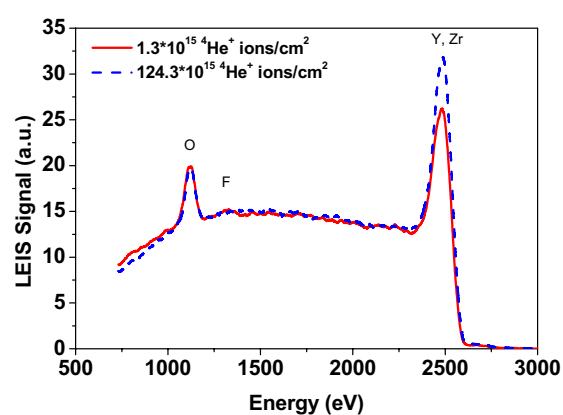


Fig. 4. LEIS spectra (3 keV, $^4\text{He}^+$) of fresh YSZ14C with different $^4\text{He}^+$ ion doses

Table 1. Composition, surface areas and suppliers of the samples used in the experiments

Catalyst	Calcination Temperature (°C)	S _g (m ² /g)	Composition (mol%)*				Surface [Y ₂ O ₃] (mol%)**	Supplier
			ZrO ₂	Y ₂ O ₃	TiO ₂	HfO ₂		
ZrO ₂	900°C	15.38±0.02	98.76	0.023	0.048	1.16	-	Tosoh, Japan
YSZ5A	900°C	14.93±0.01	95.63	3.19	0.005	1.16	14	
YSZ9A	900°C	13.12±0.02	93.74	5.13	0.005	1.13	-	
YSZ14A	900°C	13.72±0.02					11	
YSZ14B	1000°C	10.21±0.01	90.46	8.46	0.005	1.08	14	
YSZ14C	1100°C	7.03±0.02					12	
YSZ12A	900°C	22.03±0.02					19	
YSZ12B	1000°C	12.96±0.02	90.98	7.82	0.279	0.92	-	
YSZ12C	1100°C	4.46±0.03					29	

* Composition of the sample, measured with XRF

** Surface composition, measured with LEIS

3.3.2. CPOM over YSZ

3.3.2.1. ZrO₂ and YSZ

Catalytic tests were carried out over pure ZrO₂ and yttrium-stabilized ZrO₂ (YSZ) catalysts with comparable surface areas. The catalytic performance of YSZ14A is shown in Fig. 5 in a temperature window from 500°C to 900°C. Methane conversion reaches 31.5% at 650°C, when oxygen is consumed completely. CO, CO₂, H₂ and H₂O are major products of CPOM over YSZ14A, besides small amount of hydrocarbons (C₂H₄ and C₂H₆) formed via oxidative coupling in the high temperature region. Selectivities to the major products vary with reaction temperature. In contrast to temperatures above 600°C, selectivity to CO is higher than that to CO₂ at temperatures below 600°C. Similar catalytic performance was observed for YSZ5A and YSZ9A. In contrast, pure ZrO₂ and YSZ12B showed quite different catalytic activities and selectivities in the whole temperature window (500°C-900°C). For comparison, activities and selectivities of five ZrO₂-based catalysts at 600°C are presented in Fig. 6. Except for YSZ12B, YSZ catalysts are much more active than pure ZrO₂. The methane and oxygen conversions over YSZ5A, YSZ9A, and YSZ14A are twice as high as those over ZrO₂ at 600°C. However, YSZ catalysts show higher selectivities to CO and H₂ than ZrO₂. Similar catalytic performance is observed for YSZ5A, YSZ9A and YSZ14A at 600°C.

Compared with other YSZ catalysts, YSZ12B shows, in Fig. 6, much lower activity at 600°C, which is even lower than that of ZrO₂, but higher selectivity to CO and H₂. However, at 800°C, when oxygen is completely consumed, similar methane conversions are observed for all YSZ catalysts including YSZ12B. However, the product distribution over YSZ12B is quite

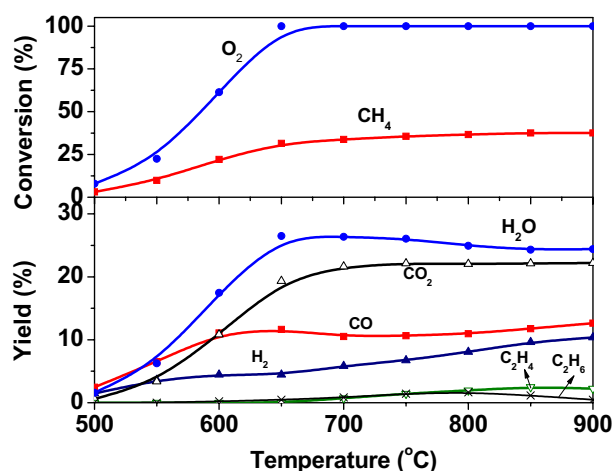


Fig. 5. Conversion/yield as a function of reaction temperature for CPOM on YSZ14A. Catalyst: 0.3 g YSZ14A diluted with 0.3 g α -Al₂O₃; CH₄:O₂:He=2:1:14, F_{total} = 170 ml/min.

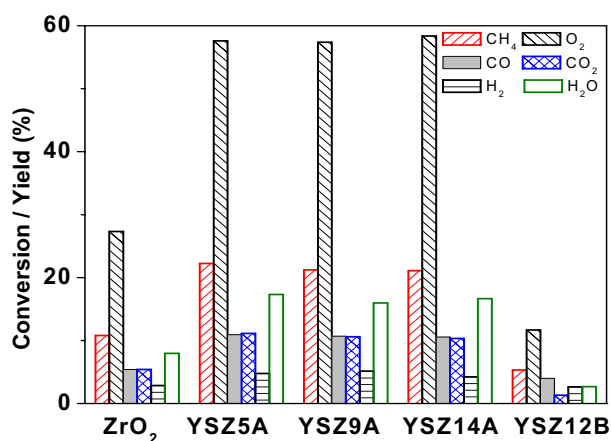


Fig. 6. Catalytic performance of ZrO₂ and YSZ catalysts at 600°C. Catalyst: 0.3 g, diluted with 0.3 g α -Al₂O₃; CH₄:O₂:He = 2: 1:14, F_{total} = 170 ml/min.

different. Comparing YSZ12B with other YSZ catalysts, significantly higher selectivities to CO and H₂O are observed, while selectivities to CO₂ and H₂ are lower. Therefore, the effect of the secondary reactions on the product distribution was studied for YSZ12 catalysts in more detail at temperatures above 900°C.

3.3.2.2. Influence of surface area

Fig. 7 shows the variation of CH₄ and O₂ conversions with the catalyst surface area and reaction temperature. A significant influence of the surface area on conversions of methane and oxygen is observed over YSZ12 catalysts. Homogeneous reactions in the gas phase started at around 900°C (empty reactor), which is more than 400°C higher than the initiation temperature of CPOM over YSZ12A. Compared with the YSZ catalyst, a minor activity of α -Al₂O₃ is observed at temperatures below 850°C. As shown in Fig. 7, the initiation temperature and T₉₀, at which 90% oxygen is converted, decrease with increasing surface area of the catalyst. Complete oxygen conversion is reached over YSZ12A with a surface area of 22 m²/g at 700°C; in contrast, e.g. on YSZ12C with a surface area of 4.5 m²/g, the oxygen conversion is well below 10% at the same temperature. CH₄ conversion increases dramatically over all catalysts with reaction temperature as long as oxygen is not exhausted. Only a slight increase in CH₄ conversion is observed after oxygen is consumed completely.

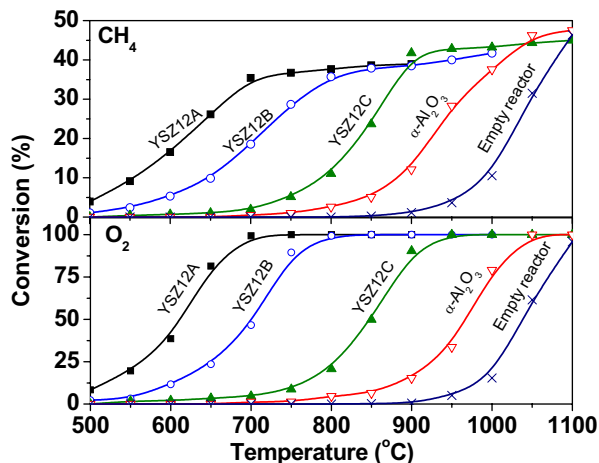


Fig. 7. CH₄ and O₂ conversions as a function of reaction temperature and surface area. Catalyst: 0.3 g, diluted with 0.3 g α -Al₂O₃; CH₄:O₂:He=2:1:14, F_{total} = 170 ml/min. Surface area: YSZ12A 22 m²/g; YSZ12B 13 m²/g; YSZ12C 4.5 m²/g.

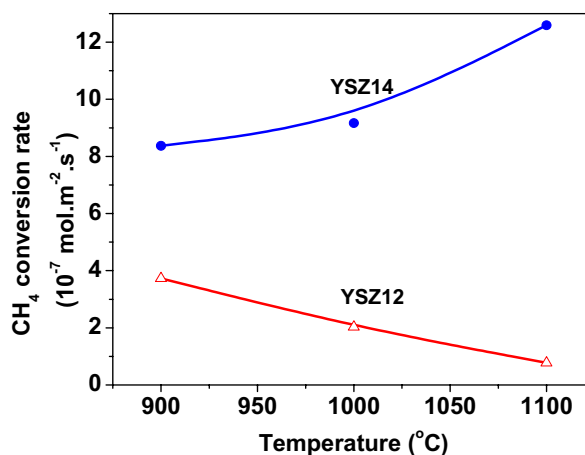


Fig. 8. CH₄ conversion rate at 600°C as a function of calcination temperature. Catalyst: 0.3 g, diluted with 0.3 g α -Al₂O₃; CH₄:O₂:He= 2:1:14, F_{total} = 170 ml/min.

3.3.2.3. Methane conversion rate

Experimental evaluation e.g. *via* the activation energy, is not feasible because the heat of reaction influences the reaction temperature and because catalysts are too active to allow

differential experiments at the space velocities that can be achieved. Therefore, any mass transfer limitation was evaluated by calculations in this work. According to the usual criteria (the Carberry number, and the Wheeler-Weisz modulus²¹), it can be concluded that mass transfer limitations can be neglected under the reaction conditions described in Fig. 6.

Fig. 8 shows CH₄ conversion rates in term of mol CH₄. m⁻².s⁻¹ at 600°C over YSZ12 and YSZ14 catalysts with varying surface area *via* sintering at different temperatures. The methane conversion rates over YSZ14 catalysts are significantly higher than those over YSZ12 catalysts. The calcination temperature influences the CH₄ conversion rate significantly. However, the trends are quite different for these two series of catalysts. For YSZ12 catalysts, CH₄ conversion rate (in mol CH₄. m⁻².s⁻¹) decreases by a factor of 5 on increasing the calcination temperature from 900°C to 1100°C. In contrast, the CH₄ conversion rate per m² over YSZ14 catalysts increases by a factor of 1.5 after calcination at 1100°C.

3.3.3. CPOM over YSZ at temperatures above 900°C

CPOM was carried out over YSZ12 series of catalysts at temperatures above 900°C in order to investigate the effect of the secondary reactions, such as CO₂- and steam-reforming of methane, and the water-gas shift reaction, on the product distribution. Fig. 9 shows conversions and yields as a function of reaction temperature for CPOM over YSZ12C. Because of the abovementioned small surface area and high impurity coverage, a low activity ($X_{\text{CH}_4} < 5\%$) was observed at temperatures below 800°C, whereas conversions of CH₄ and O₂ increased significantly above 800°C. The highest yields of water and CO₂ were obtained at 950°C; oxygen was exhausted while about 45% of the methane was converted. Yields of CO and H₂ increase dramatically at the expense of CO₂, H₂O and methane when the temperature was increased further.

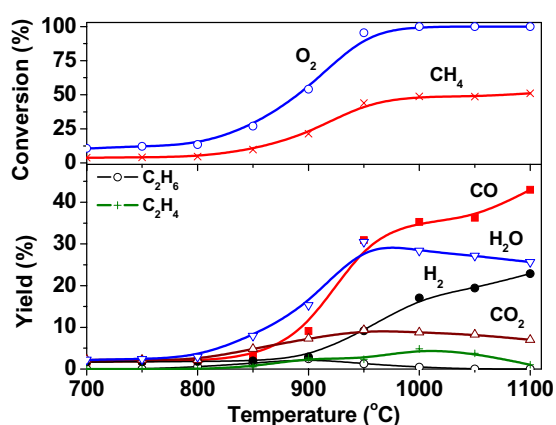


Fig. 9. Conversion/yield as a function of reaction temperature for CPOM on YSZ12C. Catalyst: 0.3 g YSZ12C diluted with 0.3 g α -Al₂O₃; CH₄:O₂:He=2:1:14, $F_{\text{total}} = 170$ ml/min.

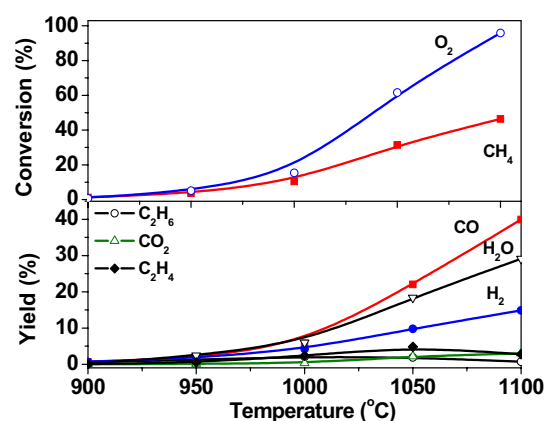


Fig. 10. Conversion/yield as a function of reaction temperature for oxidation in the empty reactor. CH₄:O₂:He=2:1:14, $F_{\text{total}} = 170$ ml/min.

Naturally, the homogeneous reaction in the gas phase will contribute more and more when the temperature is increased. As shown in Fig. 10, the contribution of the homogeneous reactions can be neglected at temperatures below 950°C. However, they will certainly contribute at temperatures above 950°C.

3.3.4. Coupling CPOM with steam or CO₂ reforming of CH₄

Effects of addition H₂O and CO₂ to the feed of CPOM over YSZ12C at 950°C are shown in Fig. 11. The product distribution obviously changes when H₂O is added to the feed, whereas the methane conversion increases slightly. Selectivities to CO and H₂ increases, while the CO₂ selectivity decreases.

Compared with adding H₂O, adding CO₂ to the feed significantly influences not only the product distribution but also methane conversion. Fig. 11 shows that methane conversion, as well as yields of CO and H₂O increase significantly, whereas the H₂ yield remains unchanged.

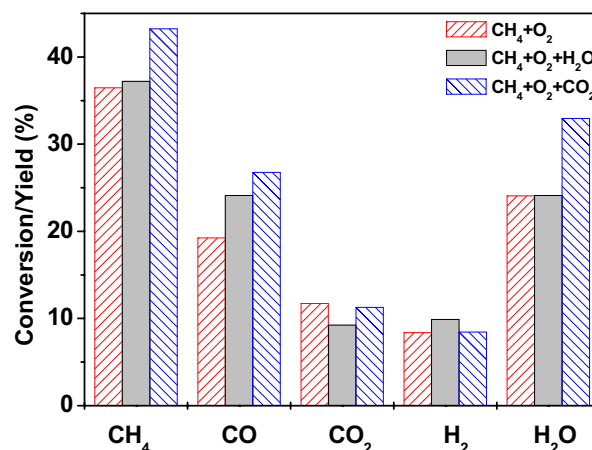


Fig. 11. Influence of CO₂ or H₂O addition to the feed on conversion and yields in partial oxidation of methane on YSZ12C at 950°C. Catalyst: 0.2g YSZ12C diluted with 0.2 g α -Al₂O₃; F_{total} = 170 ml/min. Normal feed: CH₄:O₂:He=2:1:14; H₂O addition: CH₄:O₂:H₂O:He=2:1 :0.6:13.4; CO₂ addition: CH₄:O₂:CO₂:He = 2:1:0.4:14.6.

3.3.5. Steam reforming of methane

Steam reforming reaction was carried out over YSZ12C under the same gas hourly space velocity (GHSV) of methane as used in the normal CPOM. As shown in Fig. 12, the initial reaction temperature for steam reforming of methane is about 850°C. Methane conversion reaches 18% at 1100°C. In addition to the major reforming products (CO and H₂), also CO₂ is detected in the product mixture at temperatures above 1000°C.

Steam reforming of methane was also carried out in an empty alumina reactor under identical reaction conditions. Methane conversion is only 3.8% at 1100°C, which is much smaller than that measured over YSZ12C. Except for small amounts of CO and H₂, no CO₂ was detected as a product in the effluent of the reactor.

3.3.6. CO₂ reforming of methane

Fig. 13 shows methane conversion and product distribution as a function of reaction temperature for CO₂ reforming of methane over YSZ12C. Under the same GHSV of methane as used in normal CPOM, CO₂ reforming reaction of methane starts at 800°C, and occurs significantly at temperatures above 1000°C. H₂O is also observed in the product at

temperatures above 900°C, though CO and H₂ are the major products. Methane conversion over YSZ12C reaches 20% at 1100°C; in contrast, only 4% of methane is converted in the empty alumina reactor.

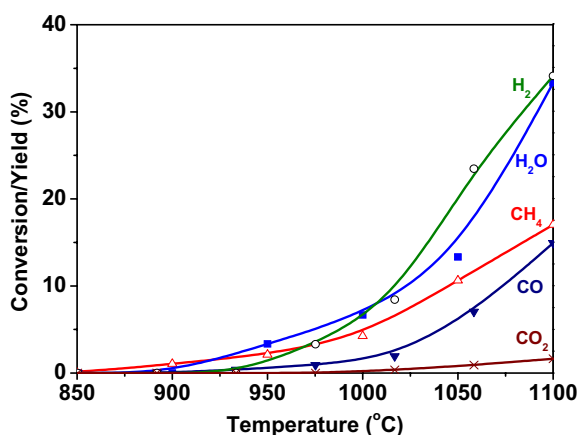


Fig. 12. Steam reforming reaction of methane on YSZ12C at different temperatures. Catalyst: 0.2g YSZ12C diluted with 0.2g α -Al₂O₃; Feed: CH₄:H₂O:He = 20:6:174 (ml/min).

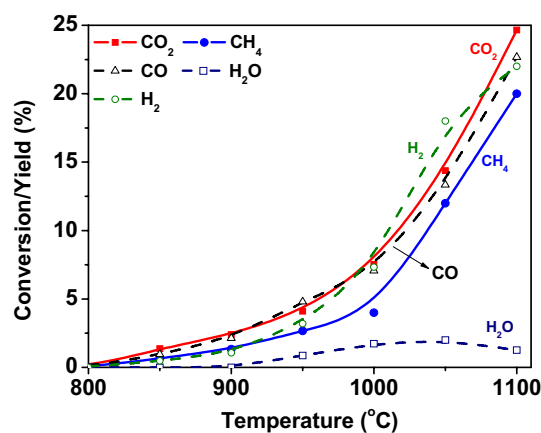


Fig. 13. CO₂ reforming reaction of methane on YSZ12C at different temperatures. Catalyst: 0.2 g YSZ12C diluted with 0.2 g α -Al₂O₃; Feed: CH₄:CO₂:He = 20:7.73:174 (ml/min).

3.4. Discussion

3.4.1. Active surface of YSZ

Comparing ZrO₂ with three YSZ catalysts, YSZ5A, YSZ9A, and YSZ14A, Fig. 6 clearly shows that yttrium-stabilized ZrO₂ is more active and selective than ZrO₂. These four catalysts were provided by TOSOH and have comparable surface areas and impurity contents. Before discussing this improved catalytic performance in more detail, the possible nature of the active sites will be discussed first.

The improvement of catalytic performance has been related to the presence of vacancies in many oxidation processes over mixed oxides²², e.g. the oxidation of propane over ZrO₂ and YSZ²³ and oxidative coupling of methane over rare earth oxides doped with strontium fluoride²⁴, Y₂O₃-CaO²⁵, and SrO- or ZnO-doped La₂O₃²⁶. The positive effect of doping is attributed to an increase in the concentration of oxygen vacancy, which favors the adsorption and activation of oxygen. The bulk properties of YSZ have been studied extensively by both experimental and theoretical methods^{27;28}. Very less is known about its surface structure. It is well known that oxygen vacancies can be created in ZrO₂ by adding ions with a low-valence such as Y³⁺, whereas pure ZrO₂ contains oxygen vacancies in very low concentration^{29;30}. Although the catalytic performance of ZrO₂-based catalyst is strongly influenced by the concentration of oxygen vacancies, the precise role of these vacancies in the activation of methane and/or oxygen is still not clear. This is the subject of ongoing work in our laboratory.

Obviously, the concentration of oxygen vacancies in YSZ increases with the Y_2O_3 concentration, which would increase the activity of YSZ. However, comparing YSZ5A with YSZ9A and YSZ14A, it is obvious that these three catalysts have similar activity and selectivity at 600°C (Fig.6). The results of LEIS measurements listed in table 1 show enrichment of Y_2O_3 in the outermost surface of these three catalysts. Almost identical compositions of the outermost surface are observed for YSZ5A and YSZ14A (12±2 mol % Y_2O_3), despite the differences in their bulk compositions. Comparable segregation phenomena were also reported by Theunissen *et al.*³¹, who studied the composition of grain boundaries as well as the surfaces of dense $(ZrO_2)_{100-x}(Y_2O_3)_x$ ($x=2\sim 16$) by AES and XPS. De Ridder *et al.*³² arrived at the same conclusion with LEIS. Therefore, the similarity in the catalytic performance of YSZ5A, YSZ9A and YSZ14A can be attributed to the similar surface composition (Y/Zr ratio), which appears to be independent of the bulk Y_2O_3 concentration. In the range of Y_2O_3 concentrations used in this work, the activity and selectivity of YSZ catalysts are apparently not influenced by the bulk composition.

3.4.2. Effects of contamination

The catalytic performance of YSZ12B is quite different from that of YSZ14A, as shown in Fig. 6, though both surface area and the Y_2O_3 concentration in the bulk are almost identical. As discussed above, the catalytic performance of ZrO_2 -based catalyst is strongly influenced by the surface composition. The major differences between YSZ12B and YSZ14A are the surface concentration of contaminants, which will be discussed first, and the Y_2O_3 concentration in the surface layer, which will be discussed secondly.

The surface of the YSZ12 catalysts is significantly contaminated with oxides, mainly CaO, as detected with LEIS (Figs. 1 and 2). The surface of the YSZ14 catalysts is much less contaminated (Figs. 3 and 4). Based on the LEIS measurements, it is estimated that about half of the outermost surface of YSZ12B is covered with these contaminations, mainly CaO. Significant segregation of traces of contaminations is consistent with the work of Brongersma and coworkers^{33,34}. These authors reported that the surface of YSZ was completely covered by contaminations after calcination at 1000°C, although the coverage with impurities was limited to only 16% after thermal treatment at 700°C for 1 h. Unlike the dense YSZ samples used by Brongersma *et al*, the surface area of the YSZ samples used in this work is up to 22 m²/g. The surface-to-bulk ratio of the samples in this work is thus much higher, resulting in less surface contamination. On the other hand, the diffusion distance for contaminations to reach the surface is much shorter which would lead to higher surface coverage of the contaminations. Moreover, calcination at high temperature not only results in the segregation of the impurities but also causes the sample to lose surface area *via* sintering (table 1), thus decreasing the surface-to-bulk ratio. These effects together lead to higher impurity coverage on the surface of YSZ12C compared to YSZ12A, as shown in Fig. 2. The segregation of CaO to the surface either simply blocks the active surface of YSZ, or forms new phases, such as calcium-

stabilized zirconia (CSZ), which should have different catalytic properties than YSZ. This explains the significant difference in catalytic performance between YSZ12B and pure YSZ catalysts (Fig. 6), as well as declining methane conversion rate (Fig. 8) with increasing calcination temperature for YSZ12 catalysts. Blocking the active surface by CaO was suggested also by Isupova *et al.*³⁵ to explain the low activity of La-Ca-Mn-O perovskites for CO oxidation.

However, at this stage it cannot be ruled out that high Y₂O₃ concentration in the surface leads to a decrease in activity, e.g. *via* clustering of the resulting oxygen vacancies. Clustering of oxygen vacancies is known to decrease the mobility of vacancies in the bulk of YSZ at concentrations above 8-12 mol%³⁶.

Two major impurities, TiO₂ and HfO₂, detected in the bulk of YSZ12B by XRF (shown in table 1) were not detected on the surface of YSZ12B by LEIS (see Fig.1 and Fig. 2). This is in agreement with the results of Ross *et al.*³⁷, who found a stronger segregation in YSZ for cations with low valence, such as Na⁺, Ca²⁺ and Mg²⁺, compared with the high valence impurities, like Ti⁴⁺ and Ce⁴⁺³⁷.

3.4.3. Effects of calcination temperature

As discussed above, calcination at high temperature results in a high coverage of impurities on the surface. The conversion rate of methane per surface area increases with the calcination temperature for the YSZ14 catalysts (Fig. 8), on which only minor surface contamination is detected with LEIS (Figs. 3 and 4). Moreover, these three catalysts have almost identical surface Y₂O₃ concentrations (Table 1). Apparently, a high calcinations temperature increases the number of active sites *via* modification of the surface structure. The same phenomenon was also observed in oxidation of CO over La-Ca-Mn-O perovskites by Isupova *et al.*³⁵. More details about the effect of calcination temperature on catalytic properties of YSZ are discussed in Chapter 6.

3.4.4. CPOM at high temperatures

The extremely high CO selectivity of YSZ12B at 800°C invoked a more detailed investigation of the catalytic performance of the YSZ12 series of catalysts at higher temperatures. As discussed above, due to the small surface area and high impurity coverage, YSZ12C shows a relatively low activity ($X_{\text{CH}_4} < 5\%$) in Fig. 9 at temperatures below 800°C. After all oxygen is exhausted, the product distribution varies with further increasing temperature, though only a slight increase of the CH₄ conversion is observed. This indicates that reactions between CH₄ and products (CO₂, H₂O), such as steam reforming and CO₂ reforming of methane, or among products, i.e., the reverse water-gas shift reaction, occur at higher temperatures. Oxidation of methane in the empty reactor, as shown in Fig. 10, occurs significantly at temperatures above 950°C. However, comparing the product distribution over YSZ12C (Fig. 9) with the product

distribution in the empty reactor (Fig. 10), significant differences are obvious, especially in the yields of H₂ and CO₂. Moreover, a significant difference in the level of conversions was observed at temperatures up to 1100°C with and without catalyst. These indicate that the catalyst still plays an important role, even at very high temperatures. The simultaneous occurrence of homogeneous and heterogeneous reactions was also reported, for example, by Leveles *et al.*³⁸ for oxidative dehydrogenation of propane over Li/MgO and by many other authors for oxidative coupling of methane^{39,40}. In addition to homogeneous and heterogeneous reactions taking place in parallel, the actual situation is much more complicated, because the catalyst may both generate and scavenge radical intermediates involved in the homogeneous reaction. This results in a complex reaction scheme, which is outside the scope of this work.

The increase in CO and H₂ yields after addition of H₂O to the feed (Fig. 11) indicates that steam reforming of methane ($\text{CH}_4 + \text{H}_2\text{O} \rightarrow \text{CO} + 3\text{H}_2$) occurs during CPOM at high temperatures, which is further confirmed by the direct observation of steam reforming of methane over the catalyst (Fig.13). The conversion of methane over YSZ12C (about 18% at 1100°C in Fig.13) is much higher than in the empty reactor, which gives only 3.8% methane conversion.

The activity of YSZ12C for CO₂ reforming of methane is obvious from the significant methane conversion observed during CO₂ reforming of methane over YSZ12C (Fig. 13), which is 5 times higher than in the empty reactor. Water formation during CO₂ reforming of methane over YSZ12C clearly indicates that the reverse water-gas shift reaction ($\text{CO}_2 + \text{H}_2 \rightarrow \text{CO} + \text{H}_2\text{O}$) occurs as well. The change in the product distribution when CO₂ is added to the feed of CPOM (Fig. 11) confirms that both CO₂ reforming of methane ($\text{CH}_4 + \text{CO}_2 \rightarrow 2\text{CO} + 2\text{H}_2$) and the reverse water-gas shift reaction take place during CPOM.

However, the reforming activity of YSZ is not sufficient to reach equilibrium, even at 1100°C. Many homogeneous and heterogeneous reactions are involved in CPOM over YSZ at temperatures above 900°C, as discussed before. The activity of the empty reactor for reforming reactions, although limited, suggests that also these reforming reactions proceed via an interweaved homogeneous-heterogeneous reaction network, similar to CPOM as discussed above.

3.5. Conclusions

Catalytic partial oxidation of methane to synthesis gas was studied over ZrO₂, pure YSZ and YSZ containing oxide contaminations in a wide temperature window. Doping ZrO₂ with Y₂O₃ generates active sites, resulting in improved catalytic performance. The composition of the outermost surface rather than the bulk of YSZ clearly determines the catalytic performance.

The composition of the outermost surface of calcined YSZ is independent of both the concentration of Y₂O₃ in the bulk and calcination temperature as long as the YSZ catalyst is not contaminated; the surface always contains 12±2 mol% Y₂O₃ due to segregation of Y₂O₃. More active sites are created per m² after calcination at higher temperatures.

Sintering causes the activity of YSZ containing traces of (earth) alkali oxides to collapse. This effect is probably due to segregation of the impurities to the surface. However, it can not be ruled out that enhanced segregation of Y_2O_3 contributes to this effect.

Heterogeneous reactions occur concurrently with homogeneous reactions at temperatures above 950°C during CPOM over YSZ. Catalytic performance of YSZ can be improved by a raise in the reaction temperature to 950°C and above, due to dry reforming, steam reforming and the reverse water-gas shift reactions. Nevertheless, thermodynamic equilibrium is not even approached, even at very high temperatures, because of insufficient reforming activity.

Acknowledgements

This work was performed under the auspices of NIOK, the Netherlands Institute of Catalysis Research. Stichting Technische Wetenschappen (STW, Dutch Foundation of Applied Sciences) is gratefully acknowledged for financial support under project number UPC-5037. The authors thank Prof. H.H. Brongersma, Dr. M. de Ridder and Mr. A. Knoester (Calipso LEIS Expertise Center) for LEIS measurements and fruitful discussions. Thanks to Ing. V. Skolnik for the measurement of the BET surface area, and to Ing. J.A.M. Vrieling for XRF analysis.

References

1. D.A.Hickam and L.D.Schmidt, *Science* 259, 343 (1993).
2. D.A.Hickman, E.A.Haupfear, L.D.Schmidt, *Catal.Lett.* 17, 223 (1993).
3. D.A.Hickam and L.D.Schmidt, *AIChE J.* 39, 1164 (1993).
4. V.R.Choudhary, V.H.Rane, A.M.Rajput, *Appl.Catal.A* 162, 235 (1997).
5. A.T.Aschcroft, P.D.F.Vernon, M.L.H.Green, *Nature* 344, 319 (1990).
6. V.R.Choudhary, B.S.Uphade, A.S.Mamman, *J.Catal.* 172, 281 (1997).
7. R.Shiozaki et al., *J.Chem.Soc., Faraday Trans.* 93, 3235 (1997).
8. P.Chen, H.B.Zhang, G.D.Lin, K.P.Tsai, *Appl.Catal.A* 166, 343 (1998).
9. T.Hayakawa et al., *Appl.Catal.A* 149, 391 (1997).
10. M.M.Karavayev, A.P.Zasorin, N.F.Kleshchev, *Catalytic oxidation of ammonia, Khimia, Moscow* (1983).
11. T.H.Chilton, *Chem.Eng.Progr.Monogr.Ser.* 3, 56 (1960).

12. K.D.Campbell, H.Zhang, J.H.Lunsford, *J.Phys.Chem.* 92, 750 (1988).
13. A.Parmaliana and F.Arena, *J.Catal.* 167, 57 (1997).
14. A.G.Steghuis, *Ph.D thesis, University of Twente, The Netherlands* (1998).
15. A.G.Steghuis, J.G.van Ommen, J.A.Lercher, *Catal.Today* 46, 91 (1998).
16. J.Zhu, M.S.M.M.Rahuman, J.G.van Ommen, L.Lefferts, *Appl.Catal.A* 259, 95 (2004); Chapter 2.
17. H.H.Brongersma et al., *Nucl.Instrum.Meth.B* 190, 11 (2002).
18. H.H.Brongersma, N.Hazewindus, J.M.van Nieuwland, A.M.M.Otten, A.J.Smets, *Rev.Sci.Instr.* 49, 707 (1978).
19. W.P.A.Jansen et al., *Surf.Interface Anal.* 36, 1469 (2004).
20. M.de Ridder, R.G.van Welzenis, H.H.Brongersma, *Surf.Interface Anal.* 33, 309 (2002).
21. R.A.van Santen, P.W.N.M.van Leeuwen, J.A.Moulijn, B.A.Averill, *Catalysis; An integrated approach* (Elsevier, Amsterdam, 1999).
22. E.N.Voskresenskaya, V.G.Rogueva, A.G.Anshits, *Catal.Rev.Sci.Eng.* 37, 101 (1995).
23. M.Labaki, S.Siffert, J.F.Lamonier, E.A.Zhilinskaya, A.Aboukais, *Appl.Catal.B* 43, 261 (2003).
24. R.Long, Y.Huang, W.Weng, H.Wan, K.Tsai, *Catal.Today* 30, 59 (1996).
25. Y.Osada et al., *Appl.Catal.A* 59, 59 (1990).
26. H.Borchert and M.Baerns, *J.Catal.* 168, 315 (1997).
27. J.P.Goff, W.Hayes, S.Hull, M.T.Hutchings, K.N.Clausen, *Phys.Rev.B* 59, 14202 (1999).
28. S.Fabris, A.T.Paxton, M.W.Finnis, *Acta Materialia* 50, 5171 (2002).
29. N.Mommer, T.Lee, J.A.Gardner, W.E.Evenson, *Phys.Rev.B* 61, 162 (2000).
30. E.Karaoetrova et al., *J.Am.Ceram.Soc.* 84, 65 (2001).
31. G.S.A.M.Theunissen, A.J.A.Winnubst, A.J.Burggraaf, *J.Mater.Sci.Lett.* 8, 55 (1989).
32. M.de Ridder et al., *Nucl.Instrum.Meth.B* 190, 732 (2002).
33. M.de Ridder, A.G.J.Vervoort, R.G.van Welzenis, H.H.Brongersma, *Solid State Ionics* 156, 255 (2003).
34. M.de Ridder, R.G.van Welzenis, H.H.Brongersma, U.Kressig, *Solid State Ionics* 158, 67 (2003).

35. L.A.Isupova et al., *Solid State Ionics* 141-142, 417 (2001).
36. A.Bogicevic and C.Wolverton, *Phys.Rev.B* 67, 24106 (2003).
37. I.M.Ross, W.M.Rainforth, D.W.Mccomb, A.J.Scott, R.Brydson, *Scripta Materialia* 45, 653 (2001).
38. L.Leveles, K.Seshan, J.A.Lercher, L.Lefferts, *J.Catal.* 218, 296 (2003).
39. K.M.Dooley, S.Y.Chen, J.R.H.Ross, *J.Catal.* 145, 402 (1994).
40. G.C.Hoogendam, K.Seshan, J.G.van Ommen, J.R.H.Ross, *Catal.Today* 21, 333 (1994).

Chapter 4

Reaction Scheme of Partial Oxidation of Methane to Synthesis Gas over Yttrium-stabilized Zirconia

Abstract

Partial oxidation of methane to synthesis gas over yttrium-stabilized zirconia (YSZ) was studied with in-situ FTIR and both steady state- and transient- experiments. The four major products, CO, H₂, CO₂ and H₂O are primary products of CPOM over YSZ. Besides these major products and traces of hydrocarbons, traces of formaldehyde and formic acid were observed in the product mixture for the first time, especially at high reaction temperatures. In-situ IR showed that formate was formed by activation of methane on the surface of YSZ catalyst under reaction conditions at temperatures between 400°C and 475°C. Adsorbed formaldehyde was never observed, due to rapid conversion to formate. Temperature-programmed desorption/decomposition (TPD/TPDE) of formate resulted in an essentially identical mixture of CO, CO₂, H₂, and H₂O to normal CPOM. Addition of formaldehyde to the CPOM reaction mixture caused the yields of CO, CO₂, and H₂ to increase without influencing the product distribution. This is a strong indication that CH₂O is indeed an intermediate product, in agreement with the fact that traces of formaldehyde were observed in the product mixture. A reaction scheme is proposed that contains exclusively reaction pathways that contribute significantly; the ratios between the competing pathways is strongly influenced by temperature but does not vary at all when formaldehyde is added. CO and H₂ are formed via decomposition of both adsorbed formaldehyde and formate, while CO₂ is produced via decomposition of formate mainly. Activation of methane is the rate-determining step at 600°C and higher temperature.

Key words: *Partial oxidation of methane; Synthesis gas; Yttrium-stabilized zirconia; Reaction mechanism; Formate; Formaldehyde.*

4.1. Introduction

The large amount of natural gas found worldwide has recently led to extensive research in the area of methane conversion. None of the catalytic processes proposed as direct methods for methane utilization, such as oxidative coupling, partial oxidation to methanol or formaldehyde etc., is yet mature for industrial exploitation due to the limited yields, in spite of the efforts and resources devoted to increase those yields¹. Therefore, indirect utilization of natural gas has attracted more and more attention. Catalytic partial oxidation of methane to synthesis gas (CPOM) is one of the most attractive options among these indirect transformation routes, because of its mild exothermic heat of reaction and suitable H₂/CO ratio for downstream processes, such as methanol synthesis and Fischer-Tropsch synthesis. Green *et al.*² discussed three main types of catalysts for CPOM in detail: the first group of catalysts are supported nickel, cobalt and iron, the second group is based on noble metals and transition metal carbide catalysts are the third group. A considerable amount of work concerning the reaction mechanism of CPOM over the metallic catalyst has been done. Two general mechanisms for the partial oxidation of methane to synthesis gas have been proposed. The so called “indirect mechanism” claims that methane is combusted to CO₂ and H₂O, followed by both steam and carbon-dioxide reforming^{3,4} as consecutive reactions. The “direct mechanism” proposed by Schmidt⁵⁻⁷ assumes that methane is directly converted to CO and H₂, without initial deep oxidation. This issue is important because the indirect mechanism will cause huge temperature gradients in the reactor.

However, metallic catalysts are suffering from deactivation by sintering of metal and/or support and from evaporation of the metal in form of volatile metal oxide formed at very high temperatures, especially in the presence of oxygen^{8,9}. Metal loss in the form of volatile oxide, which contributes to deactivation of the catalyst, is also a serious problem in the ammonia oxidation process over Pt-Rh gauzes operated at similar conditions as CPOM¹⁰.

Mixed oxides have been extensively studied for the oxidative conversion of methane to methanol¹¹⁻¹³, formaldehyde¹²⁻¹⁵, methyl formate¹⁶, hydrocarbons^{17,18} and oxidative coupling of methane^{19,20}. CPOM has often been reported as a major side reaction in these processes. Steghuis²¹ and Stobbe²² investigated oxidation of methane over some oxide catalysts, such as ZrO₂, Y₂O₃, La₂O₃/ZrO₂, yttrium-stabilized zirconia (YSZ), and TiO₂. Among these irreducible oxides, YSZ was the most active catalyst for CPOM. These catalysts show lower activity and selectivity compared to metal catalysts. However, catalyst stability is superior and the issue of lower selectivity can be dealt with by introducing a second metal-based reforming catalyst bed that can be kept stable because contact with oxygen at high temperatures is avoided as described in Chapter 2 and our previous publication²³.

Stobbe *et al.*²² concluded, based on the relation between methane conversion and selectivities over ZrO₂, that CO and H₂ are primary products of CPOM over ZrO₂, whereas CO₂ is formed by water-gas shift and oxidation of CO. Steghuis²¹ proposed a reaction mechanism of CPOM over YSZ, including homolytic dissociation of methane over O_(s) sites followed by

conversion to CO, H₂ and H₂O *via* the formation and decomposition of formaldehyde as an intermediate. CO₂ is produced by further oxidation of the reaction intermediate. However, a H₂/CO ratio in the product mixture significantly larger than one is observed²¹, implying that formaldehyde can not be the only source of CO and H₂.

The objective of the present work is to solve these issues and to complete the reaction scheme of CPOM over YSZ catalyst, including all essential reaction pathways. This information is essential to define a research strategy to achieve a higher selectivity with YSZ-based catalysts. In this work, CPOM over YSZ catalyst was studied with *in-situ* FTIR and catalytic experiments with methane and/or formaldehyde in both steady state experiments and transient experiments. Based on the obtained results, a modified reaction scheme will be proposed, including an estimation of the relative rate of each path.

4.2. Experimental

4.2.1. Catalysts

Yttrium-stabilized zirconia (YSZ) (Gimex, The Netherlands), which consists of 12 wt.% yttria in zirconia, was calcined at 600°C and 900°C respectively for 15 h. The BET surface areas of two resulted samples were 56 m²/g and 22 m²/g after calcination. We refer to these catalysts as YSZ12 and YSZ12A, respectively. YSZ12 powder was used mainly for *in-situ* infrared experiments because of its higher surface area. YSZ12A was crushed and sieved to 0.3-0.6 mm particles for catalytic testing.

4.2.2. Catalytic measurements

The CPOM was performed with a fixed-bed reactor made of an alumina tube (inner diameter, 4 mm; length, 450 mm) at atmospheric pressure. A mixture of 0.3 g YSZ12A with 0.3 g α-Al₂O₃ particles with the same particle size was fixed in the isothermal zone of the reactor by quartz wool. In order to minimize the contribution of the gas-phase reaction, two thin alumina sleeves (outer diameter, 3 mm) were placed above and below the catalyst bed in the reactor, which were used as thermocouple-wells as well. The reaction temperature was varied and the system was allowed to reach steady state within two hours. Reactants CH₄ and O₂ were diluted with helium (CH₄:O₂:He=2:1:14), and the total flow rate was about 170ml/min (STP). On-line gas chromatography with Carboxan 1000 and Haysep N columns was used to analyze the effluent gas from the reactor. N₂ was used as an internal standard. Conversions (X) and yields (Y) were calculated according to:

$$X_{CH_4} = \frac{CH_4^{in} - CH_4^{out}}{CH_4^{in}}; \quad X_{O_2} = \frac{O_2^{in} - O_2^{out}}{O_2^{in}}; \quad Y_{CO} = \frac{CO^{out}}{CH_4^{in}}; \quad Y_{CO_2} = \frac{CO_2^{out}}{CH_4^{in}}; \quad Y_{H_2} = \frac{H_2^{out}}{2CH_4^{in}}; \quad Y_{H_2O} = \frac{H_2O^{out}}{2CH_4^{in}}$$

Mass spectrometry was used to detect trace products, such as HCHO, CHOOH and C₂ products (C₂H₆, C₂H₄ and C₂H₂) by measuring mass-to-charge ratio (m/z) values¹⁵: 30 (HCHO), 46 (CHOOH) and 25 (C₂ hydrocarbons).

To study conversion of formaldehyde over YSZ under typical conditions for CPOM, a second tubular reactor was mounted to the catalytic setup, which was connected to the catalytic reactor. Para-formaldehyde with a particle size of 0.3-0.6 mm was loaded in this second reactor to generate formaldehyde gas flow by passing 100ml/min He through the reactor. The partial pressure of formaldehyde in the feed was controlled by the temperature of the second reactor. The formaldehyde stream was co-fed to the catalytic reactor with O₂ (10 ml/min), CH₄ (20 ml/min) and balanced with helium. The conversions (X) and yields (Y) were calculated according to:

$$X_{CH_4} = \frac{CH_4^{in} - CH_4^{out}}{CH_4^{in}}; \quad X_{O_2} = \frac{O_2^{in} - O_2^{out}}{O_2^{in}}; \quad Y_{CO} = \frac{CO^{out}}{CH_4^{in} + CH_2O^{in}}; \quad Y_{CO_2} = \frac{CO_2^{out}}{CH_4^{in} + CH_2O^{in}};$$

$$Y_{H_2} = \frac{H_2^{out}}{2CH_4^{in} + CH_2O^{in}}; \quad Y_{H_2O} = \frac{H_2O^{out}}{2CH_4^{in} + CH_2O^{in}}$$

Temperature-programmed oxidation of formaldehyde was carried out in the same setup. The composition of the product mixture was analyzed with mass spectrometry by following mass-to-charge ratio (m/z) values: 32 (O₂), 30 (HCHO), 16 (CH₄), 31 (CH₃OH), 28 (CO), 2 (H₂), 44 (CO₂), 18 (H₂O), 46 (CHOOH) and 25 (C₂ hydrocarbons).

4.2.3. *In-situ* Infrared spectroscopy

Fig. 1 shows a scheme of the *in-situ* IR system, which consists of a Nicolet 20SXB FTIR spectrometer and a mass spectrometer. The stainless steel IR cell was constructed as a continuously stirred tank reactor (1.5 cm³) equipped with two CaF₂ windows. Mass flow controllers were used to control all gas flow rates. The catalyst powder (about 10 mg) was pressed into a self-supporting wafer. By switching the four-port valve, the composition of the gas could be changed between inert (helium) and reactive gas. The IR spectra were collected with

resolution of 4cm⁻¹ and treated by the Nicolet OMNICTM software. IR results are presented as difference spectra by subtracting the spectrum of the catalyst sample in helium. Before measurement, the catalyst sample was activated *in-situ* at 600°C for 30 min with 20% O₂ in helium, subsequently, cooled down to the reaction temperature in helium. The effluent composition was monitored with a quadrupole mass spectrometer (Balzers QMG 420). A blank experiment was carried out with an empty cell under identical conditions; no conversion of CH₄ and O₂ was observed.

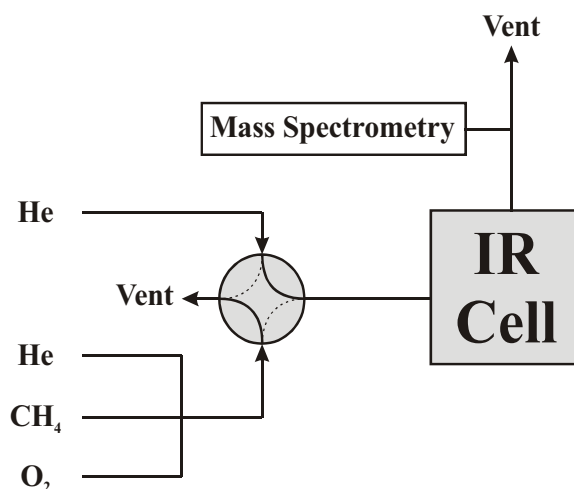


Fig. 1. Scheme of a flow system for *in-situ* IR measurement.

4.2.4. Temperature-programmed desorption/decomposition (TPD/TPDE)

4.2.4.1. TPD/TPDE in the IR cell

After formation of formate species *via* reaction of CH₄ and O₂ on YSZ12 at 400°C in the *in-situ* IR experiment (see results), the sample was cooled down to 50°C in He and kept at 50°C for 30 min in helium flow, subsequently heated up with a ramp of 10°C/min to 600°C and kept at 600°C for 10 min. The effluent composition was monitored with a quadrupole mass spectrometer (Balzers QMG 420).

4.2.4.2. TPD/TPDE in TPD setup

A homemade TPD setup equipped with a mass spectrometer (BALZERS QMS 200F) was used for temperature-programmed desorption (TPD) or temperature-programmed decomposition (TPDE) experiments. About 0.15 g of catalyst YSZ12A was placed in a quartz tube (reactor). After the catalyst was activated at 500°C and 10⁻³ mbar for 7 h, and subsequently, cooled down to 50°C, the mixture of reactants (CH₄/O₂=2:1) was introduced to the system till 7 mbar. Subsequently, the reactor was heated up to 400°C. After reaction at 400°C for 2 h, the system was evacuated at 400°C for 2 h to remove unconverted reactants and weakly adsorbed molecules. Then, the reactor was cooled down to 50°C, and TPD/TPDE was carried out with a heating rate of 10°C/min to 800°C and dwelled at 800°C for 1 h.

4.3. Results

4.3.1. Partial oxidation of methane over YSZ

Blank experiments in the empty alumina tubular reactor and with diluent α -Al₂O₃ particles exclusively, were carried out to check the activity of both reactor wall and α -Al₂O₃ particles. In the empty reactor only about 1% methane conversion was observed at 900°C. Compared with YSZ, α -Al₂O₃ was much less active for CPOM. The methane conversion over α -Al₂O₃ was less than 0.5% at 700°C, while at this temperature YSZ12A converted oxygen completely and about 40% of the methane already as shown in Fig. 2. Besides the four major products CO, H₂, CO₂ and H₂O, a small amount of hydrocarbons (C₂H₆, C₂H₄ and C₂H₂), formed *via* methane coupling, were observed as well over YSZ12A.

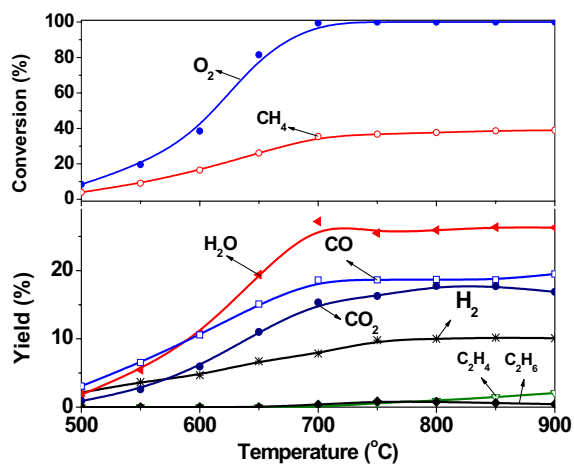


Fig. 2. Conversion / yield as a function of reaction temperature. Conditions: Catalyst 0.3 g YSZ12A diluted with 0.3g α -Al₂O₃, CH₄/O₂/He=2:1:14, F_{total}=170 ml/min.

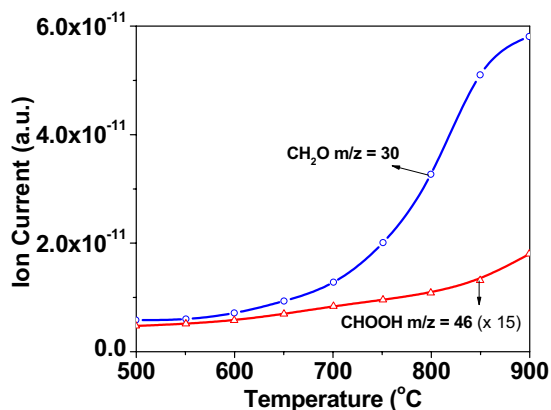


Fig. 3. Trace products in CPOM detected by mass spectrometer during CPOM over YSZ12A. Conditions: as shown in Fig. 2.

Traces of formaldehyde and formic acid were detected by mass spectrometry in the product mixture of CPOM. As shown in Fig. 3, the mass signals of HCHO (m/z , 30) and CHOOH (m/z , 46) increase with increasing reaction temperature.

Fig. 4 shows that the yields of CO, CO₂, H₂ and H₂O increase linearly with the methane conversion at 600°C up to 10% conversion, which was varied *via* the contact time by varying the amount of catalyst. In other words, the selectivities of the products are independent of the methane conversion, which indicates that CO, CO₂, H₂ and H₂O are primary products of CPOM. At 600°C, the selectivities to CO, CO₂ were 62% and 38%, and the H₂/CO and H₂/CO₂ ratios were 1.16 and 1.89 respectively.

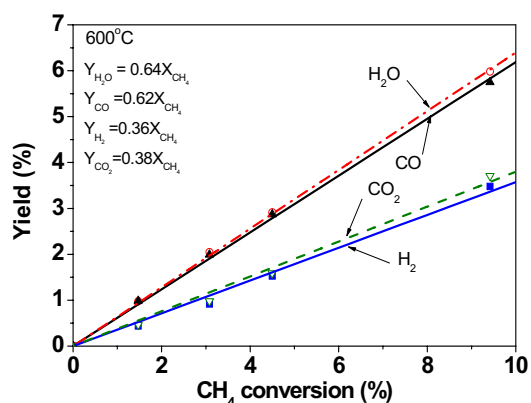


Fig. 4. Yield as a function of methane conversion. Catalyst: YSZ12A; Temperature: 600°C.

4.3.2. *In-situ* IR study

In-situ IR measurements were conducted on both YSZ12A and YSZ12 catalysts in the same gas mixture (11.8% CH₄, 5.9% O₂ and balance He) as used in the catalytic experiments. Very weak bands were observed on the surface of YSZ12A due to its low surface area. Therefore, *in-situ* IR study was carried out on YSZ12 in the present work, which has a higher surface area than YSZ12A. Fig. 5 shows FTIR absorbance spectra collected during reaction of CH₄ with O₂ on YSZ12 at different temperatures (30–475°C). Formate is the only surface intermediate observed exclusively above 400°C, characterized by the bands at 1575 ($\nu_{(as)}\text{OCO}$), 1384 (δ_{CH}) and

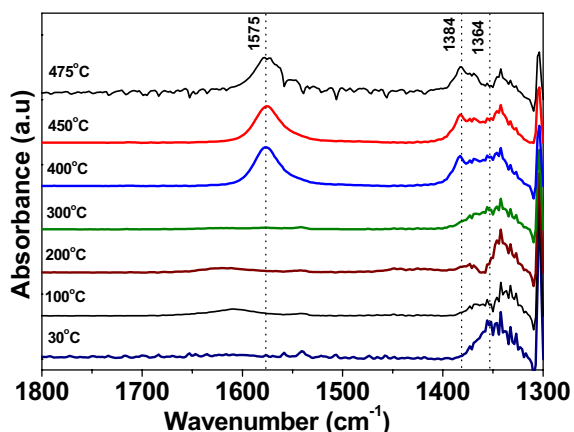


Fig. 5. *In-situ* IR spectra obtained during CPOM. Catalyst: YSZ12; Reactive gas: CH₄: O₂:He= 2:1:14; Total flow rate: 100 ml/min.

1364 cm^{-1} ($\nu_{\text{(s)}}\text{OCO}$). The ν_{CH} mode was observed at 2885 cm^{-1} , which is in agreement with the assignment to formate²⁴. The wave-numbers measured are similar to those reported by Busca et al.²⁵ for the formate species formed *via* the adsorption of formaldehyde on ZrO_2 at room temperature. The intensity of the formate bands hardly varies between 400°C to 475°C (the highest temperature that the IR cell can reach) although the noise increases at higher temperatures. No reaction products were detected in the effluent stream by mass spectrometry at any temperature from 30°C to 475°C .

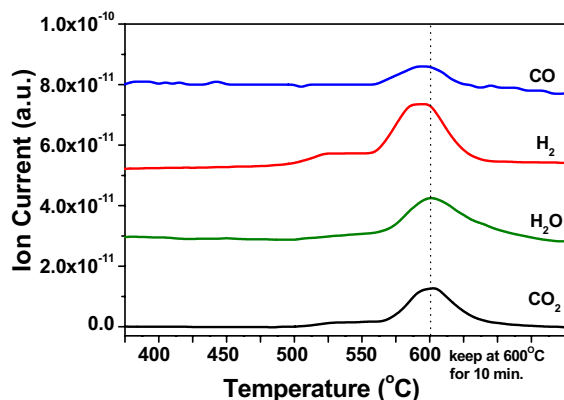


Fig. 6. TPD/TPDE profiles of formate species on YSZ12 surface (In IR cell).

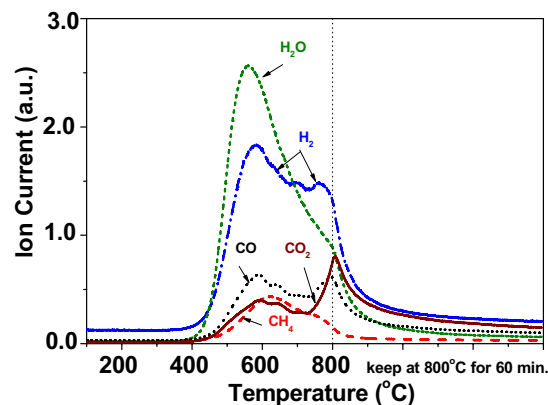


Fig. 7. TPD/TPDE after reaction of CH_4 and O_2 (2:1) at 400°C for 2 h on YSZ12A pretreated at 500°C for 7 h under 10^{-3} mbar. Evacuated at 400°C for 2 h.

4.3.3. TPD/TPDE of the formate on YSZ surface

After the formate was formed on YSZ12 in the *in-situ* IR experiment, TPD/TPDE was carried out in the infrared cell (Fig. 6). The major decomposition products of the formate species on the surface of YSZ12 are CO, CO_2 , H_2 , and H_2O .

TPD/TPDE experiments were also carried out on catalyst YSZ12A in a dedicated MS-TPD setup, which could reach a maximum temperature of 800°C (Fig. 7). Again, the same decomposition products (CO , CO_2 , H_2 , H_2O) are observed in addition of CH_4 desorbed from the surface of YSZ12A. Desorption starts between 400°C and 500°C and desorption was still not complete at 800°C . Two desorption peaks are observed for CO, H_2 , and especially CO_2 at 580°C and around 800°C respectively. The latter peak is obviously an artifact as the maximum temperature is 800°C so the actual second maximum temperature would be higher. Both water and methane do not show a convincing second desorption peak. The major amount of water is desorbed from the catalyst at relatively low temperatures with the maximum at 580°C .

4.3.4. Oxidative conversion of CH_2O

4.3.4.1. YSZ12A

Temperature-programmed oxidative conversion of CH_2O was carried out over 0.3 g YSZ12A catalyst with CH_2O and O_2 partial pressures of 0.033 bar and 0.029 bar (balanced with helium). Fig. 8 presents the product distribution at different temperatures. CO , CH_3OH and CH_4 were major products at temperatures below 350°C . Maximal yields of CO and H_2O are observed at about 350°C , coinciding with the temperature at which formaldehyde is just converted completely. At 500°C the yield of H_2 is maximal whereas the yield of H_2O exhibits a local minimum. At even higher temperatures, the yields of CO_2 and H_2O increase at the expense of CO and H_2 .

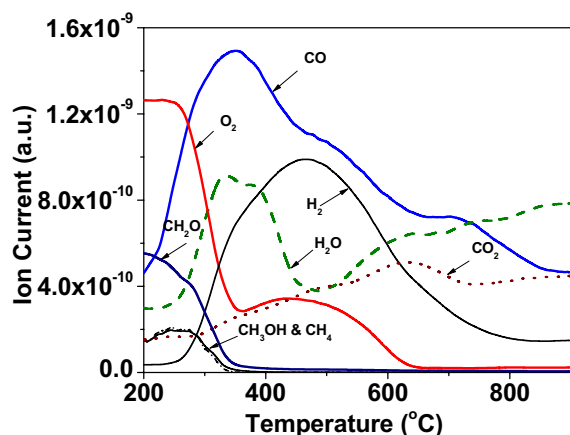


Fig. 8. Temperature-programmed oxidative conversion of CH_2O over YSZ12A with a heat rate of $10^\circ\text{C}/\text{min}$. $P_{\text{CH}_2\text{O}}=0.033$ bar; $P_{\text{O}_2}=0.029$ bar; catalyst: 0.3g YSZ12A diluted with 0.3g $\alpha\text{-Al}_2\text{O}_3$.

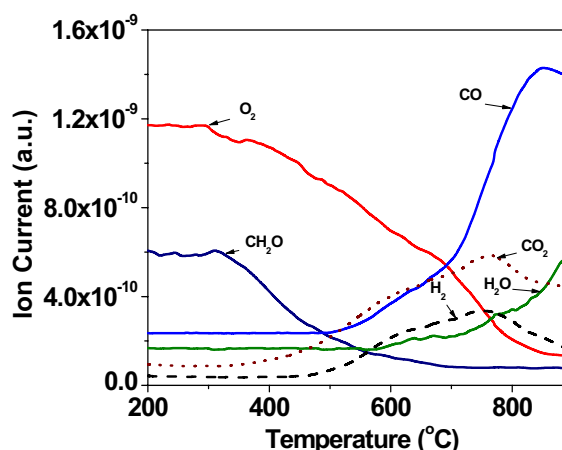


Fig. 9. Temperature-programmed oxidative conversion of CH_2O in an empty reactor with a heat rate of $10^\circ\text{C}/\text{min}$. $P_{\text{CH}_2\text{O}}=0.033$ bar; $P_{\text{O}_2}=0.026$ bar.

4.3.4.2. Empty reactor

The empty reactor gives completely different results compared to YSZ12A. Fig. 9 shows that CH_2O is not converted at all below 350°C , and the conversion is not complete even at 900°C . About 10% formaldehyde remains unconverted in the gas phase at 900°C . CH_3OH and CH_4 are not detected at any temperature between 200 and 900°C . Production of CO and H_2O increased with reaction temperature, and the maximal yields of CO_2 and H_2 were obtained at 750°C .

4.3.4.3. Co-feeding CH_2O with CH_4 and O_2

In order to study the conversion of formaldehyde over YSZ12A under typical conditions for normal CPOM, a small amount of CH_2O was added continuously to the mixture of feed gases with the same partial pressures of CH_4 and O_2 (balanced with helium) as used in the normal CPOM experiments. Conversions and yields are plotted as a function of CH_2O partial pressure in the feed gas in Fig. 10. Oxygen is completely converted at 800°C (Fig. 10a) and

the yields of CO, CO₂ and H₂ increase significantly with the increase of CH₂O partial pressure. In contrast, methane conversion and the yield of H₂O decrease with CH₂O introduced to the feed. At lower temperatures, e.g. 600°C (Fig. 10b), where oxygen is not consumed completely, the methane conversion is constant at 16%, independent of CH₂O partial pressure in the feed. The oxygen conversion and yields of CO, CO₂ and H₂ increase significantly with the CH₂O partial pressure. In contrast, the effect on the yield of H₂O is rather modest. In both experiments at 600°C and 800°C, the trace of formaldehyde detected in the effluent mixture from the reactor is about the same as detected in normal CPOM. The H₂/CO ratio and selectivities to CO and CO₂ as a function of CH₂O partial pressure at 600°C are shown in Fig. 11. Only minor changes in selectivities and H₂/CO ratio are observed when increasing the CH₂O partial pressure.

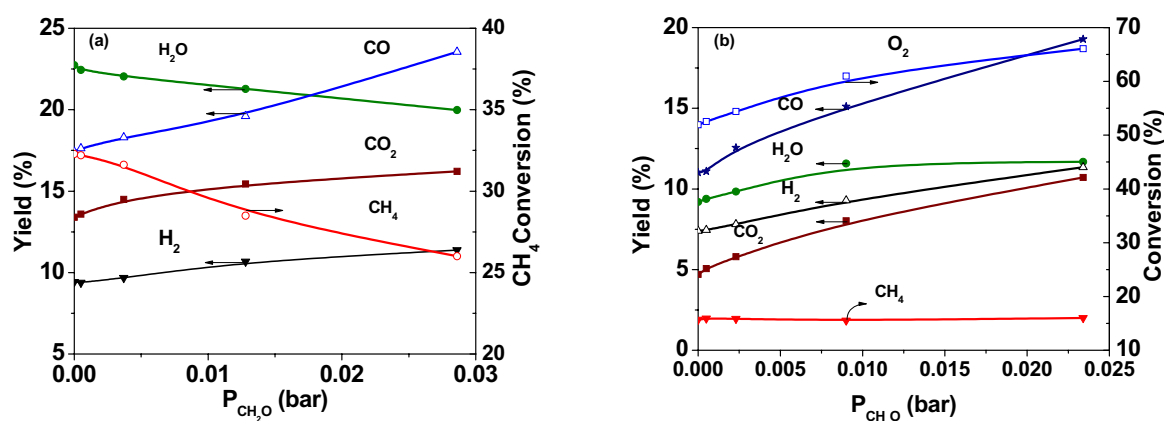


Fig. 10. The effects of CH₂O addition to the feed gas on conversions and yields at different reaction temperatures (a) 800°C (O₂ conversion: 100%), (b) 600°C. Catalyst: 0.3 g YSZ12A; Feed gases: P_{CH₄}=0.118 bar, P_{O₂}=0.059 bar, balance He. Total flow rate: 170 ml/min.

4.4. Discussion

4.4.1. Activation of methane

The formation of formate on surface of YSZ12, shown in Fig. 5, clearly indicates that methane is activated and reacts with oxygen at relatively low temperatures (around 400°C). The actual temperature of the sample wafer could be lower than that indicated in Fig. 5 because the measured temperature was that of the sample holder surrounded by heating wires. The same products (CO, CO₂, H₂, and H₂O) are observed during TPD/TPDE of formate in

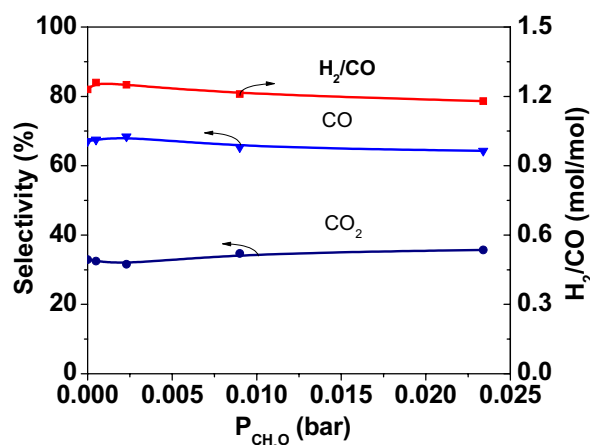


Fig. 11. Product distribution of formaldehyde oxidation over YSZ12A at 600°C under CPOM conditions. Conditions: as shown in Fig. 10.

both the IR cell and the TPD setup (quartz tube). The decomposition temperature on YSZ12 ($S_g=56 \text{ m}^2/\text{g}$) (Fig. 6) and on YSZ12A ($S_g=22 \text{ m}^2/\text{g}$) (Fig. 7) varies and the experiment in the dedicated TPD (Fig. 7) gives much more details because the IR-cell is not optimised for TPD experiments. The difference in the decomposition temperature might be caused by the different surface areas of these two catalysts. The formate species is so stable that no decomposition products could be detected in the effluent from IR cell at temperatures between 400 and 475°C, which agrees well with the results of TPD/TPDE shown in Fig. 6. This indicates that in the low temperature region, the rate-determining step of CPOM over YSZ is not the activation of methane but the decomposition of the formate. Nevertheless, the detection of a small amount of CO_2 during TPO of formaldehyde (Fig. 8) indicates that the oxidation of formate at low temperatures is possible. We will discuss the rate-determining step in more detail later.

The mechanism of activation of methane is one of the most important aspects in methane oxidation. However, the mechanism is still far from being understood on irreducible oxides. Most of the proposed mechanisms for the methane activation on irreducible oxides, like ZrO_2 , YSZ, Al_2O_3 , are based on the characterization of physical adsorbed methane on oxides at low temperatures ($<0^\circ\text{C}$)^{21;26}. Information on surface intermediates during methane oxidation over irreducible oxides under reaction conditions (e.g. temperatures above 400°C) is not available due to rapid transformation of the intermediates on oxides. In this study, it is the first time, to the best of our knowledge, that formate is observed on the surface of irreducible oxides, formed *via* oxidation of methane at relatively low temperature.

Doping ZrO_2 with yttrium results in not only the formation of a stable tetragonal or cubic phase, but also the generation of defects (oxygen vacancies) in the bulk of YSZ, strongly influencing the ionic conductivity of the material. The extent of the presence of those vacancies on the surface of YSZ is not known, but it seems reasonable to assume that the surface contains oxygen vacancies as well. The role of such oxygen vacancies or different types of surface oxygen species (e.g. O^- as reported by Steghuis²¹) in the activation of methane and oxygen on YSZ is also not clear yet. Investigation of the effects of the oxygen vacancies and surface hydroxyl groups is in progress in our lab. In this contribution we will limit ourselves to the reaction pathway, without going into details about the active sites that are involved in the reactions.

4.4.2. Reaction intermediates

Formaldehyde is often detected in the product mixture of partial oxidation of methane over many oxide catalysts^{16;20;27}. The detection of formaldehyde as an intermediate product here (Fig. 3) is not surprising. However, addition of a small amount of formaldehyde to the feed gas of CPOM results in a product mixture with identical H_2/CO ratio and selectivities to CO , CO_2 as observed in normal CPOM (Fig. 11). These identical results confirm that CH_2O is

indeed a reaction intermediate. The product distribution in Fig. 11 would have changed significantly, e.g. in the case that all formaldehyde added would have decomposed to CO and H₂.

The observation of formate on the surface of YSZ in the *in-situ* IR experiments and the similarity between the product distribution during TPD/TPDE of the formate intermediate (Figs. 6 and 7) and the product distribution during steady state CPOM (Fig. 2) indicate strongly that also formate is a reaction intermediate in CPOM. The observation of traces of formic acid in the mixture of CPOM product (Fig. 3), although very small, gives further support for this hypothesis. The surface formate was found on oxides in many processes, such as dry reforming of methane on Ru/ γ -Al₂O₃²⁸, hydrogenation of CO₂ over Ru/TiO₂²⁹, and adsorption of methanol and formaldehyde on Ce_xZr_{1-x}O₂²⁴ and on ZrO₂, TiO₂, Al₂O₃²⁵. Decomposition of formic acid and formate on oxides has been studied by many researchers^{30;31}. Two reaction routes are widely accepted for the decomposition of adsorbed formate³¹; dehydrogenation to CO₂ and H₂ versus dehydration to CO and H₂O.

Adsorption of formaldehyde on different oxides has been studied by Busca et. al²⁵ using FTIR spectroscopy between 170K and 570 K. Adsorbed formaldehyde can be observed only at extremely low temperature (around 170K), and transformation of formaldehyde to polyoxymethylene, dioxymethylene, formate and methoxy already occurs at such low temperatures. After heating up to 270~300K, only formate and methoxy species are observed on the surface of titania and zirconia. We studied adsorption of formaldehyde on YSZ by IR at room temperature. Only adsorbed formate and methoxy were observed on the surface of YSZ12. More detailed results of formaldehyde adsorption on YSZ will be reported in a future publication. However, the fast transformation of formaldehyde to formate on YSZ explains the fact that no adsorbed formaldehyde was observed on YSZ during the *in-situ* IR experiments.

Steghuis²¹ suggested that the decomposition of adsorbed formaldehyde is the only source of CO and H₂. If that would be the case, the H₂/CO ratio in the product mixture should be 1:1. It was shown in Chapter 3 as well as in Ref.²¹ that consecutive reactions, like steam reforming, CO₂ reforming, and water-gas-shift reaction, which would obviously influence the CO/H₂ ratio, can be neglected for temperature below 900°C. We have also investigated all possible reactions that may occur between CH₄ and CPOM-products, such as CO₂- and steam-reforming of methane, and among products, like water-gas shift and reverse water-gas shift reactions over YSZ catalysts in a wide temperature window (500°C-1100°C). The detailed results are presented in Chapter 3 and are consistent with Steghuis' conclusions. On the other hand, if all formaldehyde would transfer to surface formate that decomposes to CO, H₂O, CO₂, and H₂ under CPOM conditions, the ratio of H₂/CO₂ in the product mixture would be 0.5:1. However, the higher H₂/CO (>1.0) and H₂/CO₂ ratios (>0.5), shown in Fig. 4, imply that CO and H₂ are produced from both formaldehyde and formate.

Therefore, both formaldehyde and formate are reaction intermediates in CPOM over YSZ. A part of the adsorbed formaldehyde decomposes to CO and H₂, while the rest is oxidized to formate, which decomposes to CO and H₂O *via* dehydration, and to CO₂ and H₂ *via* dehydrogenation. Obviously, the H₂/CO ratio of the product mixture strongly depends on the relative rate of each reaction pathway, which will be discussed in more detail hereafter.

4.4.3. Reaction scheme

Based on the discussion so far we propose the reaction scheme shown in Fig. 12. As discussed in 4.2, activation of methane on the surface of YSZ results in the formation of surface formaldehyde (reaction 1). A part of the formaldehyde is further oxidized to formate on the surface (reaction 2). The rest of the formaldehyde decomposes on YSZ surface to CO and H₂ (reaction 5), and also possibly desorbs (step 6) and decomposes to CO and H₂ (reaction 8) in the gas phase. We also include the possibility that desorbed formaldehyde can be oxidized in gas phase to CO₂ and H₂O *via* reaction 7. Surface formate decomposes to a mixture of CO, CO₂, H₂ and H₂O (Figs. 6 and 7), which is in agreement with the reactions 3 and 4, as proposed earlier by Bianchi³¹. The surface formate species may be oxidized further to carbonate species, which decomposes to CO₂ at high temperature. Most of the water is produced in the first step (reaction 1), which explains well the fact that methane conversion influences water formation dramatically, as observed in Fig. 10a, whereas a very little contribution of CH₂O oxidation to the water formation is observed in Fig. 10b.

A number of reaction steps can be ruled out based on the experimental results. Oxidative conversion of formaldehyde was studied with temperature-programmed reaction over YSZ12A and in the empty reactor (Figs. 8 and 9). Compared with the reaction in the empty reactor, the oxidation of formaldehyde over YSZ12A is much faster. The conversion of formaldehyde in the gas phase is far from completion and does not exceed 90% even at 900°C (Fig. 9). In contrast, only a trace of formaldehyde was detected in the normal CPOM experiment under the same conditions. This suggests that the conversion of formaldehyde on the surface of YSZ12A is much faster than its desorption. Moreover, compared with decomposition of formaldehyde over YSZ, the decomposition in the gas phase is minor²¹ and this is also evident from the comparison between Fig. 8 and Fig. 9. Therefore, the conversion of adsorbed formaldehyde predominately occurs *via* decomposition and oxidation on the surface of YSZ12A (reactions 2 and 5). The contribution of reactions in the gas phase (reactions 6, 7, and 8) is not significant. Thus, the reaction paths with dotted arrows in Fig. 12 are not essential and can be neglected.

A remarkable decrease of methane conversion is observed when formaldehyde is added at 800°C, when oxygen is exhausted as shown in Fig. 10a. This indicates a competition in oxygen consumption by methane oxidation and oxidative conversion of formaldehyde. Apparently, the latter is much faster than the former, especially when it is taken into account that the formaldehyde concentration is roughly one order of magnitude lower than the

methane concentration. On the other hand, at 600°C and incomplete conversion of oxygen, the addition of formaldehyde causes a significant increase in yield of all major products due to complete conversion of the formaldehyde added to the reaction mixture. Therefore, it can be concluded that methane activation is the rate-determining step of CPOM over YSZ at 600°C and above.

Earlier we have seen that below 500°C methane is converted to adsorbed formate, without detectable further reaction to desorbed products.

Apparently, methane activation is faster than decomposition of formate. On the other hand, between 600°C and 800°C the activation of methane is rate-determining step. If this is to be explained in terms of the activation energy of both steps, it would follow that the activation energy of formate decomposition would be larger than for methane activation, which is very unlikely. Therefore, we propose that the activation of methane below 500°C proceeds *via* a reaction channel that is not accessible at higher temperatures. This might be the case, e.g. if a relatively unstable surface oxygen species is responsible, i.e. one that is not stable above 600°C.

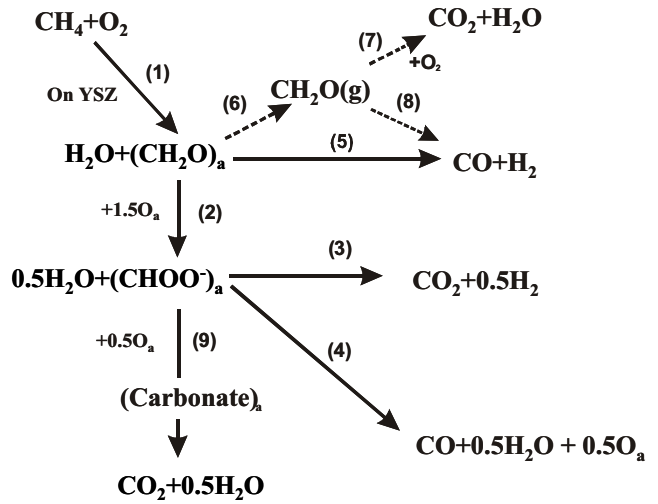


Fig. 12. The proposed reaction scheme for CPOM on YSZ.

4.4.4. Relative reaction rates

Based on the proposed reaction scheme (Fig.12), the rates of formation of the four main products and the consumption rate of oxygen can be expressed as $R_{H_2} = R_5 + 0.5R_3$; $R_{CO} = R_5 + R_4$; $R_{CO_2} = R_3 + R_9$; $R_{H_2O} = R_1 + 0.5R_2 + 0.5R_4 + 0.5R_9$; $R_{O_2} = R_1 + 0.75R_2 - 0.25R_4 + 0.25R_9$. At steady state, $R_2 = R_3 + R_4 + R_9$ and $R_1 = R_2 + R_5 = R_3 + R_4 + R_5 + R_9$.

Because $R_{H_2} = 2 \cdot Y_{H_2} \cdot F_{CH_4}$; $R_{CO} = Y_{CO} \cdot F_{CH_4}$; $R_{CO_2} = Y_{CO_2} \cdot F_{CH_4}$; $R_{H_2O} = 2 \cdot Y_{H_2O} \cdot F_{CH_4}$, and $R_{O_2} = X_{O_2} \cdot F_{O_2}$, where Y is yield, X is conversion and F is flow rate ($F_{CH_4} = 2F_{O_2}$), the relative rate of each reaction pathway can be expressed as below:

$$\text{Dehydrogenation of formate (reaction 3): } \frac{R_3}{R_3 + R_4 + R_5 + R_9} = \frac{12Y_{H_2} - 14Y_{CO} - 16Y_{CO_2} + 4X_{O_2}}{Y_{CO} + Y_{CO_2}};$$

$$\text{Dehydration of formate (reaction 4): } \frac{R_4}{R_3 + R_4 + R_5 + R_9} = \frac{4Y_{H_2} + 2X_{O_2} - 6Y_{CO} - 8Y_{CO_2}}{Y_{CO} + Y_{CO_2}};$$

$$\text{Decomposition of formaldehyde (reaction 5): } \frac{R_5}{R_3 + R_4 + R_5 + R_9} = \frac{7Y_{CO} + 8Y_{CO_2} - 4Y_{H_2} - 2X_{O_2}}{Y_{CO} + Y_{CO_2}};$$

CO₂ formation *via* decomposition of carbonate (reaction 9):

$$\frac{R_9}{R_3 + R_4 + R_5 + R_9} = \frac{14Y_{CO} + 17Y_{CO_2} - 12Y_{H_2} - 4X_{O_2}}{Y_{CO} + Y_{CO_2}}.$$

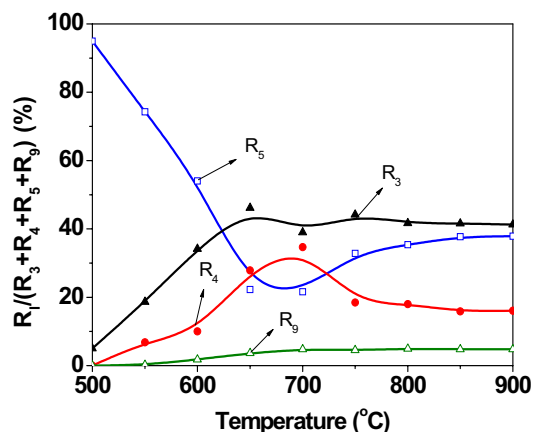


Fig. 13. The estimated relative rates of main reaction pathways as a function of reaction temperature. Based on the catalytic performance of YSZ12A presented on Fig. 1.

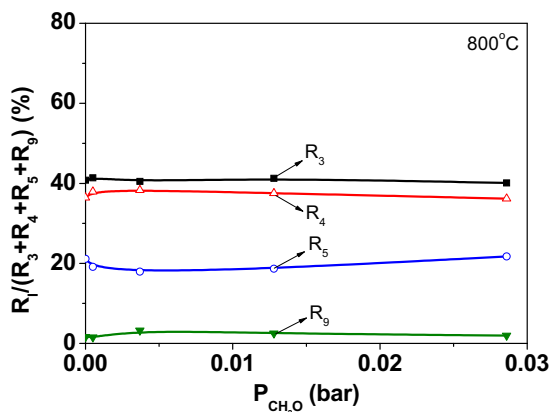


Fig. 14. Influence of formaldehyde added to the feed of normal CPOM on the relative rates, which is estimated based on product distribution as different partial pressures of formaldehyde presented on Fig.10(a).

So, the relative rate of each reaction pathway can be estimated based on the catalytic results shown in Fig. 2. Fig. 13 shows the estimated relative rates at different reaction temperatures. With increasing temperature, the rate of formaldehyde decomposition (reaction 5) decreases and reaches a constant value at about 750°C . In contrast, the relative rates of decomposition of formate (reactions 3 and 4) are almost zero at 500°C . This is in agreement with the fact that stable formate species on the surface of YSZ is observed in the TPD/TPDE experiments. Both dehydration and dehydrogenation of formate increase with increasing temperature, and only slight changes are observed at temperatures above 750°C . CO_2 is formed mainly *via* the decomposition of formate (reaction 3) and only about 10% of CO_2 is formed *via* decomposition of carbonate at temperatures above 700°C . Combining this with the fact that the carbonate species was not observed on the surface of YSZ12 in the *in-situ* IR experiment, it is concluded that the route *via* carbonate is minor in the formation of CO_2 .

Relative rates are also estimated based on the product distribution (Fig.10a) when CH_2O was co-fed with CH_4 and O_2 . The identical relative rates presented in Fig. 14, independent of partial pressure of formaldehyde in the feed, indicate that oxidation of methane on YSZ proceeds indeed *via* both decomposition and oxidative conversion of formaldehyde.

It is obvious, as shown in Fig. 12, that selectivity to synthesis gas depends strongly on the relative rates of three dominating reactions, reactions 3, 4 and 5. However, because of the fast oxidation of formaldehyde on the surface of oxide catalysts (reaction 2), the challenge in this system is to accelerate formaldehyde decomposition (reaction 5) or to prevent the oxidative conversion of formaldehyde to formate (reaction 2) in order to increase the selectivity to synthesis gas.

4.5. Conclusions

Partial oxidation of methane to synthesis gas has been investigated over YSZ. CO, H₂O, CO₂ and H₂ are primary products. Methane can be activated at 450°C to form a relatively stable formate species; however, this reaction channel is probably not available at high temperature. Formaldehyde and formate are two key reaction intermediates. CO and H₂ are formed *via* decomposition of both adsorbed formaldehyde and formate on the surface of YSZ, while CO₂ is produced *via* decomposition of the surface formate mainly. Most of H₂O is produced in the first step, the oxidation of methane to formaldehyde. Desorption of formaldehyde and subsequent decomposition or oxidation in the gas phase does not contribute significantly. Further oxidation of formate to carbonate, which decomposes to CO₂ at elevated temperatures, is also minor but still significant.

At low temperature (<500°C), the decomposition of the stable formate species is the step that prevents any reaction occurring. However, activation of methane is the rate-determining step at 600°C and above. A reaction scheme is proposed that contains exclusively reaction pathways that contribute significantly; the ratios between the competing pathways are strongly influenced by temperature but do not vary at all when formaldehyde is added.

Acknowledgements

This work was performed under the auspices of NIOK, the Netherlands Institute of Catalysis Research. Stichting technische wetenschappen (STW, the Dutch technology foundation) is gratefully acknowledged for financial support under project number UPC-5037.

References

1. J.M.Fox, *Catal.Rev.Sci.Eng.* 35, 169 (1993).
2. A.P.E.York, T.Xiao, M.L.H.Green, *Topics in Catal.* 22, 345 (2003).
3. A.T.Aschcroft et al., *Nature* 344, 319 (1990).
4. D.Dissanayake, M.P.Rosynek, C.Kharas, J.H.Lundford, *J.Catal.* 132, 117 (1991).
5. D.A.Hickman and L.D.Schmidt, *Science* 259, 343 (1993).
6. D.A.Hickman, E.A.Haupfear, L.D.Schmidt, *Catal.Lett.* 17, 223 (1993).
7. D.A.Hickman and L.D.Schmidt, *AIChE J.* 39, 1164 (1993).
8. S.Albertazzi et al., *Appl.Catal.A* 247, 1 (2003).
9. H.Jehn and J.Less, *Common Metals* 100, 321 (1984).

10. M.M.Karavayev, A.P.Zasorin, N.F.Kleshchev, *Catalytic oxidation of ammonia*, *Khimia, Moscow* (1983).
11. J.W.Chun and R.G.Anthony, *Ind.Eng.Chem.Res.* 32, 259 (1993).
12. T.Sugino, A.Kido, N.Azuma, A.Ueno, Y.Udagawa, *J.Catal.* 190, 118 (2000).
13. Q.Zhang, D.He, Z.Han, X.Zhang, Q.Zhu, *Fuel* 81, 1599 (2002).
14. T.Weng and E.E.Wolf, *Appl.Catal.A* 96, 383 (1993).
15. A.Parmaliana and F.Arena, *J.Catal.* 167, 57 (1997).
16. A.Parmaliana, F.Frusten, F.Arna, A.Mezzapica, V.Sokolovskii, *Catal.Today* 46, 117 (1998).
17. Y.Zeng, F.T.Akin, Y.S.Lin, *Appl.Catal.A* 213, 33 (2001).
18. R.Spinicci, P.Marini, S.De Rossi, M.Faticanti, P.Porta, *J.Mol.Catal.A* 176, 253 (2001).
19. K.D.Campbell, H.Zhang, J.H.Lundford, *J.Phys.Chem.* 92, 750 (1988).
20. S.Wada, T.Tagawa, H.Imai, *Appl.Catal.* 47, 277 (1989).
21. A.G.Steghuis, *Ph.d thesis, University of Twente, The Netherlands* (1998).
22. E.R.Stobbe, *Ph.d thesis, University of Utrecht, The Netherlands* (1999).
23. J.Zhu, M.S.M.M.Rahuman, J.G.van Ommen, L.Lefferts, *Appl.Catal.A* 259, 95 (2004); *Chapter 2*.
24. E.Finocjio, M.Daturi, C.Binet, J.C.Lavalley, G.Blanchard, *Catal.Today* 52, 53 (1999).
25. G.Busca, J.Lamotte, J.C.Lavalley, V.Lorenzelli, *J.Am.Chem.Soc.* 109, 5197 (1987).
26. C.Li, W.Yan, Q.Xin, *Catal.Lett.* 24, 249 (1994).
27. S.Wada and H.Imai, *Catal.Lett.* 8, 131 (1991).
28. P.F.Aparicio, I.R.Ramos, J.A.Anderson, A.G.Ruiz, *Appl.Catal.A* 202, 183 (2000).
29. M.Marwood R.Doepper and A.Renken, *Appl.Catal.A* 151, 223 (1997).
30. M.A.Henderson, *J.Phys.Chem.B* 101, 221 (1997).
31. D.Bianchi, T.Chafik, M.Khalfallah, S.J.Teichner, *Appl.Catal.A* 105, 223 (1993).

Chapter 5

Activation of O₂ and CH₄ on Yttrium-stabilized Zirconia for the Partial Oxidation of Methane to Synthesis Gas

Abstract

The isotopic exchange reaction on ZrO₂ and yttrium-stabilized ZrO₂ (YSZ) during catalytic partial oxidation of methane to synthesis gas (CPOM) was studied using transient pulse experiments. The results reveal that surprisingly CPOM over both oxides proceeds via a Mars-van Krevelen mechanism. Despite the presence of adsorbed oxygen species, as confirmed by isotopic exchange experiments under CPOM reaction conditions, methane is selectively oxidized by lattice oxygen ions on the surfaces of YSZ and ZrO₂. At 900°C, about 8% and 14% of lattice oxygen in the outermost surface layer of ZrO₂ and YSZ, respectively, can be extracted by methane. Extraction of lattice oxygen results in the formation of surface oxygen vacancies. However, the routes to replenish oxygen differ for both oxides. For ZrO₂, the extracted lattice oxygen ions are replenished by direct activation of molecular oxygen at the site of the surface vacancy. The presence of a high concentration of surface oxygen vacancies on YSZ, generated by doping ZrO₂ with Y₂O₃, enables fast activation of oxygen molecules as well as fast lattice diffusion of oxygen. The two effects together lead to a rapid replenishment of the surface lattice oxygen extracted by methane. The proposed mechanism explains both the comparatively high activity of YSZ in CPOM and the observation that, contrary to ZrO₂, lattice oxygen is found exclusively in oxidation products of methane over YSZ during the pulse experiments.

Key words: Zirconia; Yttrium-stabilized zirconia; Selective oxidation; Reaction mechanism; Oxygen vacancies; Partial oxidation of methane; Isotopic oxygen exchange.

5.1. Introduction

The use of natural gas as a raw material is a future goal of strategic importance, because of the impending decline in fossil-oil resources, and contemporarily, the large amounts of natural gas found worldwide. The direct processes to olefins and oxygenates, such as methanol and formaldehyde, are not attractive due to the low yields obtained. Therefore, considerable academic and industrial research has been focused on indirect processes proceeding *via* synthesis gas. Compared with steam reforming of methane, the conventional process for synthesis gas production, partial oxidation of methane to synthesis gas (POM), is attractive because of its mild exothermic heat of reaction and the suitable H₂/CO ratio for downstream processes, such as methanol and Fischer-Tropsch syntheses. Unlike non-catalytic partial oxidation, which needs high temperature (>1200°C) to ensure complete conversion of CH₄ and to reduce soot formation, catalytic partial oxidation (CPOM) would significantly decrease reaction temperature by using active catalysts. This makes CPOM an interesting proposition for synthesis gas production.

Normally, CPOM is carried out at a still relatively high temperature (above 900°C). The volatility of support materials or that of the active catalytic components is usually not considered as a problem. However, in the case of catalytic oxidation at these high temperatures volatilization of the active phase must be considered as an important factor for deactivation of the catalyst. As we discussed in our previous work (Chapters 2, 3 and 4)¹⁻³, metallic catalysts are suffering from deactivation due to sintering and metal loss *via* evaporation in the form of volatile metal oxides⁴. The stability of metal catalysts is still a concern, despite that CPOM over metallic catalysts has been intensively studied for about two decades⁵⁻⁷. Some hardly reducible oxides, possessing very good thermal stability, have been investigated for partial oxidation of methane to synthesis gas^{2,3;8-10}. Yttrium-stabilized zirconia (YSZ) appeared to be a promising catalyst for CPOM, despite of its insufficient reforming activity, which needs to be compensated with a reforming catalyst in a dual bed system¹, as proposed in Chapter 2.

In general, it is known that defects, e.g. oxygen vacancies, are important in the surface chemistry and catalysis of metal oxides¹¹. The number of oxygen vacancies in ZrO₂ can be increased significantly by doping with lower valence metal ions, such as Y³⁺ and Ca²⁺. Compared with ZrO₂, improved catalytic performance of YSZ in oxidation catalysis was attributed to a high concentration of oxygen vacancies^{3;12}. Lattice oxygen ions are often involved in reactions over oxide catalysts. Most of the partial oxidation reactions proceed *via* a Mars-van Krevelen mechanism, in which lattice oxygen ions are incorporated into the products¹³. The cycle for catalytic partial oxidation is closed *via* replenishing the extracted lattice oxygen ions through the dissociative adsorption of molecular oxygen at the surface¹⁴.

In Chapter 4, formaldehyde and formate were shown to be both reaction intermediates for CPOM over YSZ². Based on the results of *in-situ* FTIR and both steady-state and transient experiments, a reaction scheme was proposed. We also investigated the effect of the surface

composition of YSZ catalysts on the catalytic performance in CPOM. It was postulated that oxygen vacancies are most likely involved in CPOM³. However, the mechanistic details, in particular the role of oxygen vacancies and that of lattice oxygen ions in the partial oxidation of methane, are still not clear. Moreover, the nature of the oxygen species, e.g. surface lattice oxygen ions or adsorbed oxygen, in activation of methane is still a matter of controversy^{15;16}. In this work, we attempt to identify the active sites for activation of both oxygen and methane on the surfaces of YSZ and ZrO₂. CPOM is studied over ZrO₂-based catalysts using transient experiments. Isotopic oxygen ¹⁸O₂ exchange with the catalysts is investigated both in the absence and in the presence of methane and under reaction conditions for CPOM.

5.2. Experimental

5.2.1. Catalysts

Catalyst samples of ZrO₂ and YSZ were prepared by calcining powders of pure zirconia and stabilized zirconia with 14 wt% Y₂O₃ at 900°C, respectively. The YSZ sample used in this study is identical to the catalyst YSZ14A described in Chapter 3. After calcination for 15 h in air, the BET surface areas are 13.7 and 15.4 m²/g for YSZ and ZrO₂, respectively. TiO₂ and HfO₂ were found to be two major contaminations in the bulk, whereas no inorganic contamination was detected on the outermost layer by low-energy ion scattering (LEIS). More details about catalyst preparation and characterization are presented in Chapter 3.

2.2. Transient experiments

Pulse experiments using CH₄ and/or O₂ were performed in an alumina reactor with inner diameter of 4 mm. Helium (40 ml/min) with a purity of 99.99% was used as a carrier gas. The effluent from the reactor was analyzed by an on-line quadrupole mass spectrometry (BALZERS QMS 200F). Significant contributions of gas phase reactions and/or α -Al₂O₃ (diluent of the catalyst bed) were not observed in blank experiments using the empty reactor and/or α -Al₂O₃ instead of the catalyst. The pulse experimental data were used primarily to determine the amount of oxygen that was removed from or replenished into the catalyst during each reduction and oxidation cycle. The mass spectrometer was calibrated by pulsing different amounts of reactants or products of CPOM through the α -Al₂O₃ bed, respectively. The amount of each compound was estimated based on the area of corresponding peak of the mass signal. Prior to pulsing, the catalyst (0.3 g diluted with 0.3 g α -Al₂O₃) was pre-oxidized in a mixture of O₂ (40 ml/min) and He (40 ml/min) at 800°C for 1 h. Subsequently, the reaction system was cooled or heated to the reaction temperature, and flushed with helium (40 ml/min) for 1 h to remove any residual oxygen in the system. Then, a sequence of pulses of methane (500 μ l per pulse) was passed through the catalyst bed with an interval time of 5 min. After oxygen was exhausted from the catalyst by reaction with subsequent pulses of methane, the system was flushed with helium for 0.5 h to remove possible residual CH₄. The re-

oxidation of the catalyst was studied by pulsing with pure O₂ (99.99%) with the same sample loop of 500 μl.

2.3. Isotopic ¹⁸O₂ exchange

Isotopic oxygen exchange between ¹⁸O₂ and the catalysts was investigated in the temperature range from 30 to 900°C. The purity of the stable isotopic ¹⁸O₂ was not lower than 95 at% (Chemotrade, Germany). Quartz wool plugs were used to support and secure the 0.3 g catalyst sample in the middle of the alumina reactor. The outlet gas was analyzed by online mass spectrometry (BALZERS QMS 200F). The oxygen balance in the experiments was 98±2%. Prior to pulsing ¹⁸O₂, the sample was pre-oxidized with 80 ml/min of O₂/He (1:1) at 800°C for 1 h to remove adsorbed contaminations, e.g., H₂O and CO₂. Subsequently, the system was cooled or heated to the temperature for the oxygen exchange experiment, and flushed with He (80 ml/min) at the same temperature for 1 h. After this pretreatment, a pulse of ¹⁸O₂ was passed through the catalyst bed with 40 ml/min helium as carrier gas. Before the exchange experiment was carried out at another temperature, the catalyst was re-oxidized with O₂/He and flushed with helium again as described above. The pulse size was equivalent to 2.7×10¹⁹ oxygen atoms (500μl loop), or 1.35×10¹⁸ oxygen atoms (25μl loop). The influence of methane on the oxygen exchange reaction was studied by simultaneously pulsing CH₄ (50 μl) and ¹⁸O₂ (25μl) into the carrier gas *via* two six-port valves, resulting in one ¹⁸O₂-CH₄ pulse.

5.3. Results

5.3.1. Isotopic oxygen exchange

5.3.1.1. ¹⁸O₂ exchange in the absence of methane

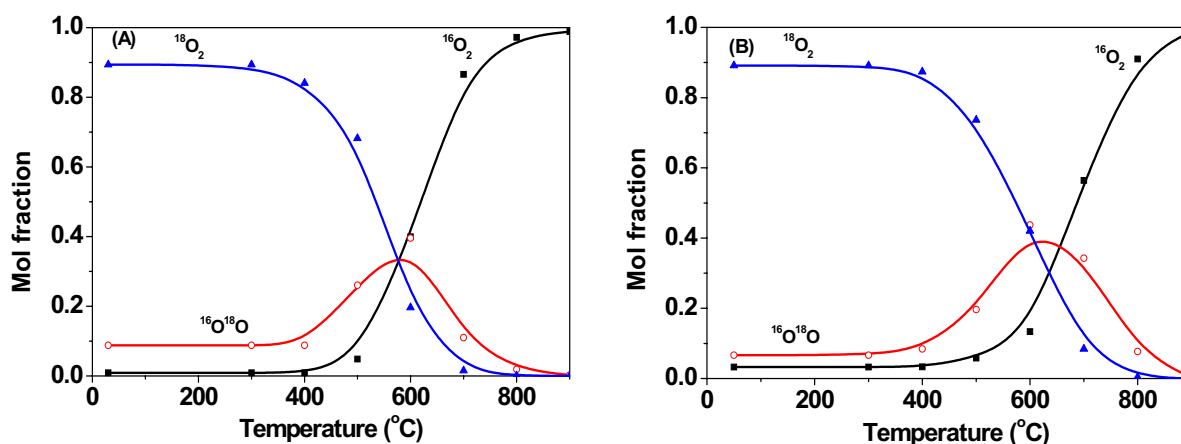


Fig. 1. Dependence of isotopic product distribution on reaction temperature when pulsing ¹⁸O₂ (1.34×10¹⁹ molecules/pulse) over (a) 0.3 YSZ (Sg=13.7 m²/g), and (b) 0.3 g ZrO₂ (Sg=15.4m²/g).

¹⁸O₂ exchange experiments were conducted at temperatures between 30 and 900°C over ZrO₂ and YSZ. These two catalysts had almost identical surface areas (14.5±1.0 m²/g). All possible oxygen molecules (¹⁸O₂, ¹⁶O¹⁸O, and ¹⁶O₂) were monitored at the reactor outlet. Blank experiments showed that the ¹⁸O₂ conversion was less than 5% in the empty alumina reactor, even at 900°C. The product distribution for the ¹⁸O₂ exchange with YSZ and ZrO₂ as a function of reaction temperature is shown in Fig. 1. Please note that each data point

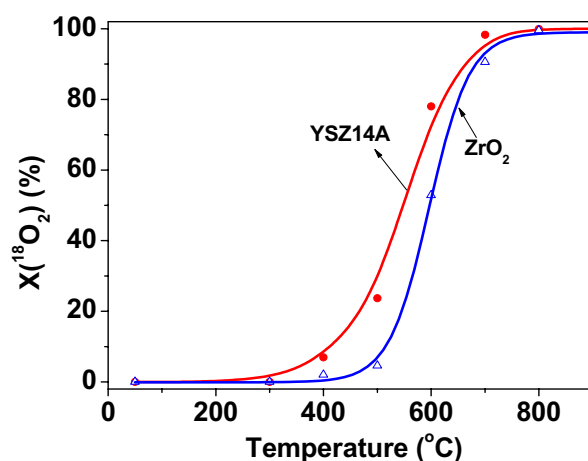


Fig. 2. Temperature dependence of the conversion of gas-phase ¹⁸O₂ (2.68×10¹⁹ atoms / pulse) in the isotopic exchange reaction with ZrO₂ and YSZ.

represents a single isothermal experiment. Very small amounts of ¹⁶O¹⁸O and ¹⁶O₂ are detected at temperatures below 300°C, which originate from impurities in the ¹⁸O₂ gas. Oxygen exchange occurs at temperatures above 300°C for both ZrO₂ and YSZ. Both ¹⁶O₂ and ¹⁶O¹⁸O are observed as isotopic exchange products when ¹⁸O₂ is pulsed over the catalysts. Unlike for ¹⁶O₂, showing a steadily increasing concentration with reaction temperature, a maximum in the amount of ¹⁶O¹⁸O is observed at 625°C for ZrO₂ and at 575°C for YSZ. ¹⁶O¹⁸O was the major isotopic product at temperatures below 575°C for YSZ, whereas the presence of ¹⁶O₂ increases significantly at the expense of ¹⁶O¹⁸O at temperatures above 575°C. Exclusively ¹⁶O₂ was detected at temperatures above 800°C for both ZrO₂ and YSZ. Even after ten ¹⁸O₂ pulses with a loop of 500 μl, ¹⁶O₂ was detected exclusively.

The temperature dependence of the conversion of ¹⁸O₂ during the exchange with ZrO₂ and YSZ is shown in Fig. 2. At temperatures below 700°C, the oxygen exchange reaction is found to be significantly slower for ZrO₂, compared with that of YSZ. Complete exchange is observed for both ZrO₂ and YSZ at temperatures above 800°C.

5.3.1.2. ¹⁸O₂ exchange in the presence of methane

The influence of methane on the oxygen exchange reaction was investigated by pulsing CH₄ (50 μl/pulse) and ¹⁸O₂ (25 μl/pulse) simultaneously over 0.3 g YSZ or ZrO₂. All possible products (H₂, H₂¹⁶O, H₂¹⁸O, C¹⁶O, C¹⁸O, C¹⁶O₂, C¹⁶O¹⁸O, C¹⁸O₂) were monitored with mass spectrometry at the outlet of the reactor. The product responses of the ¹⁸O₂-CH₄ pulse over YSZ and ZrO₂ at 600°C are shown in Figs. 3a and 3b. Surprisingly, the products detected for YSZ (Fig. 3a) are limited to C¹⁶O, C¹⁶O₂, H₂¹⁶O and H₂, whereas no products containing ¹⁸O could be detected. Similar results were obtained at 800°C. Obviously, these products are formed *via* oxidation of methane with ¹⁶O originating from YSZ. Compared with pulsing CH₄

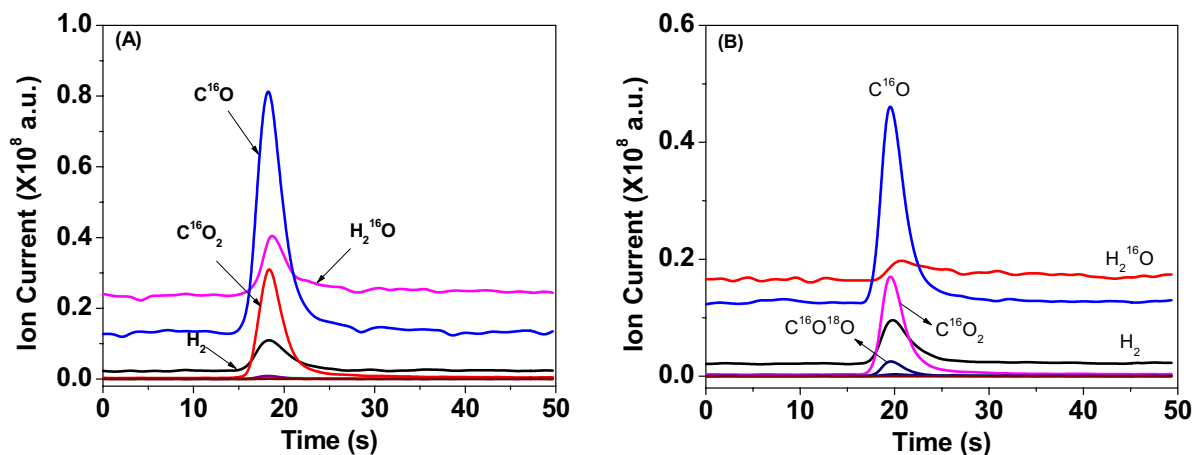


Fig. 3. Product response of $^{18}\text{O}_2\text{-CH}_4$ pulse ($25\mu\text{l } ^{18}\text{O}_2$ plus $50\mu\text{l CH}_4$) over (a) 0.3 g YSZ and (b) 0.3 g ZrO_2 at 600°C .

exclusively, as described in Section 3.2.1, all product responses increase significantly when CH_4 is pulsed together with $^{18}\text{O}_2$. Unlike for YSZ, a significant amount of $\text{C}^{16}\text{O}^{18}\text{O}$ was detected when pulsing $^{18}\text{O}_2\text{-CH}_4$ over ZrO_2 , although ^{16}O -containing products were again found to be dominant (Fig. 3b). Fig. 4 compares the oxygen responses when pulsing $^{18}\text{O}_2$ and $^{18}\text{O}_2\text{-CH}_4$ over YSZ at 600°C . The presence of methane induces a strong decrease in the amounts of $^{16}\text{O}_2$ and $^{16}\text{O}^{18}\text{O}$ detected, whereas the amount of $^{18}\text{O}_2$ decreases only slightly.

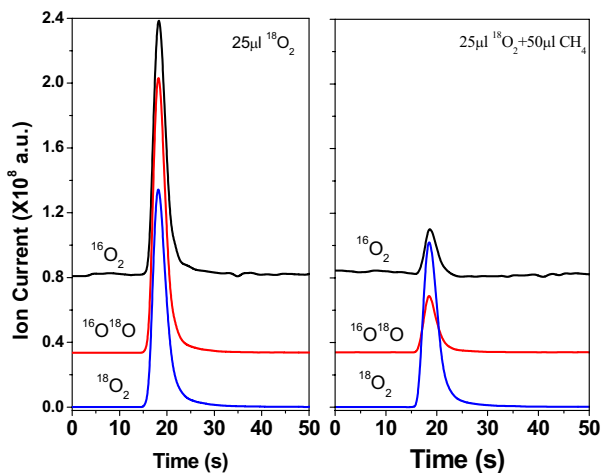


Fig. 4. Oxygen response during $^{18}\text{O}_2$ pulse and $^{18}\text{O}_2\text{-CH}_4$ pulse over 0.3 g YSZ at 600°C .

5.3.2. Methane activation

5.3.2.1. CH_4 -pulse experiments

CH_4 pulse experiments over both ZrO_2 and YSZ were carried out in the absence of oxygen at 900°C and 1 bar. Possible traces of oxygen in the carrier gas (helium) were not significant, because variation of the interval time between two CH_4 pulses did not influence the experimental results. The product responses of a CH_4 pulse over pre-oxidized YSZ are shown in Fig. 5. A mixture of CO , H_2 , CO_2 and H_2O is produced during the pulse experiments, which is in agreement with the product slate in steady-state experiments². Unlike other products, a delayed signal is observed for H_2O , suggesting a strong adsorption of H_2O on YSZ catalysts. The formation of CO , CO_2 and H_2O may result from CH_4 reacting with active

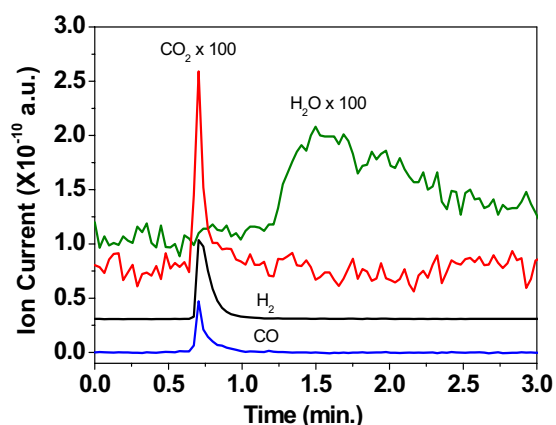


Fig. 5. Response of a methane pulse over 0.3 g YSZ at 900°C. The catalyst was preoxidized for 1 h, followed by flush with helium for 1h, both at 800°C.

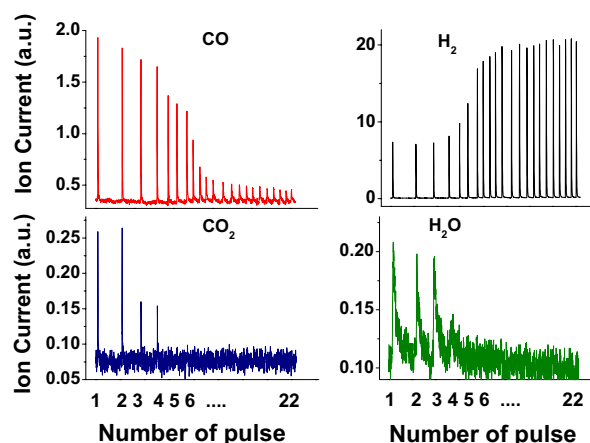


Fig. 6. Effluent gases from methane pulsing experiment at 900°C over 0.3 g YSZ ($S_g=13.7 \text{ m}^2/\text{g}$), which was preoxidized at 900°C for 1 h and subsequently flushed with helium for 1 h.

oxygen species on/in YSZ. The product distribution vs. pulse number is shown in Fig. 6. CO₂ and H₂O are formed only during the first four pulses, whereas CO and H₂ are formed during all methane pulses. The concentration of active oxygen species on/in YSZ is apparently too low to deeply oxidize CH₄ after 4 pulses. After about 10 ~13 pulses, very small but constant signals for m/e of 28 were observed. These can be attributed to a trace of N₂ (about 20 ppm) in CH₄ gas, which has the same mass-to-charge ratio ($m/e=28$) as CO. Upon further pulsing, dissociation of CH₄ resulted in a higher H₂ signal and carbon deposition occurred on the YSZ surface after oxygen was exhausted from the catalyst. Similar results were obtained for ZrO₂. After subtracting the contribution of the trace of nitrogen in CH₄ gas, it was estimated that about $6.3 \pm 0.5 \times 10^{17}$ and $5.5 \pm 0.5 \times 10^{17}$ oxygen atoms per m² (O/m²) were extracted by CH₄ pulses from pre-oxidized ZrO₂ and YSZ, respectively. These values were estimated from the amounts of CO, CO₂ and H₂O formed.

Identical pulse experiments were carried out over pre-reduced YSZ and ZrO₂, which were treated with 5% H₂ in argon at 900°C for 1 h before pulsing CH₄. Besides H₂ formed by decomposition of CH₄, no oxygen-containing products were detected.

5.3.2.2. O₂-pulse experiments

O₂ pulses were conducted over the catalyst at 900°C and 1 bar, after oxygen was exhausted by 22 CH₄-pulses as described above. Before pulsing O₂, the catalyst was flushed with pure helium at 900°C for 30 min. The responses of oxidation products and oxygen during oxygen pulses over YSZ are shown in Fig. 7. CO and CO₂ are two oxidation products observed when pulsing oxygen, i.e., H₂ and H₂O were not detected. During the first 12 pulses, only CO is formed. An increasing CO₂ signal is observed starting from the 13th pulse at the expense of CO. Oxygen is first detected at the 17th pulse, where very small amounts of CO and CO₂ are

produced. Constant oxygen signals are observed after 18 pulses, while no products are detected.

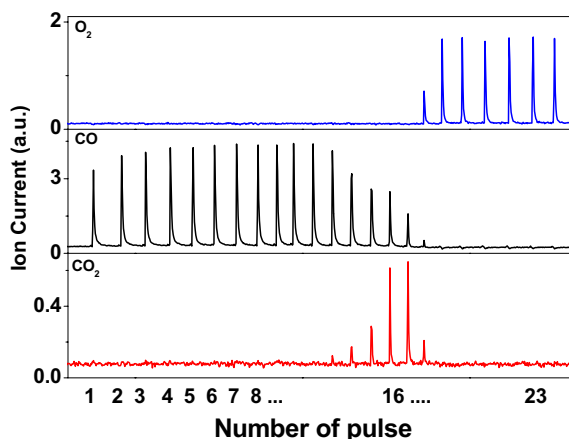


Fig. 7. Effluent gases from O₂ (50 μl/pulse) pulsing experiment at 900°C over 0.3 g YSZ (S_g=13.7 m²/g) after 22 methane pulses.

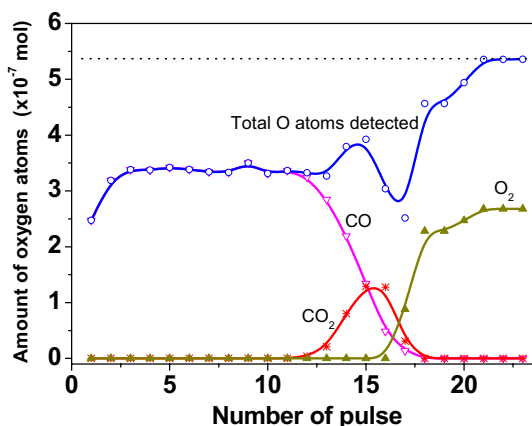


Fig. 8. Amounts of oxygen atom contained in the effluent gases of each oxygen pulse over 0.3g YSZ after 22 methane pulses.

The amount of oxygen atoms in the effluent gas after each pulse is shown in Fig. 8. In this figure, the dotted line displays the amount that is contained in each single oxygen pulse. Obviously, the total amount of oxygen atoms in O₂, CO and CO₂ detected in the effluent is less than the oxygen pulsed for the first 21 pulses. The missing oxygen is apparently stored in the oxide catalyst *via* re-oxidation of the catalyst. The integral amounts of oxygen stored in YSZ and ZrO₂ are about $6.1 \pm 0.5 \times 10^{17}$ O/m² and $10.3 \pm 1.0 \times 10^{17}$ O/m², respectively.

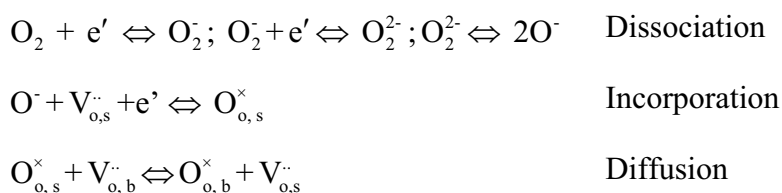
5.4. Discussion

5.4.1. Oxygen activation

Fig. 1 clearly shows ¹⁸O₂ isotopic exchange with ZrO₂ and YSZ at temperatures above 300°C. Each pulse contains 2.7×10^{19} ¹⁸O-atoms, which is approximately equivalent to the number of oxygen ions in one monolayer of 0.3 g ZrO₂ or YSZ, each having a total surface area of 4.5 m². At temperatures above 800°C, ¹⁸O₂ is completely exchanged with ¹⁶O originating from ZrO₂ or YSZ, even after ten pulses.

It has been recognized that anionic defects, e.g., oxygen vacancies and F centers (an oxygen vacancy capturing one or two electrons) favors the oxygen exchange reaction¹⁷⁻²¹. This would explain the observation in Fig. 2 that oxygen exchange is much slower on ZrO₂ than on YSZ. The latter has a much higher concentration of oxygen vacancies generated by doping Y₂O₃ in ZrO₂.

Isotopic oxygen exchange has been studied on many oxides including YSZ²²⁻²⁴, and several strongly resembling mechanisms have been proposed. According to the generally adopted kinetic scheme^{25;26},



several species can occur as intermediates for the reduction of molecular oxygen, e.g. O₂⁻, O₂²⁻ and O⁻. In this work we do not attempt to distinct between these three surface oxygen species, and therefore they are denoted as O* hereafter. The Kroger-Vink notation is used for lattice defects: V_o^{··} denotes an oxygen vacancy, O_o[×] a regular lattice oxygen ion and e' an electron. The footnotes, s and b refer to “surface” and “bulk”, respectively. Thereby we make a distinction between lattice oxygen ions fully coordinated in the bulk versus lattice oxygen ions in the surface, which are not coordinatively saturated. This distinction is necessary because only the surface lattice oxygen will be accessible for the catalytic reaction. The same argument also holds for oxygen vacancies. In principle, each of the indicated reaction steps may be rate determining.

The distribution of isotopic exchange products depends on the relative rates of the dissociation, incorporation and diffusion steps. Note that the randomization of isotopic components can only occur after dissociation of the oxygen molecule at the surface. Hence, if the incorporation reaction and subsequent diffusion are faster, ¹⁶O₂ will be the dominating product. In contrast, faster dissociation of oxygen compared to oxygen incorporation will lead to formation of ¹⁶O¹⁸O. Fig. 1 shows that more ¹⁶O¹⁸O is formed than ¹⁶O₂ at temperatures below 575°C for YSZ and 625°C for ZrO₂. This shows that the dissociation of oxygen is relatively fast at these temperatures. This observation is in good agreement with results obtained by Manning et al.^{23;24}, who reported that incorporation of oxygen species with YSZ is rate determining below 700°C, while dissociation is rate determining above this temperature.

5.4.2. Methane activation

Surprisingly, Fig. 3a shows exclusive formation of ¹⁶O-containing products during CH₄-¹⁸O₂ pulsing experiments. This is, first of all, strong evidence for the participation of oxygen originating from YSZ in the catalytic oxidation of methane. Furthermore, the fact that no ¹⁸O-containing products are detected excludes the possibility of methane oxidation in the gas phase at temperatures up to 800°C. The formation of ¹⁶O₂ and ¹⁶O¹⁸O in Fig. 4 confirms the existence of both ¹⁶O* and ¹⁸O* on the surface of YSZ during the CH₄-¹⁸O₂ pulse. In essence, this is consistent with the data of oxygen exchange experiments shown in Fig. 1. The formed amounts of ¹⁶O₂ and ¹⁶O¹⁸O in Fig. 4 are about similar, indicating comparable surface concentrations of ¹⁶O* and ¹⁸O* at 600°C. The combined observations made in Figs. 3a and 4

thus leads to the conclusion that the type of oxygen that reacts with methane is lattice oxygen ion ($O_{O,s}^{\times}$) in the outermost surface layer of YSZ, as opposed to adsorbed surface oxygen (O^*) that is also present. The data also imply that no accumulation of $^{18}O_{O,s}^{\times}$ occurs in the outermost surface layer during the CH_4 - $^{18}O_2$ pulse, which in turn suggests that incorporation of oxygen and subsequent diffusion into the bulk, and *vice versa*, is comparatively fast as compared to methane activation. A similar conclusion was drawn from data of isotopic exchange experiments carried out by Ishihara *et al*²⁰.

Finally, Fig. 4 shows that the oxidation of CH_4 in a way competes with isotopic oxygen exchange. In spite of a slightly enhanced $^{18}O_2$ conversion in the presence of CH_4 (c.f. $^{18}O_2$ signals in Figs. 4a and b), the consumption of lattice oxygen ions ($^{16}O_{O,s}^{\times}$) by methane suppresses the formation of $^{16}O^*$ at the surface, which is why the formation rates of $^{16}O_2$ and $^{16}O^{18}O$ decrease significantly. The enhanced conversion of $^{18}O_2$ in the presence of CH_4 suggests that CH_4 and O_2 molecules at the surface are *not* competing for the same adsorption sites, as one would expect for a redox mechanism.

Figs. 5 and 6 demonstrate that methane is preferentially oxidized by lattice oxygen when YSZ or ZrO_2 are pre-oxidized. No oxidation products are observed when CH_4 is pulsed over pre-reduced YSZ or ZrO_2 at 900°C (not shown). It should be noted that the amount of removable oxygen of both ZrO_2 and YSZ were found to be below the detection limit of conventional TPR. Partial reduction of ZrO_2 has been reported by other researchers^{27;28}, although ZrO_2 and YSZ are normally considered as hardly reducible oxides. Re-oxidation of oxygen-exhausted YSZ and ZrO_2 confirms that CPOM over both YSZ and ZrO_2 proceeds *via* a Mars-van Krevelen mechanism²⁹. Corresponding data are shown in Figs. 6 and 8. Compared with the amount of oxygen replenished ($6.1 \pm 0.5 \times 10^{17}$ O/m² and $10.3 \pm 1.0 \times 10^{17}$ O/m² for YSZ and ZrO_2 , respectively) (Fig. 8), the amount of the oxygen extracted by pulses of CH_4 (Fig. 6) is lower ($5.5 \pm 0.5 \times 10^{17}$ O/m² and $6.3 \pm 0.5 \times 10^{17}$ O/m² for YSZ and ZrO_2 , respectively). First of all, these numbers are in the same order of magnitude, although the difference for ZrO_2 is significant. The reason for this is the fact that quantitative analysis of water with MS is unreliable in general because of adsorption of water on the equipment as well as the unavoidable presence of water in the background of the vacuum. Moreover, it was not possible to calibrate the MS for water in the correct low concentration range. The experiments with ZrO_2 are more affected than with YSZ because the amount of water produced on ZrO_2 is significantly larger. Nevertheless, in the O_2 -pulse experiments no water is formed, therefore providing the most reliable numbers for amount of oxygen that can be removed: 6.1×10^{17} O/m² and 10.3×10^{17} O/m² for YSZ and ZrO_2 , respectively. If it is assumed that solely the (100) faces of monoclinic ZrO_2 and cubic YSZ are exposed to the CH_4 gas, the integral amounts of extracted lattice oxygen correspond to only 13.6% and 8.5%, respectively, of a single monolayer. Data of LEIS and XRF experiments exclude significant contributions from reducible metal oxide contaminations at the surface.

Fig. 6 shows formation of CO₂, CO, H₂ and H₂O when pulsing CH₄ over the pre-oxidized catalyst. These are all primary products of CPOM². Deep oxidation of methane to CO₂ and H₂O occurs during the first four pulses, whereas partial oxidation to CO and H₂ is found to dominant during the subsequent pulses. This shows that the amount of extractable lattice oxygen of the catalyst has a significant influence on the relative rates of reactions, which is in accordance with a kinetic model presented elsewhere². A low concentration of extractable lattice oxygen favors selective oxidation of methane to CO and H₂, produced mainly *via* decomposition of adsorbed formaldehyde. In contrast, a high concentration of extractable lattice oxygen promotes further oxidation of surface formaldehyde to CO₂ and H₂O via surface formate and carbonate intermediates.

5.4.3. Reaction model

The role of lattice oxygen in heterogeneous catalytic reactions has been subject of many studies^{13;30-33}. It has been shown that conventional redox catalysts can act as the source of active oxygen and sustain oxidation for a certain period of time in the absence of oxygen in the gas phase³¹⁻³³. Our results show that this also holds for ZrO₂ and YSZ.

In pure ZrO₂, the intrinsic concentration of oxygen vacancies is low^{34;35}. Doping with Y₂O₃ leads to formation of extrinsic oxygen vacancies. On the other hand, oxygen vacancies on the surface of ZrO₂ and YSZ are created by extraction of lattice oxygen ions, as revealed by characterization of adsorbed CO with *in situ* FTIR³⁶, or directly illustrated by EPR spectroscopy^{12;37}. This is possible if the valence state of the catalyst rapidly adjust itself to the external conditions. In a localized description, this leads to the formation of two Zr³⁺ surface cations associated with a single vacancy. In Kröger-Vink notation, the formed associate can be presented as $Zr'_{Zr} - V_{O,S}^{\bullet\bullet} - Zr'_{Zr}$. These Vacancies can be re-filled with oxygen, either by direct transfer of oxygen from the gas phase or by lattice oxygen diffusion. The reversed view is that surface lattice oxygen coordinated by Zr⁴⁺ cations is active in the methane oxidation reaction.

Though doping ZrO₂ with Y₂O₃ increases the concentration of extrinsic oxygen vacancies, it also decreases the concentration of surface lattice oxygen (O_{O,s}^x) because the Y₂O₃ concentration in the surface is significant³. This explains why significantly more oxygen could be removed by subsequent methane pulses from pre-oxidized ZrO₂ than from pre-oxidized YSZ (see Section 4.2). The extent of reduction is about 13.6% and 8.5% of the total number of oxygen in a single monolayer for ZrO₂ and YSZ, respectively.

Surface lattice oxygen ions are extracted during reaction with methane. In the case of ZrO₂, re-oxidation of the vacant sites by O₂ is the main route to replenish the surface lattice oxygen. Fig. 3b shows formation of C¹⁶O¹⁸O during a ¹⁸O₂-CH₄ pulse over ZrO₂, which is taken as evidence that the extracted oxygen on the ZrO₂ surface is replenished by direct activation of molecular oxygen at the surface oxygen vacancy site. In the case of YSZ, fast activation of

oxygen and fast lattice oxygen diffusion provides an alternative pathway for replenishment of the surface lattice oxygen. The presence of extrinsic oxygen vacancies promotes the oxygen activation on the surface, but also facilitates rapid diffusion of oxygen in the lattice. This explains the higher conversion rate of methane over YSZ, $8.4 \times 10^{18} \text{ mol.m}^{-2}.\text{s}^{-1}$ at 600°C , as compared to ZrO_2 , $4.3 \times 10^{18} \text{ mol.m}^{-2}.\text{s}^{-1}$ at the same temperature³. It also explains why ^{16}O -containing products are exclusively produced during $^{18}\text{O}_2\text{-CH}_4$ pulses over YSZ (see Fig. 3a).

The emerging picture, as depicted in Fig. 9, is that CPOM over both YSZ and ZrO_2 proceeds *via* the Mars-van Krevelen reduction-oxidation mechanism. For ZrO_2 , the rate of methane oxidation is balanced by the rate of re-oxidation of the vacant sites by O_2 . In the case of YSZ, fast diffusion of oxygen in conjunction with rapid oxygen transfer at extrinsic oxygen vacancies at the surface provides an alternative pathway for replenishment of the oxygen consumed by methane. The present results make apparent that it is the activation of methane on the YSZ surface, rather than the activation of molecular oxygen, that is the rate-determining step during CPOM (see Fig. 4b).

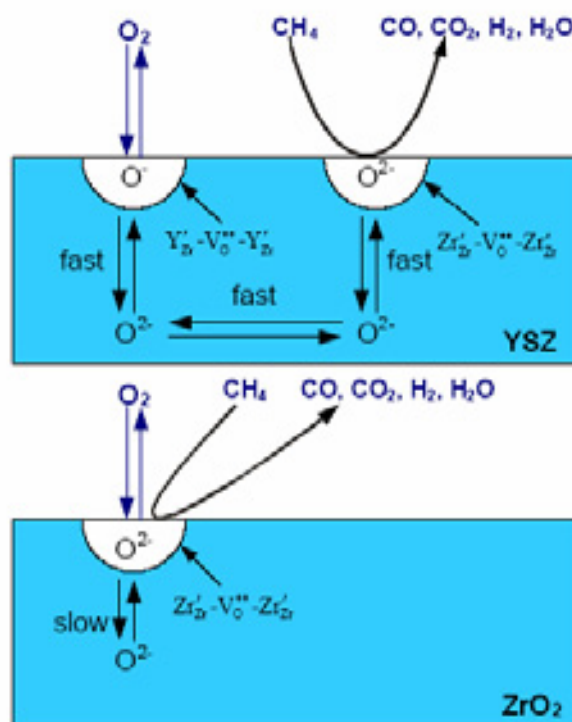


Fig. 9. The reaction models proposed for CPOM over YSZ and ZrO_2 catalysts.

5.5. Conclusions

The results of this study clearly demonstrate that CPOM over ZrO_2 and YSZ proceeds *via* a Mars-van Krevelen mechanism. Methane is selectively oxidized by surface lattice oxygen. At 900°C , about 8% and 14% of lattice oxygen in the outermost surface layer of ZrO_2 and YSZ, respectively, can be extracted by methane. Extraction of lattice oxygen by methane results in the formation of surface oxygen vacancies. After this oxidation step, the route to replenish surface oxygen differs for both oxides. For ZrO_2 , the replenishment occurs by direct activation of molecular oxygen at the surface oxygen vacancy site. Extrinsic oxygen vacancies in YSZ, generated by doping ZrO_2 with Y_2O_3 , facilitate fast activation of molecular oxygen as well as fast lattice diffusion of oxygen. The two effects together lead to a rapid replenishment of the surface lattice oxygen extracted by methane. The proposed mechanism explains both the comparatively high activity of YSZ in CPOM and the observation that,

contrary to ZrO₂, lattice oxygen is found exclusively in oxidation products of methane over YSZ during the pulse experiments.

Acknowledgements

This work was performed under the auspices of NIOK, the Netherlands Institute of Catalysis Research. Stichting Technische Wetenschappen (STW, the Dutch technology foundation) is gratefully acknowledged for financial support under project number UPC-5037. The authors thank Mr. Sander Albertsma for part of the CH₄ pulse experiments and Ing. Bert Geerdink for technical support.

References

1. J.Zhu, M.S.M.M.Rahuman, J.G.van Ommen, L.Lefferts, *Appl.Catal.A.* 259, 95 (2004); *Chapter 2*.
2. J.Zhu, J.G.van Ommen, L.Lefferts, *J.Catal.* 225, 388 (2004); *Chapter 4*.
3. J.Zhu, J.G.van Ommen, A.Knoester, L.Lefferts, *J.Catal.* 230, 300-309 (2005); *Chapter 3*.
4. R.A.Dalla Betta, *Catal.Today* 35, 129 (1997).
5. A.T.Aschcroft, P.D.F.Vernon, M.L.H.Green, *Nature* 344, 319 (1990).
6. D.A.Hickman and L.D.Schmidt, *Science* 259, 343 (1993).
7. D.A.Hickman and L.D.Schmidt, *AIChE J.* 39, 1164 (1993).
8. A.G.Steghuis, *Ph.D thesis, University of Twente, The Netherlands* (1998).
9. A.G.Steghuis, J.G.van Ommen, J.A.Lercher, *Catal.Today* 46, 91 (1998).
10. E.R.Stobbe, *Ph.D thesis, University of Utrecht, The Netherlands* (1999).
11. M.A.Barteau, *J.Vac.Soc.Technol.A.* 11, 2162 (1993).
12. M.Labaki, S.Siffert, J.F.Lamonier, E.A.Zhilinskaya, A.Aboukais, *Appl.Catal.B.* 43, 261 (2003).
13. Z.X.Liu, Q.X.Bao, N.J.Wu, *J.Catal.* 113, 45 (1988).
14. A.Belansky and J.Haber, *Marcel Dekker, New York* (1996).
15. Z.Zhang, X.E.Verykios, M.Baerns, *Catal.Rev.- Sci.Eng.* 36, 507 (1994).
16. J.H.Lunsford, *Stud.Surf.Sci.Catal.* 81, 1 (1994).
17. E.R.S.Winter, *J.Chem.Soc.A.* 2889 (1968).

18. E.R.S.Winter, *J.Chem.Soc.A.* 1832 (1969).
19. S.Z.Lacombe, H.M.Zanthoff, C.Mirodatos, *J.Catal.* 155, 106 (1996).
20. T.Ishihara et al., *Solid State Ionics* 113-115, 593 (1998).
21. E.N.Voskresenskaya, V.G.Roguleva, A.G.Anshits, *Catal.Rev.- Sci.Eng.* 37, 101 (1995).
22. N.Sakai et al., *Phys.Chem.Chem.Phys.* 5, 2253 (2003).
23. P.S.Manning, J.D.Sirman, J.A.Kilner, *Solid State Ionics*, 93, 125 (1997).
24. P.S.Manning, J.D.Sirman, R.A.De Souza, J.A.Kilner, *Solid State Ionics* 100, 1 (1997).
25. B.A.Boukamp, B.A.van Hassel, I.C.Vinke, K.L.de Vries, A.J.Burggraaf, *Electrochem.Acta* 38, 1817 (1993).
26. R.Merkle and J.Marier, *Phys.Chem.Chem.Phys.* 4, 4140 (2002).
27. S.Sharma, S.Hilaire, J.M.Vohs, R.J.Gorte, H.W.Jen, *J.Catal.* 190, 199 (2000).
28. S.M.Stagg, E.Romeo, C.Padro, D.E.Resasco, *J.Catal.* 178, 137 (1998).
29. P.Mars and D.W.van Krevelen, *Chem.Eng.Sci.* 3, 41 (1954).
30. M.E.Lashier and G.L.Schrader, *J.Catal.* 128, 113 (1991).
31. V.D.Sokolowsky, *Catal.Rev.- Sci.Eng.* 32, 1 (1990).
32. T.V.Andrushkevich, *Catal.Rev.- Sci.Eng.* 35, 213 (1993).
33. Y.Schuurman, J.T.Gleaves, J.R.Ebner, M.J.Munney, *Stud.Surf.Sci.Catal.* 82, (1994).
34. N.Mommer, T.Lee, J.A.Gardber, W.E.Evenson, *Phys.Rev.B.* 61, 162 (2000).
35. E.Karaoetrova et al., *J.Am.Ceram.Soc.* 84, 65 (2001).
36. C.Morterra, E.Giamello, L.Orio, M.Volante, *J.Phys.Chem* 94, 3111 (1990).
37. Q.Zhao, X.Wang, T.Cai, *Appl.Surf.Sci.* 225, 7 (2004).

Chapter 6

The Role of Defect Structure in Activation of O₂ and N₂O on ZrO₂ and Yttrium-stabilized ZrO₂

Abstract

The relationship between the structure of both yttrium-stabilized zirconia (YSZ) and ZrO₂ catalysts and their abilities to activate N₂O and O₂ is studied by determination of catalytic properties and characterization with TPD, SEM and XRD. Furthermore, the role of oxygen species formed via dissociation of either O₂ or N₂O in catalytic partial oxidation of methane (CPOM) is determined. N₂O can be activated at both structural defects (e.g. Zr cations located at corners) and intrinsic oxygen vacancies ($Zr'_{Zr}-V_{O}''-Zr'_{Zr}$) and forms two types of oxygen species (α -O and β -O) on the surface, respectively. In contrast, molecular oxygen gives rise to only one type of oxygen species (β -O), i.e. surface lattice oxygen. This type of oxygen species can be extracted by reaction with methane, forming the intrinsic oxygen vacancies again during CPOM. However, the structural defects are not active for oxygen activation during CPOM. Doping ZrO₂ with Y₂O₃ significantly decreases the number of the structural defects via replacement of Zr⁴⁺ cations by Y³⁺ cations, located at corners, steps, kinks and edges of the crystallites. Calcination at higher temperatures results in less structural defects due to both increasing crystallite size as well as transformation to more regularly shaped crystallites. High temperature calcinations also increase the activity of YSZ in CPOM. This is attributed to the increase in the exposition of low index planes, especially those (111) with the lowest surface energy and the highest coordination numbers, induced by the thermal treatment.

Key words: *Oxygen vacancies; Activation of oxygen; Yttrium-stabilized zirconia; Partial oxidation of methane; Decomposition of N₂O; Structural defects.*

6.1. Introduction

Natural gas is forecasted to outlast oil by about 60 years¹ despite the relatively underdeveloped state of the gas industry. Plenty of natural gas found in many locations around the world stimulates study on its utilization. Catalytic partial oxidation of methane to synthesis gas (CPOM) is an attractive process for conversion of natural gas to synthesis gas, as alternative to steam reforming of methane. Most of the studies on CPOM were focused on metallic catalysts, like supported cobalt, nickel as well as noble metals (Rh, Pt). In contrast, irreducible metal oxides were hardly studied for CPOM, despite the fact that formation of synthesis gas is often observed as side reactions on oxide catalysts, e.g. in the oxidative conversion of methane to methanol²⁻⁴, formaldehyde^{5;6}, methyl formate⁷, as well as oxidative coupling of methane^{8;9}.

The performance of hardly reducible oxides in CPOM, e.g. ZrO₂, yttrium-stabilized zirconia (YSZ) was reported previously¹⁰⁻¹³. Compared with metal catalysts, ZrO₂-based oxide catalysts are less active and selective. However, YSZ is a very stable catalyst, because of both thermal stability as well as prevention of evaporation of the catalyst, as takes place for metal catalysts. Low activity of YSZ can be compensated by introducing a second metal-based reforming catalyst¹⁰. The metal catalyst is in this case protected for metal loss *via* evaporation of precious metal oxides because contact with oxygen at high temperatures is completely avoided.

A Mars-van Krevelen mechanism was proposed for CPOM over ZrO₂ and YSZ catalysts in Chapter 5¹³, in which methane is oxidized by lattice oxygen ions (O_o[×]) in the surface layer. The extraction of the lattice oxygen ion results in the formation of oxygen vacancies (Zr'_{Zr}-V_O^{••}-Zr'_{Zr}) associated with two Zr³⁺ cations in the surface, which are replenished by molecular oxygen. YSZ contains a much higher concentration of oxygen vacancies (Y'_{Zr}-V_O^{••}-Y'_{Zr}) both on the surface and in the bulk, which are generated extrinsically. This results in, on one hand, faster activation of oxygen on vacancies residing at the surface, and on the other hand, in enhanced diffusion of oxygen ions through the bulk. This pathway appears faster than direct O₂ activation on intrinsic vacancies for ZrO₂, speeding up both oxygen activation as well as the reaction rate in CPOM.

Although previous work elucidated the role of both intrinsic and extrinsic defects in CPOM, the effect of the morphology of YSZ remains unclear. This work focuses on the role, if any, of structural defects (such as corners, edges, steps and kinks) on ZrO₂ and YSZ. Therefore, in this study the morphology of YSZ is modified and carefully characterized to reveal the effect on the interaction with oxygen as well as on the catalytic properties in CPOM. Secondly, N₂O is used as a probe molecule to study the nature of defects, as has been done on many defective oxides, e.g. Li/MgO¹⁴, Fe-ZSM5 zeolite¹⁵ and ZrO₂^{16;17}. In short, the present work aims on identification of the structural requirements for CPOM over YSZ catalysts.

6.2. Experimental

6.2.1. Catalysts

All catalysts (YSZ14A, YSZ14B, YSZ14C and ZrO₂) were prepared by calcining yttrium-stabilized zirconia (YSZ) or zirconia powder in air for 15 h, as described previously in Chapter 3¹². In the sample code, YSZ means yttrium-stabilized zirconia, the number “14” refers to the weight percentage of Y₂O₃ in the sample, and A, B and C denote the different calcination temperatures, 900°C, 1000°C and 1100°C respectively. BET surface areas for all catalysts used in the present work are listed in table 1. As described in Chapter 3, TiO₂ and HfO₂ are two major contaminations in the bulk, whereas no inorganic contamination was detected on the outermost layer by low-energy ion scattering (LEIS).

6.2.2. Catalytic measurement

Catalytic performance of the catalysts was examined in a fixed-bed reactor made of an alumina tube (inner diameter, 4 mm; length, 450 mm) at atmospheric pressure. A mixture of 0.3 g catalyst diluted with 0.3 g α-Al₂O₃ particles was positioned in the isothermal zone of the reactor by quartz wool. Reactants, CH₄ and O₂, were diluted with helium (CH₄:O₂:He=2:1:14), and total flow rate was 170 ml/min (STP); GHSV was about 6×10³ h⁻¹. More details can be found in Chapter 4 and our previous publication¹¹.

N₂O decomposition was carried out in the same setup as used for CPOM. Diluted N₂O (N₂O/He= 3:14) was passed through the catalyst bed with a total follow rate of 170ml/min (STP); GHSV was about 6×10³ h⁻¹. On-line gas chromatography with Carboxan 1000 and Haysep N columns was used to analyze the effluent gas from the reactor. Conversions (X) and yields (Y) were calculated according to:

For CPOM:

$$X_{CH_4} = \frac{CH_4^{in} - CH_4^{out}}{CH_4^{in}}; X_{O_2} = \frac{O_2^{in} - O_2^{out}}{O_2^{in}}; Y_{CO} = \frac{CO^{out}}{CH_4^{in}}; Y_{CO_2} = \frac{CO_2^{out}}{CH_4^{in}}; Y_{H_2} = \frac{H_2^{out}}{2CH_4^{in}}; Y_{H_2O} = \frac{H_2O^{out}}{2CH_4^{in}}$$

$$\text{For N}_2\text{O decomposition: } X_{N_2O} = \frac{N_2O^{in} - N_2O^{out}}{N_2O^{in}}$$

6.2.3. TPD of adsorbed oxygen species

Temperature-programmed desorption (TPD) experiments were carried out using a homemade vacuum-TPD setup equipped with a mass spectrometer (BALZERS QMS 200F). The adsorbed oxygen species were formed either *via* dissociative adsorption of N₂O on the catalyst or *via* oxidation of the catalyst with O₂. The O₂ MS signal was normalized by surface area of the catalyst sample. For quantitative estimation of desorbed oxygen, the online mass spectrometer was calibrated for O₂.

In the case of N_2O dissociative adsorption, the experiment was conducted according to the following procedure: about 0.15 g of catalyst was placed in a quartz tube (reactor). The catalyst was pre-activated at 800°C at 10^{-3} mbar for 3 h, and subsequently, cooled to 300°C . After this pre-activation, N_2O was introduced (7 mbar). The reactor was held at 300°C for 2 h. Subsequently, the system was cooled to 50°C and evacuated at 50°C for 2 h to remove weakly adsorbed species. Then, TPD was carried out with a heating rate of $10^\circ\text{C}/\text{min}$ to 800°C and dwelled at 800°C for 10 min. Adsorption at 300°C for 2 h is sufficient to reach equilibrium, because longer adsorption time resulted in identical amounts of adsorbed oxygen.

In the case of oxidation with O_2 , the sample was pre-activated at 800°C and 10^{-3} mbar for 3 h first, followed by treatment with pure O_2 at 7 mbar and 800°C for 2 h. Subsequently, the system was slowly cooled to 50°C under 7 mbar O_2 and evacuated for 2 h. Finally, TPD was carried out with the same conditions as mentioned above.

6.2.4. SEM and XRD

The structure of the samples was determined with powder X-ray diffraction (XRD, Philips PW1830). The diffraction patterns were obtained with nickel-filtered $\text{CuK}\alpha_1$ radiation ($\lambda=1.5405\text{\AA}$) with scanning speed 2° in 2θ min^{-1} .

The morphology of catalyst particle was studied with scanning electron microscopy (SEM) (LEO 1550 FEG SEM).

6.3. Results

6.3.1. CPOM

CPOM was carried out over ZrO_2 and three YSZ catalysts calcined at different temperatures. Methane conversions over four different catalysts as a function of reaction temperature are compared in Fig. 1. Almost complete oxygen conversion is achieved at about 700°C for all catalysts (not shown here). Before oxygen is consumed completely at temperatures below 700°C , CH_4 conversion increases with reaction temperature rapidly, whereas a slight increase in CH_4 conversion is observed after oxygen is depleted at 700°C and above. Compared with ZrO_2 , all three YSZ catalysts show much higher activities for CPOM. The three YSZ catalysts show only small differences in CH_4 conversion rate when based on

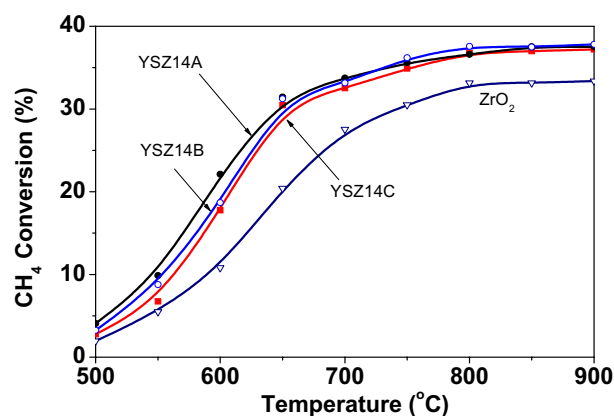


Fig. 1. CH_4 conversion as a function of reaction temperature. Catalysts: ZrO_2 , YSZ14A, YSZ14B and YSZ14C. Feed: $\text{CH}_4:\text{O}_2:\text{He}=2:1:14$, total flow rate 170 ml/min.

catalyst weight. However, the activity per m^2 of these three YSZ catalysts varies significantly. The CH_4 conversion rates at 600°C were estimated to be $8.4 \times 10^{17} \text{ mol.m}^{-2}.\text{s}^{-1}$, $9.2 \times 10^{17} \text{ mol.m}^{-2}.\text{s}^{-1}$, and $12.6 \times 10^{17} \text{ mol.m}^{-2}.\text{s}^{-1}$ for YSZ14A, YSZ14B and YSZ14C respectively. According to the usual criteria (the Carberry number and the Wheeler-Weisz modulus¹⁸) calculated under the experimental conditions, the mass transfer limitation can be neglected at 600°C . Apparently, high-temperature calcination increases the rate per m^2 .

6.3.2. Decomposition of N_2O

Steady state decomposition of N_2O was carried out over ZrO_2 and three YSZ catalysts at temperatures from 400 to 850°C . N_2O conversions are shown as a function of temperature in Fig. 2. All four catalysts start to decompose N_2O at about 450°C . Compared with YSZ catalysts, ZrO_2 is much more active for N_2O decomposition. Complete conversion of N_2O is observed over ZrO_2 at about 700°C , while only about 70%, 28% and 12% of the N_2O is converted over YSZ14A, YSZ14B and YSZ14C respectively. The activity appears to decrease with increasing calcination temperatures for YSZ catalysts. Blank experiments showed that N_2O conversion over $\alpha\text{-Al}_2\text{O}_3$ was less than 1% at 750°C , indicating that contributions of both gas phase reaction as well as $\alpha\text{-Al}_2\text{O}_3$ can be neglected.

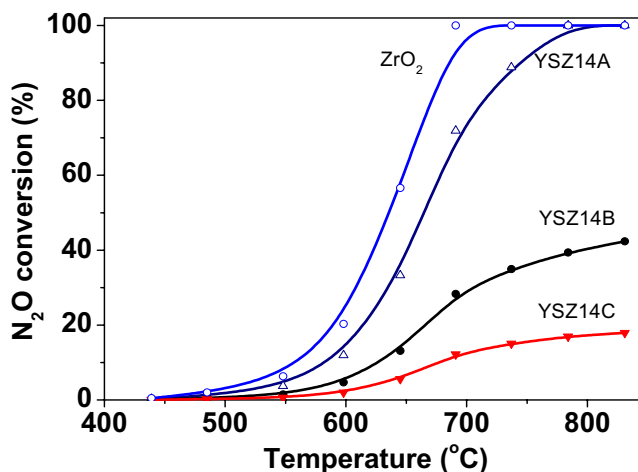


Fig. 2. N_2O conversion as a function of reaction temperature. Catalysts: ZrO_2 , YSZ14A, YSZ14B and YSZ14C. Feed: $\text{N}_2\text{O}:\text{He}=3:14$, total flow rate 170 ml/min .

6.3.3. TPD of adsorbed oxygen species

Fig. 3 shows the TPD profiles of adsorbed oxygen species formed *via* decomposition of N_2O over ZrO_2 at 300°C . The TPD result reveals that two types of oxygen species are present on ZrO_2 : $\alpha\text{-O}$ (desorption peak at 370°C) and $\beta\text{-O}$ (desorption peak at 670°C). Note that $\alpha\text{-O}$ mentioned in the present work is not related to $\alpha\text{-O}$ as defined for Fe/ZSM5^{15} , although both species are formed out of N_2O . A small N_2O desorption peak is observed at 500°C , accompanied by small N_2 and O_2 peaks. Similar results are obtained for YSZ catalysts.

TPD profiles of oxygen formed *via* N_2O decomposition and *via* oxidation with O_2 are compared in Fig. 4. A blank experiment was also carried out over ZrO_2 , which was preactivated at 800°C and cooling down to 50°C at 10^{-3} mbar for 3 h. Almost no desorption of

oxygen species is observed during the blank experiment. In contrast, when ZrO_2 was treated by either N_2O at 300°C or by O_2 at temperature between 50 to 800°C , two oxygen desorption peaks are obtained at identical desorption temperatures (370°C and 670°C). However, treatment with N_2O results in much more $\alpha\text{-O}$ on ZrO_2 as compared to treatment with O_2 , whereas almost identical amounts of the $\beta\text{-O}$ are formed out of N_2O and O_2 .

TPD profiles of oxygen species formed *via* decomposition of N_2O

are compared in Fig. 5 for three YSZ catalysts calcined at different temperatures. Intensity of MS signals was normalized by the surface area of the catalyst. Compared with the results for ZrO_2 in Fig. 4, much less $\alpha\text{-O}$ desorbs from all YSZ14 catalysts. Moreover, the amount of $\alpha\text{-O}$ decreases with increasing calcination temperature ($\text{YSZ14A} > \text{YSZ14B} > \text{YSZ14C}$), but the amount of $\beta\text{-O}$ increases concurrently. Furthermore, the desorption temperature of $\beta\text{-O}$ seems to decrease with increasing calcination temperature. The amounts of both types of oxygen are estimated based on the peak areas (table 1).

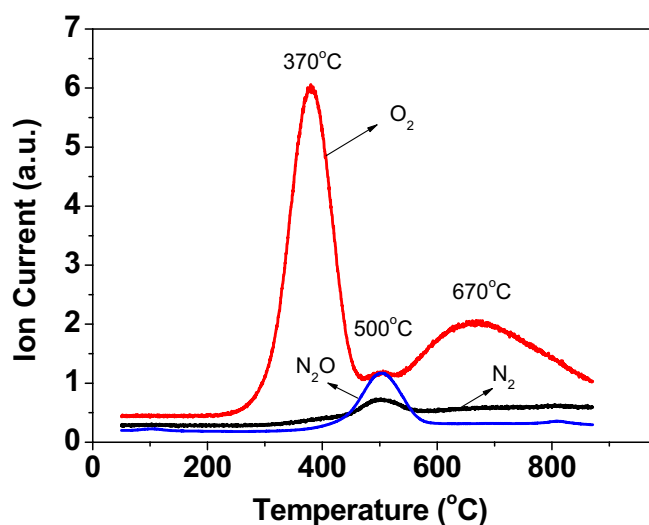


Fig. 3. TPD profiles obtained after N_2O decomposition over ZrO_2 ($S_g=15.4 \text{ m}^2/\text{g}$) at 300°C for 2 h. The intensity is normalized by surface area.

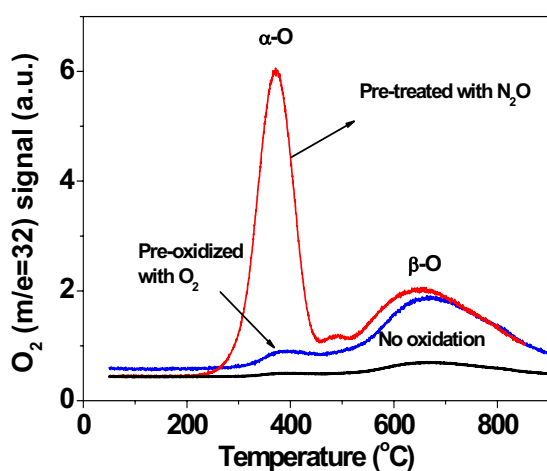


Fig. 4. TPD profiles of oxygen species formed *via* N_2O decomposition and *via* pre-oxidation with O_2 . The intensity is normalized by surface area.

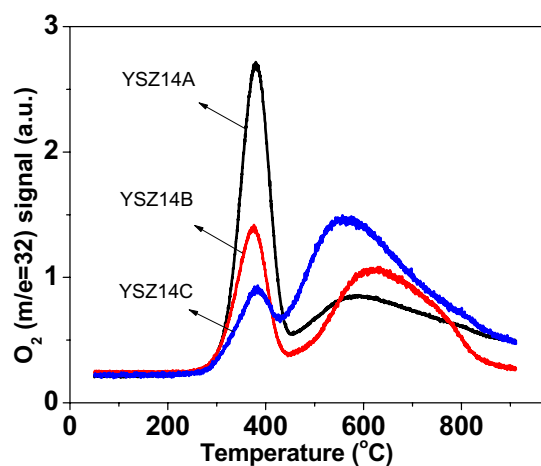


Fig. 5. TPD profiles of oxygen species formed *via* decomposition of N_2O over YSZ14A, YSZ14B, and YSZ14C. The intensity is normalized by surface area.

6.3.4. Characterization

6.3.4.1. SEM

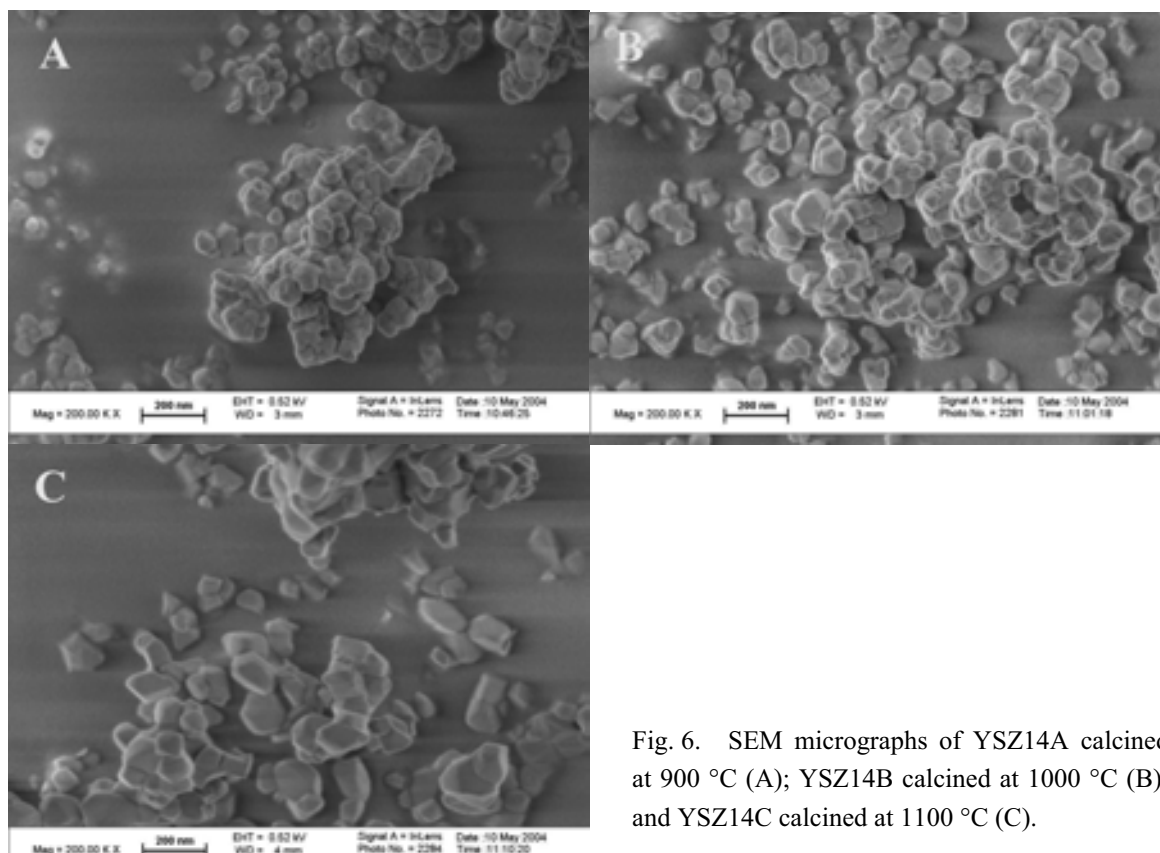


Fig. 6. SEM micrographs of YSZ14A calcined at 900 °C (A); YSZ14B calcined at 1000 °C (B); and YSZ14C calcined at 1100 °C (C).

The morphology of catalyst particles is shown in Fig. 6. The crystallite sizes of YSZ14A, YSZ14B and YSZ14C, estimated from their SEM images, are in the order of nanometers and increase with increasing calcination temperature. The estimated particle sizes are 50nm for YSZ14A, 75 nm for YSZ14B, and about 100 nm for YSZ14C. Moreover, calcination at higher temperature also results in more regularly shaped crystallites with an apparently increasing presence of low index planes.

6.3.4.2. XRD

XRD patterns of ZrO_2 , YSZ14A and YSZ14C are shown in Fig. 7. All YSZ catalysts possess the cubic crystallite structure, whereas the ZrO_2 structure is monoclinic. Based on the most intensive Bragg peak ($2\theta=30.14^\circ$) of the XRD spectrum, the grain size was also estimated by the Scherrer equation. As shown in table 1, the particle sizes

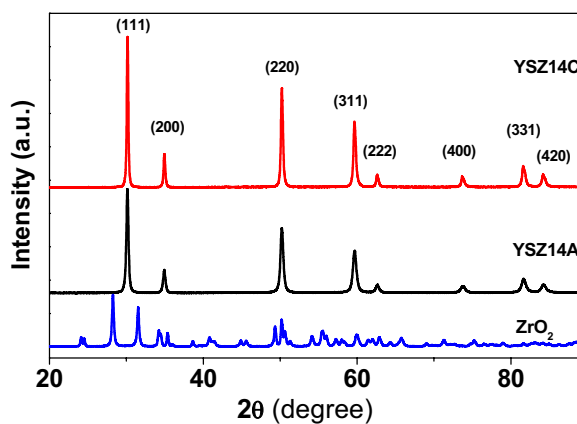


Fig. 7. XRD patterns of ZrO_2 and YSZ catalysts.

estimated based on both XRD and SEM are in reasonable agreement.

Table 1. Results of TPD and SEM, and theoretic estimation

Catalysts	Calcination temperature (°C)	Sg (m ² /g)	TPD of O ₂ species (atoms /m ²)		Surface Zr* (atoms/m ²)	Crystallite size (nm)	
			α-O	β-O		SEM	XRD
ZrO ₂	900	15.4	7.7×10 ¹⁶	4.7×10 ¹⁶	3.8×10 ¹⁸	~50	-
YSZ14A	900	13.7	3.4×10 ¹⁶	3.4×10 ¹⁶	2.9×10 ¹⁸	~50	39.4
YSZ14B	1000	10.2	1.8×10 ¹⁶	4.0×10 ¹⁶		~75	61.1
YSZ14C	1100	7.0	1.2×10 ¹⁶	6.4×10 ¹⁶		~100	77.6

* Estimated based on stoichiometry and LEIS measurements¹².

6.4. Discussion

6.4.1. Surface oxygen species

TPD of oxygen formed *via* decomposition of N₂O revealed the presence of two types of oxygen species, desorbing from the surfaces of ZrO₂ and YSZ catalysts (α-O and β-O species). YSZ14A and ZrO₂ have almost identical surface areas and comparable particle sizes. However, the amount of α-O atoms desorbed from ZrO₂ is about double as compared with YSZ14A (table 1). Apparently, the number of sites able to dissociatively adsorb N₂O decreases as a result of doping ZrO₂ with Y₂O₃. This indicates that the α-O atoms are associated to Zr, rather than to Y. As shown in Fig. 5 and table 1, the amount of α-O per m² decreases with decreasing the specific surface area of YSZ (YSZ14A>YSZ14B>YSZ14C). This difference must be caused by the change in structure of the surface of the YSZ catalysts because the surface composition is known to remain unchanged, as reported in Chapter 3 and our previous publication¹². Therefore, we conclude that the α-O atoms are adsorbed at the structural defects with low oxygen-coordination numbers, e.g. corners, edges, kinks and steps, as the amount of the α-O decreases with increasing crystallite size and with increasing regularity of the crystallite shape (table 1, Fig. 6). Doping Y₂O₃ in ZrO₂ causes the amount of α-O to decrease much more than one would expect from the fact that the surface-coverage of Y₂O₃ is only 14% (mol%). Apparently yttrium resides preferentially on the structural defects, effectively replacing Zr with Y at these sites, thus preventing the formation of α-O.

Based on the surface composition measured by LEIS¹², the total number of Zr cation per m² is estimated for both monoclinic ZrO₂ and cubic YSZ catalysts (table 1). The amount of α-O is as low as 2% of the surface zirconium cations for ZrO₂, and even less for all YSZ samples (1.2%, 0.6% and 0.4% for YSZ14A, YSZ14B and YSZ14C, respectively). The fact that α-O is a minority species is in agreement with the conclusion above that α-O resides on low coordination sites as the order of magnitude agrees with what one would expect for edges, corners, kinks and steps on not too well defined crystals shown in Fig. 6. Zhao *et. al.*¹⁹ studied

the nature of different Zr sites on ZrO₂ by ESR and reported that corners of ZrO₂ crystallites are mainly Zr³⁺ cations. Miller *et al.*,²⁰ studied N₂O adsorption and decomposition on ZrO₂ with FT-IR and observed that the number of surface Zr³⁺ sites significantly decreased when the surface of ZrO₂ was exposed to N₂O at 350°C. This was attributed to oxygen atoms formed *via* the dissociation of N₂O, however, no distinction would be made between the intrinsic oxygen vacancies and the structural defects (e.g. corners).

Adsorption of molecular N₂O at Zr⁴⁺ sites on the surface of ZrO₂ was observed by Miller *et al.*¹⁷ with FT-IR spectroscopy, which is in agreement with the small amount of N₂O desorbed at about 500°C from ZrO₂ (Fig. 4). Simultaneous formation of O₂ and N₂ at 500°C might be caused by decomposition of the desorbing N₂O at active sites, which are regenerated by desorption of the α-O at temperatures above 370°C.

The amounts of the β-O formed during TPD correspond to 0.62% and 0.47% of oxygen ions in one monolayer of ZrO₂ and YSZ, respectively. It was reported previously¹³ that about 13.6% and 8.5% of oxygen ions in the outermost layer can be extracted from ZrO₂ and YSZ respectively by H₂ or CH₄ at 900°C. Those conditions cause a much lower effective oxygen pressure as compared to conditions (up to 800°C, and 10⁻³ mbar vacuum) used in the present work. Therefore, this small amount of β-O can be reasonably attributed to partial reduction of the surface at high temperatures under high vacuum, forming oxygen vacancies ($Zr'_{Zr} - V''_O - Zr'_{Zr}$). Consistently, Deibert *et al.*²¹ observed the reduction of ZrO₂ surface layer after exposure to UHV at temperatures above 550°C. It is also important to note that there is also solid evidence from others that the surface of ZrO₂ can be partly reduced by reducing gases, e.g., CO^{22;23}, although ZrO₂ is not normally considered to be reducible.

6.4.2. Activations of N₂O and O₂

Fig. 8 shows that the decomposition rate of N₂O over ZrO₂ and YSZ at 600°C increases with the surface-concentration of α-O as determined by TPD. This strongly suggests that the structural defects (corners, edges, kinks and steps) are active sites for N₂O decomposition. The presence of Y₂O₃ in the surface decreases both the number of adsorption sites as discussed in Section 4.1 as well as the number of active sites.

It is well known that oxygen vacancies ($Y'_{Zr} - V''_O - Y'_{Zr}$) are generated extrinsically by doping ZrO₂ with Y₂O₃ as the effective charge of the incorporation of two Y³⁺ ions is balanced with an oxygen vacancy^{24;25}. However the significant lower activity of YSZ (Fig. 2), as compared with ZrO₂, implies that these extrinsic oxygen vacancies are not active sites for N₂O decomposition.

Desorption of oxygen from ZrO₂ (Fig. 3) and YSZ (Fig. 5) clearly shows that decomposition of N₂O already occurs at temperature as low as 300°C. Comparable results have been reported even at room temperature^{16;20}. However, apparently, N₂O conversion at temperatures below 450°C at GHSV of 6×10³ h⁻¹ is below the detecting limit in this work (Fig. 2). Oxygen

vacancies were generally proposed as the active sites for N_2O decomposition over many oxides, e.g. ZrO_2 ¹⁶, $YBa_2Cu_3O_7$ and Gd_2CuO_4 ²⁶. Miller *et al.*²⁰ proposed that decomposition of N_2O over ZrO_2 proceeds *via* an electron transfer reaction from Zr^{3+} site to form N_2O^- as a transient intermediate, which decomposes to a molecular N_2 and an adsorbed oxygen atom.

The amount of β -O on ZrO_2 is identical after oxidation with either

N_2O or O_2 . This indicates that the surface oxygen vacancies ($Zr'_{Zr}-V_O''-Zr'_{Zr}$) formed by partially reduction (removal of surface lattice oxygen ions *via* high temperature vacuum treatment) are able to activate both N_2O and O_2 . This is consistent with our previous conclusion¹³ that molecular oxygen can directly activated on this type of oxygen vacancies, based on the observation that $C^{18}O^{16}O$ was produced during $^{18}O_2-CH_4$ pulse over ZrO_2 at 600°C. However, almost no α -O desorbed from ZrO_2 oxidized with O_2 at temperatures between 50 and 800°C (Fig. 4). This indicates that oxygen molecules hardly dissociate at the structural defective sites (e.g. corners and edges) at temperatures below the desorption temperature of α -O. Similar observations were reported by Nakamura *et al.*²⁷ for CaO treated with either N_2O or O_2 . It was proposed by Winter²⁸ that one-electron defects are responsible for N_2O activation while activation of O_2 occurs mainly at two-electron vacancies. Intrinsic oxygen vacancies ($Zr'_{Zr}-V_O''-Zr'_{Zr}$) are associated with two Zr^{3+} cations, from which two electrons are available. In contrast, the isolated structural defective site at corners and edges can supply only one electron. This explains why structural defects are *not* active sites for oxygen activation during CPOM, although they can adsorb N_2O dissociatively. This conclusion is also supported by the fact shown in Fig. 1 that ZrO_2 is less active in CPOM than YSZ catalysts, although ZrO_2 has more structural defective sites than YSZ as discussed above.

6.4.3. Effect of calcination temperature

Methane conversion rate per m^2 increases with increasing calcination temperature (Fig. 1), although these catalysts have an identical bulk composition and surface composition (12 ± 2 mol% Y_2O_3 in the outermost layer)¹². The amounts of β -O desorbed from YSZ14 catalysts also increase with increasing calcination temperature (Fig. 5, Table 1). Fig. 9 demonstrates a linear relationship between the methane conversion rate per m^2 and the amount of β -O per m^2 .

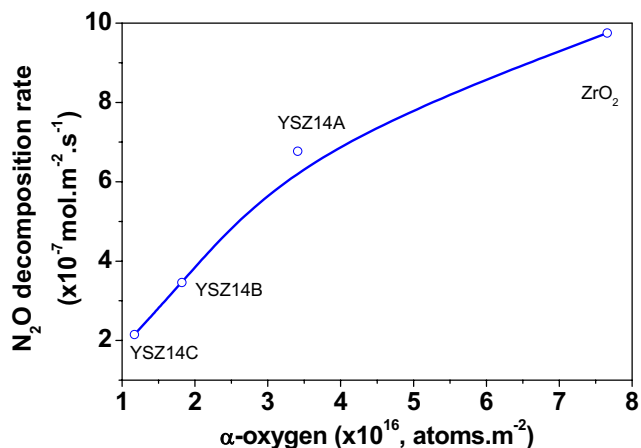


Fig. 8. Dependence of N_2O conversion rate on the amount of α -O observed during TPD.

This leaves the question why the activity and amount of β -O increase with calcination temperature. SEM images of three YSZ catalysts shows that calcination at higher temperature results in more regularly shaped crystallites with an increasing presence of low index planes (Fig. 6), suggesting that low index planes contain more β -O. The formation of low-index planes during thermal treatment is well known. It was reported that oxygen-terminated (111) surface of oxides with the fluorite structure is energetically favorable since this structure does not create a dipole moment²⁹. Indeed, the (111) face has the lowest surface energy for cubic YSZ (with fluorite structure)³⁰ as compared to the (110) and (100) faces. Therefore, especially the exposure of (111) planes is expected to increase with calcination temperature. The same trend was also reported for monoclinic ZrO_2 by Morterra et al.³¹.

Fig. 5 demonstrates that more active catalysts appear to desorb not only more β -O but also more easily, i.e. at lower temperatures. We propose that the surface reducibility of YSZ increases with the oxygen coordination number of the zirconium cation in the surface. The coordination number of Zr cation depends on the orientation of the surface plane. On the (111) Zr is coordinated with 7 oxygen ions, while the coordination numbers are 6 for Zr on both (110) and (100) surface-faces as compared to 8 in the bulk³⁰. As discussed above, the most stable surface seems indeed to be the surface with the highest oxygen coordination number. It seems reasonable to assume that surface lattice oxygen is more easily removed when the original coordination number is higher. The results in Fig. 5 indicate that the average coordination number of Zr in the surface of YSZ increases with calcination temperature and that therefore surface lattice oxygen is easier to be extracted, enhancing the activity for CPOM.

6.5. Conclusion

The role of the defective structure of both ZrO_2 and YSZ in activation of O_2 and N_2O has been studied. N_2O can be activated at both structural defects (e.g. Zr cations located at corners) and intrinsic oxygen vacancies ($Zr_{Zr}'-V_O^{\bullet\bullet}-Zr_{Zr}'$) and forms two types of oxygen species (α -O and β -O) on the surface, respectively. In contrast, molecular oxygen gives rise to only one type of oxygen species (β -O), i.e. surface lattice oxygen. This type of oxygen species can be

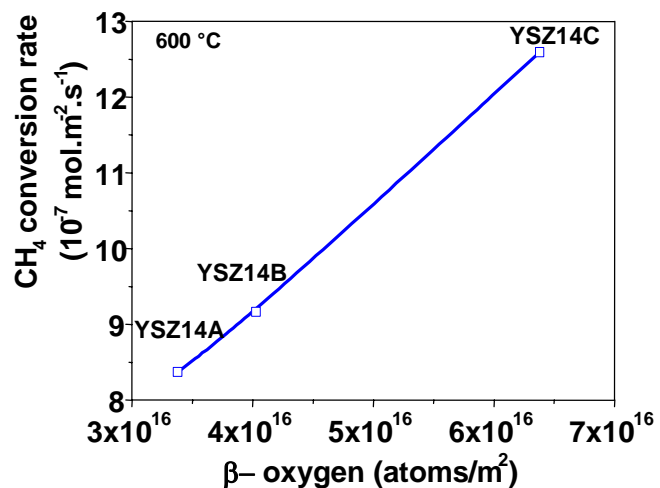


Fig. 9. Dependence of methane conversion rate on the amount of β -O observed during TPD.

extracted by reaction with methane, forming the intrinsic oxygen vacancies again during CPOM. However, the structural defects are not active for oxygen activation during CPOM. Doping ZrO₂ with Y₂O₃ significantly decreases the number of the structural defects via replacement of Zr⁴⁺ cations by Y³⁺ cations, located at corners, steps, kinks and edges of the crystallites. Calcination at higher temperatures results in less structural defects due to both increasing crystallite size as well as transformation to more regular shaped crystallites. High temperature calcinations also increase the activity of YSZ in CPOM. This is attributed to the increase in the exposition of low index planes, especially those (111) with the lowest surface energy and the highest coordination numbers, induced by the thermal treatment.

Acknowledgements

This work was performed under the auspices of NIOK, the Netherlands Institute of Catalysis Research. Stichting Technische Wetenschappen (STW, the Dutch technology foundation) is gratefully acknowledged for financial support under project number UPC-5037. The authors thank Dr. Henny J.M. Bouwmeester (IMS, university of Twente, The Netherlands) for valuable discussion, Ing. J.A.M. Vrielink, Dr. R. Keim and Mr. H. Koster for BET, SEM and XRD measurements, respectively, and Ing. Bert Geerdink for technical support.

References

1. S.Cornot-Gandolphe, *Energy Explor.Exploit.* 13, 3 (1995).
2. J.W.Chun and R.G.Anthony, *Ind.Eng.Chem.Res.* 32, 259 (1993).
3. T.Sugino, A.Kido, N.Azuma, A.Ueno, Y.Udagawa, *J.Catal.* 190, 118 (2000).
4. Q.Zhang, D.He, Z.Han, X.Zhang, Q.Zhu, *Fuel* 81, 1599 (2002).
5. T.Weng and E.E.Wolf, *Appl.Catal.A* 96, 383 (1993).
6. A.Parmaliana and F.Arena, *J.Catal.* 167, 57 (1997).
7. A.Parmaliana, F.Frusten, F.Arna, A.Mezzapica, V.Sokolovskii, *Catal.Today* 46, 117 (1998).
8. K.D.Campbell, H.Zhang, J.H.Lundford, *J.Phys.Chem.* 92, 750 (1988).
9. S.Wada, T.Tagawa, H.Imai, *Appl.Catal.* 47, 277 (1989).
10. J.Zhu, M.S.M.M.Rahuman, J.G.van Ommen, L.Lefferts, *Appl.Catal.A.* 259, 95 (2004); *Chapter 2.*
11. J.Zhu, J.G.van Ommen, L.Lefferts, *J.Catal.* 225, 388 (2004); *Chapter 4.*

12. J.Zhu, J.G.van Ommen, A.Knoester, L.Lefferts, *J.Catal.* 230, 300-309 (2005); *Chapter 3*.
13. J.Zhu, J.G.van Ommen, H.J.M.Bouwmeester, L.Lefferts, *submitted to Angewandte chemie* (2005); *Chapter 5*.
14. M.Nakamura, H.Yanagibashi, H.Mitsubishi, N.Takezawa, *Bull.Chem.Soc.Jpn* 66, 2467 (1993).
15. G.I.Panov, V.I.Sobolev, A.S.Kharitonov, *J.Mol.Catal.* 61, 85 (1990).
16. J.Lin, H.Y.Chen, L.Chen, K.L.Tan, H.C.Zeng, *Appl.Surf.Sci.* 103, 307 (1996).
17. T.M.Miller and V.H.Grassian, *J.Am.Chem.Soc.* 117, 10969 (1997).
18. R.A.van Santen, P.W.N.M.van Leeuwen, J.A.Moulijn, B.A.Averill, *Catalysis; An integrated approach* (Elsevier, Amsterdam, 1999).
19. Q.Zhao, X.Wang, T.Cai, *Appl.Surf.Sci.* 225, 7 (2004).
20. T.M.Miller and V.H.Grassian, *Catal.Lett.* 46, 213 (1997).
21. M.C.Deibert and R.Kahraman, *Appl.Surf.Sci.* 37, 327 (1989).
22. S.M.Stagg, E.Romeo, C.Padro, D.E.Resasco, *J.Catal.* 178, 137 (1998).
23. S.Sharma, S.Hilaire, J.M.Vohts, R.J.Gorte, H.W.Jen, *J.Catal.* 190, 199 (2000).
24. N.Mommer, T.Lee, J.A.Gardber, W.E.Evenson, *Phys.Rev.B.* 61, 162 (2000).
25. E.Karaetrova et al., *J.Am.Ceram.Soc.* 84, 65 (2001).
26. D.Belapurkar, N.M.Gupta, G.M.Phatak, R.M.Iyer, *J.Mol.Catal.* 87, 287 (1994).
27. M.Nakamura, H.Mitsubishi, N.Takezawa, *J.Catal.* 138, 686 (1992).
28. E.R.S.Winter, *J.Catal.* 34, 431 (1974).
29. J.C.Conesa, *Surf.Sci.* 339, 337-352 (1995).
30. G.Ballabio, M.Bernasconi, F.Pietrucci, S.Serra, *Phys.Rev.B* 70, 075417 (2004).
31. G.Cerrato, S.Bordiga, S.Barbera, C.Morterra, *Surf.Sci.* 377-379, 50-55 (1997).

Chapter 7

Concluding Remarks and Recommendations:

A Promising Concept for Catalytic Partial Oxidation of Hydrocarbons to Synthesis Gas

7.1. CPOM over ZrO₂ and YSZ

7.1.1. Catalytic chemistry

The understanding of the catalytic chemistry on the surface of catalysts is a critical step for catalyst design, although it is always a challenge for fundamental research in catalysis and surface science. The work presented in this thesis mainly aims to study on the reaction mechanism of CPOM over ZrO₂ and YSZ catalysts. Emphasis is put on (i) the active sites for both oxygen and methane activation; and (ii) the reaction scheme of CPOM, which consists of multiple pathways. The relative rates of these multiple pathways are influenced by the reaction conditions and certainly also depend on the nature of the catalysts. These two concepts are keys to understand the surface catalytic chemistry and to explain different catalytic performance of ZrO₂ and YSZ.

1) Reaction scheme

The work described in this thesis (Chapter 4) revealed that formaldehyde and formate are two major reaction intermediates for CPOM over ZrO₂ and YSZ catalysts. CO and H₂ are produced mainly *via* decomposition of formaldehyde. On the other hand, formaldehyde can be further oxidized to surface formate, which decomposes either to CO and H₂O *via* dehydration, or to CO₂ and H₂ *via* dehydrogenation. Obviously, selectivity to synthesis gas depends on the relative rates of both decomposition and oxidation of formaldehyde, which vary with reaction conditions e.g. temperature, ratio of CH₄/O₂, and the nature of the catalyst. Formation of H₂O is intrinsically unavoidable due to reaction: CH₄+O₂→ CH₂O + H₂O, which occurs during methane activation. Because ZrO₂ and YSZ are insufficiently active for steam and CO₂ reforming of CH₄ even at temperatures above 900°C, CH₄ conversion and selectivity to H₂ are always less than 50% for a stoichiometric feedstock (CH₄/O₂=2:1).

This information about the reaction scheme, on one hand, indicates that it is impossible to reach reaction equilibrium using ZrO₂-based oxide catalysts alone. It is necessary to compensate their insufficient activities in CH₄ reforming with a reforming catalyst in a dual bed system as described in Chapter 2. On the other hand, this information is also very essential to define a research strategy to achieve higher selectivity by modifying ZrO₂-based catalysts. To further enhance the selectivity of ZrO₂-based oxide catalysts to synthesis gas by accelerating the decomposition of surface formaldehyde and/or preventing its oxidation, modification of YSZ with alkali or rare earth oxides would be an interesting subject for further research. It was already reported in Chapter 3 that YSZ contaminated with CaO is significantly more selective than pure YSZ, although it was less active at low temperatures. Additionally, promoters with lower valence of cations (<4) could be more efficient than higher valent cations because they prefer to be in the surface and subsurface layers after calcination at high temperatures. Assuming that CPOM over CaO-contaminated YSZ also

proceeds *via* a Mars-van Krevelen mechanism as proposed for ZrO_2 and normal YSZ in Chapter 5, the enhanced selectivity is possibly caused by lower concentration of the extractable lattice oxygen on the surface of the CaO-contaminated YSZ as compared with normal YSZ. However, to explain in detail the reason for the enhanced selectivity is still a challenge, which can be one of the subjects for future work.

2) Active sites

The most important contribution of this thesis is in understanding the effects of extrinsic oxygen vacancies in YSZ on CPOM, which are formed by doping Y_2O_3 in ZrO_2 (Chapter 5). To the best of our knowledge, it is the first time that experimental evidence is given for the oxidation of CH_4 by the surface lattice oxygen ions of ZrO_2 or YSZ instead of adsorbed surface oxygen. CPOM over ZrO_2 and YSZ is proposed to proceed *via* a Mars-van Krevelen mechanism. A high concentration of oxygen vacancies is generated by doping ZrO_2 with Y_2O_3 , which not only enable fast activation of oxygen molecules but also facilitate fast lattice diffusion of oxygen ions. The two effects together lead to a rapid replenishment of the surface lattice oxygen extracted by methane. Both reactivity and selectivity are strongly influenced by the concentration of surface lattice oxygen for CPOM over YSZ. The higher the concentration, the more active but the less selective YSZ is.

It has been observed that for some reactions the reaction rate changes dramatically with morphological structure of the catalyst; for example, the reaction rate increases significantly from single-crystal surfaces to small particles in which there are a large number of intrinsically structural defects, e.g. corners, edges, kinks and steps. In contrast, for other reactions, the reaction rate is independent of the catalyst structure. Qualitatively, two classes of catalytic processes have therefore been named: the structure-sensitive and structure-insensitive reactions¹. It is revealed in Chapter 6 that CPOM over ZrO_2 and YSZ is not a structure sensitive reaction. The structural defects are not the active sites for oxygen activation.

It is clear that to be more active catalysts ZrO_2 -based oxides need both a high concentration of the surface lattice oxygen and fast replenishment of the consumed oxygen ions. Doping ZrO_2 with Y_2O_3 increases the concentration of oxygen vacancy significantly, but it also decreases the concentration of surface lattice oxygen. CPOM over YSZ14 (ZrO_2 doped with 14 wt.% Y_2O_3) has shown that CH_4 activation is the rate-determining step. This implies that the active sites for oxygen activation, i.e. the Y_2O_3 -induced surface oxygen vacancies, are excess. For an optimized YSZ catalyst, activation rates of both oxygen and methane should be comparable. Therefore, reduction of the Y_2O_3 content would be one of the options. However, as described in Chapter 3 segregation of Y_2O_3 to the surface during calcination at high temperatures results in almost identical surface composition, which is independent of Y_2O_3 content in the bulk. Modifying YSZ by doping traces of partly reducible oxides, e.g. CeO_2 , MnO_2 , Fe_2O_3 , V_2O_5 ,

7.1.2. Technical concept for synthesis gas production

As we discussed in Chapter 1, normal supported metallic catalysts, e.g. Rh, Pt, Ni, are suffering from loss of metal *via* evaporation in the form of volatile metal oxides at high temperatures, especially in the presence of oxygen under CPOM conditions. Therefore, hardly reducible oxides as highly stable catalysts for selective oxidation of methane to synthesis gas are subject of this thesis. Major work is focused on ZrO₂ and YSZ catalysts. The results are very promising. The defective oxide YSZ showed good selectivity to synthesis gas and excellent stability, although CO₂ and H₂O are formed. Its reforming activity is insufficient even at very high temperatures as pointed out in Chapter 3. However, this insufficient reforming activity can be compensated by introducing a second reactor with a metal catalyst. It was demonstrated in Chapter 2 that the dual bed concept for conversion of methane to synthesis gas is indeed possible and renders advantages compared to the single metal catalyst bed.

Key issues here to arrive at cheaper and more stable catalysts are:

- Limit the high temperatures (hot spot formation) compared to metallic catalysts by taking advantage of the fact that these oxide catalysts form synthesis gas as a primary product.
- Prevent contact with O₂ of the second (metallic) catalyst used for reforming, thus preventing metal loss in the form of volatile metal oxide formed at very high temperature and in the presence of oxygen.

Both approaches help to increase catalyst stability, which is still a major problem of metal catalysts.

It was demonstrated in Chapter 2 that operation of the first reactor (catalyst YSZ12C, S_g = 4.5 m²/g) at 1000°C with undiluted methane/oxygen mixtures and the second reactor (catalyst LaCoO₃) at 800°C results in complete selective conversion with GHSV in the same order of magnitude (10⁴ h⁻¹) as reported in literature for supported Rh catalysts^{4,5}. The necessary temperature for the first reactor can be significantly reduced when YSZ with higher surface area is applied, as discussed in Chapter 3 (Fig. 7). Moreover, compared with YSZ12 catalysts that are contaminated with CaO, uncontaminated YSZ14 catalysts are much more active. If YSZ14A with a surface area of 13.7 m²/g is used in the first reactor of the dual bed system, a reaction temperature of 650°C is required for this catalyst bed to consume all oxygen. It also can be expected that the GHSV can be further enhanced if Rh, the most active catalyst for methane reforming⁶, is used in the second catalyst bed instead of supported Co catalyst.

A system to generate 1 mol H₂ per second (roughly 100 kWh) would need a 2-liter YSZ reactor and a 1-liter metal catalyzed reforming reactor. This indicates that this dual bed system is an option to arrive at fairly small reactors. More importantly, this can result in an improved process control and improved catalyst stability, compared to supported metal catalysts.

7.1.3. Challenges in the application

As observed in this work, ZrO₂-based oxides, e.g. YSZ, directly catalyze partial oxidation of methane to synthesis gas with a high selectivity of 50 to 75%. It was demonstrated in Chapter 2 that synthesis gas with an equilibrium composition (almost 100% CO and H₂ yields) can be produced with the dual bed concept. However, the ZrO₂-based oxides need a relatively high startup temperature due to their low activities as compared with metal catalysts, especially compared with noble metals. Secondly, because mainly

direct partial oxidation occurs over YSZ, insufficient reaction heat generated makes it difficult to maintain adiabatic operation. Therefore, the major challenge of the dual bed approach is to lower the startup temperature and to maintain the CPOM reaction in adiabatic operation.

The essential difference compared with metallic catalysts is that decreasing the reaction temperature over YSZ does not initiate deep oxidation, which liberates lots of energy to drive the temperature up again. Fig. 1 shows the relation between the temperatures of operation *versus* the adiabatic temperature when CPOM is operated over YSZ catalyst bed with diluted methane-oxygen mixtures (CH₄:O₂:He=2:1:14). A lower dilution degree will result in a larger adiabatic temperature rise.

It may be possible to use the reaction heat, which is generated during CPOM over ZrO₂-based oxides, to heat up the feed stream to the reaction temperature by heat exchange between outlet-stream and inlet-stream. Based on these data in Fig. 1, it is roughly estimated what heat exchange efficiency is required according to the following equation:

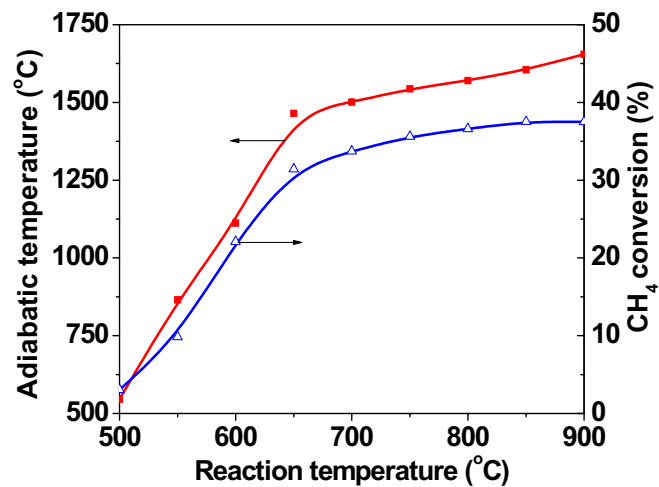


Fig. 1. Adiabatic temperature as a function of reaction temperature. Catalyst: 300 mg YSZ14A (Sg=13.7 m²/g), CH₄:O₂:He=2:1:14, total flow rate: 170 ml/min. (Estimated with HSC chemistry package)

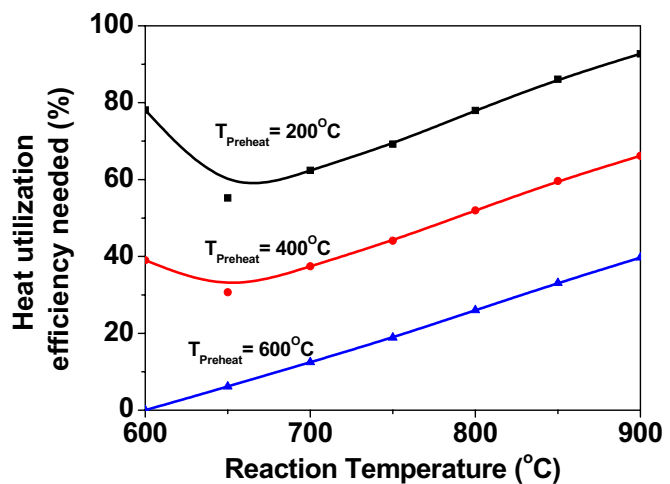


Fig. 2. Heat utilization efficiencies needed as a function of reaction temperature at different preheat temperatures.

$$\text{Heat utilization efficiency} = \frac{T_{\text{Reaction}} - T_{\text{Preheat}}}{T_{\text{Adiabatic}} - T_{\text{Reaction}}} \times 100\%$$

where C_p and flow rate are assumed to be unchanged after reaction. The calculations (Fig. 2) reveal that to reach a reasonable heat exchange efficiency (<50%) the feed stream still needs to be preheated up to 400 or 600°C.

To start up CPOM, probably it is not a big problem for metal catalyst because of their high activities. However, for YSZ to arrive at the high temperatures around 700°C, which is necessary for complete conversion of oxygen, is still a challenge. A conceptual solution would be to reverse the flow directions during startup as illustrated in Fig. 3, using the reforming catalyst for CPOM for a short time to heat up the dual bed system. Then reverse the flow and start to use the oxide catalyst for the oxidation step.

There are also other possibilities to develop catalysts, which require a lower temperature for both startup and stable adiabatic operation: (1) enhancing the catalytic activity by increasing surface area and/or adding small amount of precious metals or partly reducible metal oxides; (2) adding higher hydrocarbons or compounds like methanol to methane, which are easier to be activated than methane.

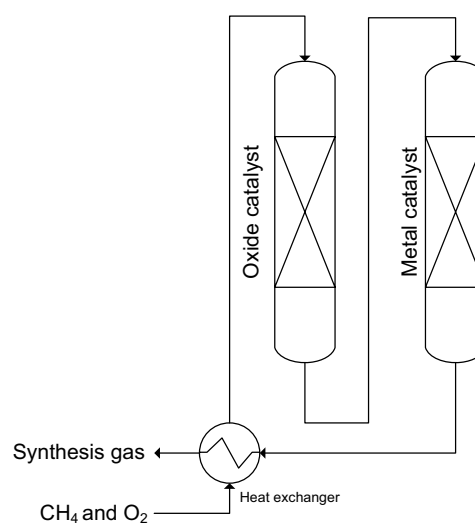


Fig. 3. Dual bed system for CPOM

7.2. Catalytic partial oxidation of liquid hydrocarbons

In addition of synthesis gas used as a starting material for production of chemicals, high-content hydrogen stream (e.g. synthesis gas) is also needed for fuel cell and internal combustion engines. While past research efforts have mainly focused on partial oxidation of methane due to its high H/C ratio, there has been an increasing emphasis on discovering new ways to convert well-distributed fuels like gasoline and diesel to hydrogen. The efficient conversion of these fuels to a high-content H_2 stream would greatly aid in the introduction of fuel cells into the automotive market because infrastructure of both gasoline and diesel has existed already. Then, the H_2 generation could be carried out anywhere using an on board reactor⁷. Similarly, the conversion of small amounts of these fuel to a synthesis gas mixture would improve spark ignition engine and catalytic performance of the exhaust catalyst, thus lowering emissions because hydrogen/fuel/air mixtures provide a more homogeneous combustion than normal fuel/air mixture⁸. The common feature shared by these processes is that they require the rapid, efficient conversion of liquid hydrocarbons to synthesis gas under a variety of conditions.

However, the knowledge about partial oxidation of hydrocarbons to synthesis gas is almost exclusively for CPO of methane. CPO of higher hydrocarbons has not got much attention so far. Therefore, study on this subject would be significantly important from both scientific and technical points of view.

Compared with methane, liquid hydrocarbons are much easier to be activated. CPO of liquid hydrocarbons can start up at a relative low temperature. There are, however, several problems demanding for extra attention, such as soot formation associated with combustion of fuel-rich gases, and deactivation of the catalyst due to also the soot formation. Therefore, major work in CPO of liquid hydrocarbons is to develop stable and active catalysts.

Based on our experience in CPO of methane, YSZ supported metallic catalysts are proposed for CPO of liquid hydrocarbons. As pointed out above, YSZ oxides are not active enough to start up at low temperatures and to maintain the CPO reaction in adiabatic operation, although it is beyond any doubt that YSZ oxides are active catalysts for CPO. To improve the activity of YSZ, especially the activity at low temperatures, small loadings of noble metal e.g. Rh, Pt, (ranging from the ppm region up to 0.1%) may be added to YSZ. Because of poor electron conductivity of YSZ, the electron transfer dominates the oxygen activation over YSZ. Obviously, adding very small amount of metal will significantly accelerate activation of molecular oxygen *via* enhancing electron conductivity of the catalyst. The effect of small amount of metal has been shown to significantly reduce the activation enthalpy for surface oxygen exchange on YSZ.

As mentioned in Chapter 1, normal metal catalysts are suffering from poor thermal stability that handicaps industrialization of metal-based CPO process. However, compared with the normal supported metal catalyst, a stronger interaction would be expected between noble metal and the defective oxide support YSZ, especially, the interaction between metal clusters and defective oxides. The strong interaction between metal and defective ZrO₂-based supports has been reported for many catalytic systems, e.g. CuO/YSZ for CO oxidation^{9;10}, Pt/YSZ for CO₂ reforming of methane¹¹. It was reported that oxygen vacancies on the surface of YSZ directly interact with the interfacial terminal oxygen ions of metal oxide. Similar effect of oxygen vacancies in support on stability of the supported metal catalysts was observed for Au/TiO₂ catalyst. Zhang *et al.*¹² found that a sputtered TiO₂ surface (with oxygen vacancies) can limit cluster size and simultaneously increase the cluster density. More recently, Wahlstrom *et al.*¹³ showed that oxygen vacancies on TiO₂ can serve as nucleation sites to immobilize Au particles.

Moreover, by special preparation methods, like sol-gel, small amount of noble metal can be dispersed homogeneously in the matrix of defective oxide support. In this way, the possibility of migration of small metal particles would be significantly reduced. Thus, the stability of the catalyst will significantly increase by efficiently preventing sintering of the metal species. Less deep oxidation would be expected for the proposed catalysts than for normal metal catalyst, because of very low metal loadings and good activity of support (ZrO₂ or YSZ) in

direct oxidation of hydrocarbon (methane) to synthesis gas. Therefore, the possibility of losing metal via formation of volatile metal oxide will be significantly reduced due to the smaller amount of reaction heat generated (and therefore lower surface temperature of the catalyst) during the reaction.

Deactivation of the catalysts due to carbon deposition is a problem for CPO of methane over metal catalysts, e.g. Ni, as discussed in Chapter 1. This problem will be more serious for CPO of liquid hydrocarbons because of low H/C ratio in their molecules. To increase resistance of the catalyst to carbon formation will be a big challenge for CPO of liquid hydrocarbons. ZrO₂ was frequently reported to be a unique catalyst support for various catalytic reactions. It was reported by Lercher *et al.*^{14;15} that ZrO₂ as a support is crucial for platinum and nickel catalysts to minimize coke deposition under CO₂/CH₄ reforming conditions. The anti-carbon formation property of ZrO₂ support was also reported by others¹⁶. Compared with ZrO₂, YSZ is a better oxygen ion conductor. A high concentration of oxygen vacancies (active sites for oxygen activation) created by doping Y₂O₃ in ZrO₂ results in both fast activation of molecular oxygen and rapid diffusion of oxygen ions in the bulk. Therefore, an even better anti-carbon formation property would be expected for YSZ.

To design a better catalyst for CPO of liquid hydrocarbons, the following questions need to be addressed: Does a high concentration of oxygen vacancies prevent carbon deposition on the surface? Or, even if the surface of the catalyst is partially covered by cook, is the catalyst still active enough? Moreover, as discussed in this thesis, YSZ itself is already an active catalyst for CPOM. What will be the role of YSZ when a small amount of metal is present? What are effects of oxygen vacancies and their interaction with metal or metal clusters supported? More interestingly, what is essential for this reaction, metal particles or metal clusters as reported for the water-gas shift reaction over Au/CeO₂ or Pt/CeO₂¹⁷? To answer these scientific questions, more detailed studies are necessary.

References

1. M.Boudart, *J.Mol.Catal.* 30, 27 (1985).
2. M.A.Johnson, E.V.Stefanovich, T.N.Truong, *J.Phys.Chem.B* 101, 3196-3201 (1997).
3. T.Ito, J.X.Wang, C.H.Lin, J.H.Lunsford, *J.Am.Chem.Soc.* 1075062-1075068 (1985).
4. P.M.Witt and L.D.Schmidt, *J.Catal.* 163, 465 (1996).
5. P.D.F.Vernon, M.L.H.Green, A.K.Cheetham, A.T.Ashcroft, *Catal.Lett* 6, 181 (1990).
6. A.P.E.York, T.Xiao, M.L.H.Green, *Topics in Catal.* 22, 345 (2003).
7. L.D.Schmidt, E.J.Klein, C.A.Leclerc, J.J.Krummenacher, K.N.West, *Chem.Eng.Sci.* 58, 1037 (2003).

8. Y.Jamal and M.L.Wyszynski, *Inter.J.Hydrogen Energy*. 19, 557 (1994).
9. W.P.Dow and T.J.Huang, *J.Catal.* 160, 171-182 (1996).
10. W.P.Dow, Y.P.Wang, T.J.Huang, *J.Catal.* 160, 155-170 (1996).
11. Y.Z.Chen, B.J.Liaw, C.F.Kao, J.C.Kuo, *Appl.Catal.A* 217, 23-31 (2001).
12. L.Zhang, F.Cosandey, R.Persaud, T.E.Madey, *Surf.Sci.* 439, 73 (1999).
13. E.Wahlstrom et al., *Phys.Rev.Lett.* 90, 026101 (2003).
14. J.A.Lercher, J.H.Bitter, W.Hally, W.Niessen, K.Seshan, *Stud.Surf.Sci.Catal.* 101, 463 (1996).
15. J.H.Bitter, K.Seshan, J.A.Lercher, *J.Catal.* 171, 279 (1997).
16. J.M.Wei, B.Q.Xu, J.L.Li, Z.X.Cheng, Q.M.Zhu, *Appl.Catal.A* 196, L167 (2000).
17. Q.Fu, H.Saltsburg, M.Flytzani-Stephanopoulos, *Science* 301, 935-938 (2003).

Referred Publications

1. Jianjun Zhu, M.S.M.M. Rahuman, Jan G. van Ommen, Leon Lefferts, “**Dual Catalyst Bed Concept for Catalytic Partial Oxidation of Methane to Synthesis Gas**”, *Appl. Catal. A*. **259**, 95-100 (004).
2. Jianjun Zhu, M.S.M.M. Rahuman, Jan G. van Ommen, Leon Lefferts, “**Partial Oxidation of Methane to Synthesis Gas in Dual Catalyst Beds Combining Irreducible Oxide and Metallic Catalysts**”, *Stud. Surf. Sci. Catal.* **147**, 205-210 (2004)
3. Jianjun Zhu, Jan G. van Ommen, Arie Knoester, Leon Lefferts, “**Effect of Surface Composition of Yttrium-Stabilized Zirconia on Partial Oxidation of Methane to Synthesis Gas**”, *J. Catal.* **230**, 300-309 (2005).
4. Jianjun Zhu, Jan G. van Ommen, Leon Lefferts, “**Reaction Scheme of Partial Oxidation of Methane to Synthesis Gas over Yttrium-stabilized Zirconia**”, *J. Catal.* **225**, 388-398 (2004)
5. Jianjun Zhu, Jan G. van Ommen, Henny J.M. Bouwmeester, Leon Lefferts “**Activation of O₂ and CH₄ on Yttrium-stabilized Zirconia for the Partial Oxidation of Methane to Synthesis Gas**”, *submitted to J. Catal.* (2005).
6. Jianjun Zhu, Jan G. van Ommen, Henny J.M. Bouwmeester, Leon Lefferts “**Partial Oxidation of Methane to Synthesis Gas over Yttrium-stabilized Zirconia: A Surface Redox Mechanism**”, *submitted to Angewandte Chemie* (2005).
7. Jianjun Zhu, Sander Albertsma, Jan G. van Ommen, Leon Lefferts, “**The Role of Defect Structure in Activation of N₂O and O₂ on ZrO₂ and Yttrium-stabilized ZrO₂**”, *submitted to J. Phy. Chem. B.* (2005).
8. Jianjun Zhu, Jan G. van Ommen, Leon Lefferts, “**Partial Oxidation of Methane by O₂ and N₂O to Syngas over Yttrium-stabilized ZrO₂**”, *submitted to Catal. Today* (2005).
9. Jianjun Zhu, Jan G. van Ommen, Leon Lefferts, “**Activation of Methane by Active Oxygen on Oxide catalysts: Abstraction or Insertion?**”, in preparation.
10. Jianjun Zhu, Henny J.M. Bouwmeester, Jan G. van Ommen, Leon Lefferts, “**Study on Oxygen Exchange between Gas Phase and Yttrium-stabilized ZrO₂ with Transient Methods**”, in preparation.
11. Jianjun Zhu, Jan G. van Ommen, Leon Lefferts, “**Effect of Water on Catalytic Partial Oxidation of Methane to Synthesis Gas over ZrO₂-based Oxide**”, in preparation.

Lectures in Conferences

1. Jianjun Zhu, Jan G. van Ommen, Leon Lefferts, “**Reaction Scheme of Partial Oxidation of Methane to Synthesis Gas over Yttrium-stabilized Zirconia**”, *Netherlands' Catalysis and Chemistry Conference V (NCCCCV)*, March 8-10, 2004, Noordwijkerhout, The Netherlands.
2. Jianjun Zhu, M.S.M. Mujeebur Rahuman, Jan G. van Ommen, Leon Lefferts, “**Dual Bed Concept for Partial Oxidation of Methane to Synthesis Gas**”, *The 7th Natural gas conversion symposium*, June 6-10, 2004, Dalian, P.R. China.
3. Jianjun Zhu, Jan G. van Ommen, L. Lefferts, “**Transient Studies on Oxygen Activation in the Partial Oxidation of Methane over ZrO₂-based Catalysts**”, *the 228th ACS National meeting*, August 22-26, 2004, Philadelphia, USA.
4. Jianjun Zhu, Jan G. van Ommen, L. Lefferts, “**Reactivity of Oxygen Species on Yttrium-stabilized Zirconia in Partial Oxidation of Methane to Synthesis Gas**”, *The first conference of the european union coordination action: “CO-ordination of Nanostructured Catalytic Oxides Research and Development in Europe (CONCORDE)”*, “*Understanding the dynamic and transient behavior of oxide catalysts in working conditions and the relationships with their catalytic performances*”, January 26-28, 2005, Louvain-la-Neuve, Belgium.
5. Jianjun Zhu, Jan G. van Ommen, Henny J.M. Bouwmeester, L. Lefferts, “**Activation of Oxygen and Methane on Yttrium-stabilized Zirconia for Partial Oxidation of Methane to Synthesis Gas**”, *the 19th North American Catalysis Society Meeting*, May 22-27, 2005, Philadelphia, USA. (Accepted)

Acknowledgements

Time flies! It is still a fresh memory that Dr. Jan van Ommen picked me up at train station on 4th April, 2001. Now it is already time to look back over the last four years I have spent in the Netherlands. To make my stay as pleasant and meaningful as possible, there are many people who had provided me help and support. Here, I would like to take this opportunity to express my sincere acknowledgments.

My special thanks to Prof. dr. ir. Leon Lefferts for having offered me a Ph. D position in Catalytic Processes and Materials Group (CPM). It is my honor to discuss with my project with him and have him as my promoter. Thanks a lot, Leon, also for the clear arguments and ideas during our discussions. I enjoyed your comments and questions very much, which always pushed me to think deeper and deeper. Dr. Jan G. van Ommen, my assistant promoter, working with you was a great experience. I really enjoyed the freedom in our discussions very much. We always started our discussion with the project, and ended with something else. Thanks a lot for correcting this booklet and translating the summary to the samenvatting. I owe a special thank to Dr. Henny J.M. Bouwmeester for helping me to understand the defect chemistry of yttrium-stabilized zirconia better, and for helping me to improve this booklet.

I feel grateful to Mr. Bert Geerdink not only for technical help during my work, but also for his private help, e.g. dealing with my Dutch letters; Dr. Barbara for her struggle to make this group more socially disciplined; Dr. Seshan for regularly organizing our group seminars and creating a very nice academic atmosphere for us; Karin for her enthusiasm for letting me know what is not allowed in the lab; Louise for XRF and some BET measurements; Herman Koster for XRD analysis; Lianne for being the most helpful and efficient secretary. I also did not forget our former secretary, Cis, thanks for her kindness and help.

I also appreciated my students, Sander and Eva, for their contribution to this work. We had a good time during our working together.

Grateful to my present and former colleagues: Jiang Xu, Fahong Li, Mingshi Li, Pingle Liu for having the same heritage and discussing very broad issues. Rahuman for having worked in the same project for two years; Laszlo for sharing his experience in automatically sampling during the catalytic measurements; further, Jeroen, Igor, Sune, Valer, Daryl, Partrick, Hans, Dejan, Nabeel, Cristiano, Khalid, Kazu and others I have not mentioned their names here, thanks a lot for unforgettable time we had during the group activities, and also for offering me a sharp insight to the various cultures.

The contribution of the promotion committee constituted probably the most feedback from the outside. I would like to thanks all committee members for their valuable comments.

I would like to express my deep gratitude to my parents, brothers and parents-in-law for their unconditional support and understanding, although they were not really happy to see my family moving far away to the Netherlands.

Acknowledgements

My wife Lei Feng and my son Jiayi, you are everything that matters me on this earth. For ups and downs in research and life abroad, you were the only persons who really understood. There are no words that can express my feelings at this moment. But, I would like to say that without your love, your support and understanding, this work not only could not have been fulfilled properly, but also would not make sense for me!

Jianjun Zhu
March 2005
Enschede, the Netherlands

Curriculum Vita

Jianjun Zhu was born on April 8, 1966 in Nantong, P.R. China. He started his study in chemical engineering at Jiangsu Polytechnic University (originally, Jiangsu Institute of Chemical Technology, SINOPEC) in 1983. After he received his BS degree in 1987, he worked in Department of Chemical Engineering at the same university. Four years later, he went to East China University of Science & Technology (Shanghai) to continue his study as a master student and started his research career in applied catalysis. He returned to Jiangsu Polytechnic University with his MSc degree in June 1994, and worked there as a lecturer in applied catalysis till 2000. In 2000, he was promoted as an associate professor in heterogeneous catalysis. He gave lectures in applied catalysis and catalytic reaction engineering. His major research interests included application of fractal geometry in catalysis, new methods for catalyst preparation, multifunctional catalysts and computer simulation of chemical processes. In 1999, he co-organized the 6th Chinese national conference in applied chemistry. Because of his outstanding achievements in both teaching and research, he won many awards in both university and province levels.

In 2000, he went to Technical university of Denmark (DTU), and worked there as an assistant researcher. He collaborated with Dr. J.Z. Jiang, Prof. Ib Chorkendorff and Dr. C.J.H. Jacobsen (Haldor Topsoe A/S) in preparation and characterization of ternary nitrides and carbides, promising catalysts for ammonia synthesis. From April 2001 to April 2005, he was employed as A.I.O. by University of Twente, the Netherlands. Under the supervision of Prof. Leon Lefferts and Dr. Jan G. van Ommen, he devoted his four years in research in “Catalytic partial oxidation of methane to synthesis gas, new concept and new materials”. The main results are described in this thesis.

ISBN 903652142-4



9 789036 521420